



U.S. Department
of Transportation
Federal Railroad
Administration

Office of Research,
Development and Technology
Washington, DC 20590

Wheel Failure Investigation Program: Phase 2



NOTICE

This document is disseminated under the sponsorship of the Department of Transportation in the interest of information exchange. The United States Government assumes no liability for its contents or use thereof. Any opinions, findings and conclusions, or recommendations expressed in this material do not necessarily reflect the views or policies of the United States Government, nor does mention of trade names, commercial products, or organizations imply endorsement by the United States Government. The United States Government assumes no liability for the content or use of the material contained in this document.

NOTICE

The United States Government does not endorse products or manufacturers. Trade or manufacturers' names appear herein solely because they are considered essential to the objective of this report.

REPORT DOCUMENTATION PAGE

Form Approved
OMB No. 0704-0188

The public reporting burden for this collection of information is estimated to average 1 hour per response, including the time for reviewing instructions, searching existing data sources, gathering and maintaining the data needed, and completing and reviewing the collection of information. Send comments regarding this burden estimate or any other aspect of this collection of information, including suggestions for reducing the burden, to Department of Defense, Washington Headquarters Services, Directorate for Information Operations and Reports (0704-0188), 1215 Jefferson Davis Highway, Suite 1204, Arlington, VA 22202-4302. Respondents should be aware that notwithstanding any other provision of law, no person shall be subject to any penalty for failing to comply with a collection of information if it does not display a currently valid OMB control number.

PLEASE DO NOT RETURN YOUR FORM TO THE ABOVE ADDRESS.

1. REPORT DATE (DD-MM-YYYY) December 2021		2. REPORT TYPE Technical Report		3. DATES COVERED (From - To) September 2017 – March 2020	
4. TITLE AND SUBTITLE Wheel Failure Investigation Program: Phase 2				5a. CONTRACT NUMBER DTFR53-12-D-00001L	
				5b. GRANT NUMBER	
				5c. PROGRAM ELEMENT NUMBER	
6. AUTHOR(S) Steven Chrismer 0000-0003-3902-4459 , Eric Sherrock 0000-0001-6004-7490 , Dan Stone (retired), Alejandro Alvarez-Reyes 0000-0002-5631-0660				5d. PROJECT NUMBER	
				5e. TASK NUMBER Task Order 7	
				5f. WORK UNIT NUMBER	
7. PERFORMING ORGANIZATION NAME(S) AND ADDRESS(ES) ENSCO Inc. 5400 Port Royal Road Springfield, VA 22151				8. PERFORMING ORGANIZATION REPORT NUMBER SERV-REPT-0002842	
9. SPONSORING/MONITORING AGENCY NAME(S) AND ADDRESS(ES) U.S. Department of Transportation Federal Railroad Administration Office of Railroad Policy and Development Office of Research, Development and Technology Washington, DC 20590				10. SPONSOR/MONITOR'S ACRONYM(S)	
				11. SPONSOR/MONITOR'S REPORT NUMBER(S) DOT/FRA/ORD-21/36	
12. DISTRIBUTION/AVAILABILITY STATEMENT This document is available to the public through the FRA website .					
13. SUPPLEMENTARY NOTES COR: Monique Ferguson Stewart					
14. ABSTRACT Although rare, broken wheel derailments tend to be more catastrophic than other derailment types as a sudden fracture can occur in service at revenue train speeds. It is very difficult to detect the hidden defects which cause such events, prior to failure. In February 2016, the Federal Railroad Administration's (FRA) Office of Railroad Safety (RRS) and Office of Research, Development and Technology (RD&T) established a multi-phase research program tasked with arriving at a better understanding of vertical split rims (VSR) and other wheel failure modes with a focus on failure causes, detection and prevention as well as overall life cycle understanding to help mitigate this risk and establish an approach to minimizing wheel failure-related derailments. This report highlights interim findings during Phase 2 of the project which focused on additional laboratory testing of failed wheels and the evaluation of approaches to analyzing industry data to identify root causes of the failures.					
15. SUBJECT TERMS Wheel failure, vertical split rims, VSR, shattered rims, broken flange, thermal cracking in flange, plate cracking, thin rim overload, rolling stock					
16. SECURITY CLASSIFICATION OF:			17. LIMITATION OF ABSTRACT	18. NUMBER OF PAGES 95	19a. NAME OF RESPONSIBLE PERSON Monique Ferguson Stewart
a. REPORT	b. ABSTRACT	c. THIS PAGE			19b. TELEPHONE NUMBER (Include area code) (202) 493-6358

METRIC/ENGLISH CONVERSION FACTORS

ENGLISH TO METRIC

LENGTH (APPROXIMATE)

1 inch (in) = 2.5 centimeters (cm)
 1 foot (ft) = 30 centimeters (cm)
 1 yard (yd) = 0.9 meter (m)
 1 mile (mi) = 1.6 kilometers (km)

AREA (APPROXIMATE)

1 square inch (sq in, in²) = 6.5 square centimeters (cm²)
 1 square foot (sq ft, ft²) = 0.09 square meter (m²)
 1 square yard (sq yd, yd²) = 0.8 square meter (m²)
 1 square mile (sq mi, mi²) = 2.6 square kilometers (km²)
 1 acre = 0.4 hectare (he) = 4,000 square meters (m²)

MASS - WEIGHT (APPROXIMATE)

1 ounce (oz) = 28 grams (gm)
 1 pound (lb) = 0.45 kilogram (kg)
 1 short ton = 2,000 pounds (lb) = 0.9 tonne (t)

VOLUME (APPROXIMATE)

1 teaspoon (tsp) = 5 milliliters (ml)
 1 tablespoon (tbsp) = 15 milliliters (ml)
 1 fluid ounce (fl oz) = 30 milliliters (ml)
 1 cup (c) = 0.24 liter (l)
 1 pint (pt) = 0.47 liter (l)
 1 quart (qt) = 0.96 liter (l)
 1 gallon (gal) = 3.8 liters (l)
 1 cubic foot (cu ft, ft³) = 0.03 cubic meter (m³)
 1 cubic yard (cu yd, yd³) = 0.76 cubic meter (m³)

TEMPERATURE (EXACT)

$$[(x-32)(5/9)] \text{ } ^\circ\text{F} = y \text{ } ^\circ\text{C}$$

METRIC TO ENGLISH

LENGTH (APPROXIMATE)

1 millimeter (mm) = 0.04 inch (in)
 1 centimeter (cm) = 0.4 inch (in)
 1 meter (m) = 3.3 feet (ft)
 1 meter (m) = 1.1 yards (yd)
 1 kilometer (km) = 0.6 mile (mi)

AREA (APPROXIMATE)

1 square centimeter (cm²) = 0.16 square inch (sq in, in²)
 1 square meter (m²) = 1.2 square yards (sq yd, yd²)
 1 square kilometer (km²) = 0.4 square mile (sq mi, mi²)
 10,000 square meters (m²) = 1 hectare (ha) = 2.5 acres

MASS - WEIGHT (APPROXIMATE)

1 gram (gm) = 0.036 ounce (oz)
 1 kilogram (kg) = 2.2 pounds (lb)
 1 tonne (t) = 1,000 kilograms (kg)
 = 1.1 short tons

VOLUME (APPROXIMATE)

1 milliliter (ml) = 0.03 fluid ounce (fl oz)
 1 liter (l) = 2.1 pints (pt)
 1 liter (l) = 1.06 quarts (qt)
 1 liter (l) = 0.26 gallon (gal)

1 cubic meter (m³) = 36 cubic feet (cu ft, ft³)

1 cubic meter (m³) = 1.3 cubic yards (cu yd, yd³)

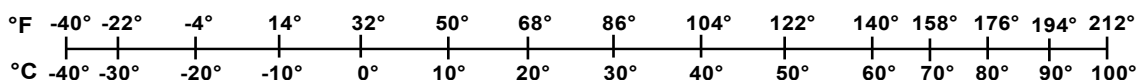
TEMPERATURE (EXACT)

$$[(9/5) y + 32] \text{ } ^\circ\text{C} = x \text{ } ^\circ\text{F}$$

QUICK INCH - CENTIMETER LENGTH CONVERSION



QUICK FAHRENHEIT - CELSIUS TEMPERATURE CONVERSION



For more exact and or other conversion factors, see NIST Miscellaneous Publication 286, Units of Weights and Measures. Price \$2.50 SD Catalog No. C13 10286

Updated 6/17/98

Contents

Executive Summary	1
1. Introduction	3
1.1 Background	3
1.2 Objectives	5
1.3 Overall Approach	5
1.4 Scope	6
1.5 Organization of the Report	6
2. Current Understanding of VSR Wheel Failures	7
2.1 Proposed Mechanism of Delamination	10
2.2 Interpretation of the Cause of VSR Failures	10
3. Considerations of Industry Data	11
3.1 WILD Data as an Indicator of Impending VSR Failure	11
3.2 Wheel Temperature Data and VSR Failures	26
4. Laboratory Testing	29
4.1 Test Wheels	29
4.2 Metallurgical Analysis	30
4.3 Residual Stress	31
4.4 Observations and Conclusions from Laboratory Testing	32
5. Conclusion	33
6. References	35
Appendix A. Results of Laboratory Testing of Individual Failed Wheels	37

Illustrations

Figure 1. Example of Vertical Split Rim, Shattered Rim, and Thermal Crack Failed Wheels [1]...	4
Figure 2. Typical VSR Defect	7
Figure 3. Potential Directions of Propagation from the Zone of Origin for a Subsurface Initiated Crack and Subsequent VSR Failure.....	8
Figure 4. Crack Initiation Locations of Broken Wheels [8]	9
Figure 5. Example of WILD Data for VSR Failure with Small Impact Loads—Car 6.....	11
Figure 6. Example of WILD Data for VSR Failure with Small Impact Loads—Car 8.....	12
Figure 7. Example of WILD Data for VSR Failure with Small Impact Loads—Car 10.....	12
Figure 8. Example of WILD Data for VSR Failure with Small Impact Loads—Car 20.....	12
Figure 9. Illustration of Monotonically Increasing and Non-Monotonically Increasing Data Trends	13
Figure 10. Example of WILD Data for a VSR Failed Wheel Showing Increasing Dynamic Augment.....	14
Figure 11. Example Calculation of “kip-days” at Time of VSR Failure	15
Figure 12. Further Examples Showing Number of Kip-Days at VSR Failure	16
Figure 13. Examples of VSR Failure Well Before Suggested 11,000 Kip-Days Limiting Criterion	17
Figure 14. WILD Data for a VSR Wheel with a Large Impact Load Before Failure [9].....	18
Figure 15. WILD Data for a VSR Wheel with a Small to Moderate Impact Load Before Failure [9].....	19
Figure 16. Example of Fatigue Crack Growth Rate in Rail [11].....	19
Figure 17. Measured Increase in Rail Fatigue Crack Size with Cumulative Tonnage [12]	20
Figure 18. Example Calculation of $P*\Delta$ for Rapid Increase of Initially Large Impact Load	21
Figure 19. Example Calculation 1 of $P*\Delta$ for Rapid Increase of Initially Small Impact Load	21
Figure 20. Example Calculation 2 of $P*\Delta$ for Rapid Increase of Initially Small Impact Load	22
Figure 21. Example Calculation 3 of $P*\Delta$ for Rapid Increase of Initially Small Impact Load. ...	22
Figure 22. Comparing Kip-Days with $P*\Delta$ for a VSR Failed Wheel for Car 1.....	23
Figure 23. Comparing Kip-Days with $P*\Delta$ for a VSR Failed Wheel for Car 21.....	23
Figure 24. Comparing Kip-Days with $P*\Delta$ for a VSR Failed Wheel for Car 18.....	24
Figure 25. Comparing Kip-Days with $P*\Delta$ for a VSR Failed Wheel for Car 16.....	24
Figure 26. Comparing Kip-Days with $P*\Delta$ for a VSR Failed Wheel for Car 5.....	25
Figure 27. Comparing Kip-Days with $P*\Delta$ for a VSR Failed Wheel for Car 2.....	25

Figure 28. Wheel Temperature Above Ambient History for Sample VSR Failed Wheel..... 27

Tables

Table 1. “Kip-days” Calculations for Wheel History Shown in Figure 11	15
Table 2. Maximum Measured Wheel Temperature and Wheel Failure Mode for Sample Failed Wheel Dataset	27
Table 3. Tread Geometry for Phase 2 Failed Wheels Using LazerView® Measurements	29
Table 4. Available Impact and Out-of-Round Measurements for Failed Wheels Considered in Phase 2	30
Table 5. Chemical Composition Determined by Check Analysis for Wheels Tested in Phase 2.	30
Table 6. Microcleanliness Ratings of Failed Wheels Considered in Phase 2.....	31
Table 7. Residual Stress States in Failed Wheels BNSF7 and UP9 and Their Mates	31

Executive Summary

This report summarizes the results of the second phase of a multi-phase study to determine the underlying mechanism(s) for catastrophic wheel failures such as shattered rims and vertical split rims (VSRs) and potential solutions and strategies to minimize derailments due to these types of failures. ENSCO, Inc., and Engineering Systems, Inc. led this study with significant contributions made by Railinc, members of the Association of American Railroads (AAR), car owners and wheel suppliers.

Between 2013 and 2015, accidents associated with wheel failures represented 11 percent of all equipment-caused accidents.¹ Although rare, broken wheel derailments tend to be more catastrophic than other derailment types due to sudden fracture which can occur at revenue train speeds. Coupled with increased movement of hazardous material including crude oil, this scenario poses an increasing risk to public and railroad safety. In response to this increased risk, the Federal Railroad Administration's (FRA) Administrator, Ronald Batory, tasked the FRA Office of Railroad Safety (RRS) with arriving at a better understanding of VSRs and other wheel failure modes. RRS' objectives include improved insight into failure causes, the development of detection and prevention methods and establishment of approaches to minimize wheel failure-related derailments.

Past studies and research supported by FRA have focused on developing an understanding of wheel failures from various perspectives. A definitive study to determine the underlying mechanism(s) for wheel failures such as shattered and vertical split rims and potential solution(s) and strategies to minimize derailments due to these types of wheel failures remains to be completed. In response to a request from RRS, FRA's Office of Research, Development and Technology (RD&T), established a multi-phase research program in February 2016 to develop a comprehensive understanding of various wheel failure mechanisms, identify major contributing factors to these failures, and arrive at potential strategies to mitigate the failures and consequently improve safety of rail network operations and reduce risks. The initial vision of this FRA program includes the following phases:

- Phase 1: Problem Definition and Size Analysis
- Phase 2: Review and Analysis of Tests and Analytic Studies on Investigation of Wheel Failure Mechanisms
- Phase 3: Modeling and Analysis of Underlying Wheel Failure Mechanisms and Failure Prevention and Mitigation Strategies

A key element of FRA's approach is its creation of an industry Stakeholder Working Group (SWG) made up of members of the AAR, car owners, and researchers as active participants. Researchers working with FRA and the SWG identified the following wheel failures to consider under this program: VSR; shattered rims; broken flange; plate cracking; thermal cracking in flanges; and thin rim overloads. Based on the prevalence of VSR and shattered rim failures, much of the Phase 1 activities and subsequent Phase 2 efforts were focused on these failure modes.

¹ Based on equipment-caused accident data available from [FRA's Office of Railroad Safety](#), November 2016.

During Phase 2 of the effort, the research team focused on two approaches to further the investigation of wheel failures:

- An analysis of sample industry data to find trends that would identify contributions to failures. An investigation of data sources included AAR MD-115² database records, Wheel Impact Load Detector (WILD) history and wheel temperature data for wheels confirmed to be VSR failures. This investigation identified several key issues with the data sources that must be overcome to arrive at an analysis plan that is likely to successfully identify contributing factors.
- Conduct laboratory-based tests on eight failed wheels and their mates donated by Class I railroads and industry members. Testing included an evaluation of wheel profile contours, out-of-round assessments, microhardness tests, microcleanliness tests, fracture toughness tests and evaluations of residual stress.

The following are conclusions drawn from the efforts conducted under Phase 2 and prior research activities:

- Wayside wheel impact data and wheel temperature data currently captured by the industry are not able to reliably identify wheels that failed due to VSR. Wheel impact data collected on wheels prior to VSR failure appear to contain information that may provide an early indication of failure. One method that shows promise based on a very small sampling of VSR wheels identifies and quantifies a sudden upward trend in impact load before failure that is indicative of discontinuities on the tread surface that may indicate that a wheel is at risk for VSR formation. The research group recommends this data source be looked at in more detail once a relationship between these discontinuities and factors influencing VSR formations are definitively established.
- Given the lack of definitive trends in data considered to date, initiation of VSR failures appears to be the result of a combination of factors. These factors are likely rolling contact fatigue, moderate-to-high heat inputs from on-tread braking, and, possibly, impact loads that altered the beneficial residual stress state that was imparted during heat-treatment.

This research group recommends a parametric study using finite element analysis to answer the following questions:

- What are the major factors that cause a crack below the surface of the wheel tread to turn towards the surface of the rim?
- What are the relative roles of contact mechanics and operating conditions including the development of thermal stresses in the wheel that will lead to the development of VSR?
- What information collected by industry, either presently or in the future, can identify conditions that could be indicators of at-risk wheels?

² AAR's Railinc MD-115 database, is formed from mechanical defect reports on wheels removed from service collected by railroads and submitted to Railinc. The database includes reports represented by Why Made Codes: 66, 68, 69, 71, 83, and 85. More details on AAR's Field Manual – Rule 41. (Minimum requirements for removing defective wheels)

1. Introduction

This report summarizes the results of the second phase of a multi-phase study initiated in February 2016, to determine the underlying mechanism(s) for catastrophic wheel failures such as shattered rims and vertical split rims (VSRs) and potential solutions and strategies to minimize derailments due to these types of failures.

1.1 Background

The Federal Railroad Administration (FRA) continuously evaluates derailment causes to identify trends in the industry that merit additional research to improve the safety and efficiency of railroad operations. Accidents resulting from in-service failure of freight rail vehicle wheels is one such area in which additional efforts are required.

Between 2013 and 2015, accidents associated with wheel failures represented 11 percent of all equipment-caused accidents.³ Broken wheel derailments tend to be more catastrophic than other derailment types due to the sudden fracture and ensuing derailment which can occur at high train speeds. Coupled with movements of hazardous materials, including crude oil, this scenario poses an increasing risk to public and railroad safety. In response to this increased risk, the FRA Administrator tasked the FRA Office of Railroad Safety (RRS) with developing a better understanding of VSRs and other wheel failure modes. RRS' objectives include improved insight into failure causes, the development of detection and prevention methods and establishment of approaches to minimize wheel failure-related derailments.

Broken wheel derailments occur when a wheel experiences a fracture that removes a significant portion of the wheel or causes the wheel to become loose on the axle. The FRA Derailment Cause Codes⁴ and the Association of American Railroads (AAR) Field Manual of Interchange Rules, Rule 41 details the different types of broken wheels which can cause derailments. [Figure 1](#) illustrated the wheel failures that have historically been the most problematic:

- **Vertical Split Rim (VSR):** A VSR occurs when sub-surface tread cracking reaches a critical location within the rim. A tread surface or subsurface horizontal crack is initiated and grows. These horizontal cracks can be surface initiated (i.e., shelling/spalling/RCF/thermal cracking) or subsurface initiated (i.e., delamination) [1]. This crack then turns in a “vertical” direction and propagates towards the wheel tread resulting in a loss of wheel material. Unfortunately, current research has not completely identified the root cause of or proper mitigation actions for VSR failures. Although some railroads noted a decrease in VSR failures over the past several years, this wheel failure mode continues to represent a derailment risk.
- **Shattered Rim:** Shattered rim failures are due to contact stress creating subsurface fatigue cracking initiated at voids or inclusions. Thin rim thickness and impact loads can increase the contact stresses in proximity to subsurface voids and inclusions. Bending stresses

³ Based on equipment-caused accident data available from [FRA's Office of Railroad Safety](#), November 2016.

⁴ Train Accident Cause Codes (Appendix C of FRA Guide for Preparing Accident/Incident Reports) Namely: Broken Flange (E60C, E60L), Broken Hub (E63C, E63L), Broken Plate (E62C, E62L), Broken Rim (E61C, E61L), Other Wheel Defects (E69C, E69L), Thermal Crack (flange or tread) (E6AC, E6AL)

then cause the subsurface fatigue crack to grow to be quite large before fracture, causing an extensive loss of wheel rim material.

- **Thermal Crack Extended Into Plate:** A thermal crack is a transverse fatigue crack initiated at the surface of the tread or flange that occurs when the rim hoop residual stress is transformed from the beneficial compressive stress to the detrimental tensile stress. This stress reversal occurs due to significant tread braking. If the fatigue crack grows during repeated heating cycles to the point where it eventually reaches the critical size, a large transverse overload fracture will propagate into the plate and can turn to remove a large portion of the rim and plate, or go to the hub and cause the wheel to become loose on the axle.



Vertical Split Rim

Shattered Rim

Thermal Crack Extending Into Plate

Figure 1. Example of Vertical Split Rim, Shattered Rim, and Thermal Crack Failed Wheels [1]

Past studies and research supported by FRA focused on developing an understanding of wheel performance from various perspectives, including material properties (i.e., metallurgy, strength, and toughness), manufacturing processes (i.e., casting, forging, heat treatment, surface treatment, and residual stresses), design parameters (i.e., wheel diameter, rim thickness, and plate type), and the operating environment (i.e., axle load, maximum operating speed, tread braking capacity, wheel-rail interaction under curving and traction conditions, and track perturbations, etc.). However, a definitive study to determine the underlying mechanism(s) for catastrophic wheel failures such as shattered rims, VSRs, and potential solution(s) and strategies to minimize derailments due to these types of failures remains to be completed.

In response to this need, FRA's Office of Research, Development and Technology (RD&T), working in cooperation with RRS, established a multi-phase research program to establish a comprehensive understanding of the various wheel failure mechanisms, identify major contributing factors to these failures, and arrive at potential strategies to mitigate the failures and consequently improve rail network operations safety and reduce risks. The initial vision of this FRA program includes the following phases:

- Phase 1: Problem Definition and Scope Analysis
- Phase 2: Review and Analysis of Tests and Analytic Studies on Investigation of Wheel Failure Mechanisms

- Phase 3: Modeling and Analysis of Underlying Wheel Failure Mechanisms and Failure Prevention and Mitigation Strategies

A key element of FRA’s approach is its creation of an industry Stakeholder Working Group (SWG) made up of railroads, car owners, and researchers as active participants in the research program. Membership in the SWG included personnel from:

- AAR
- Burlington Northern Santa Fe Railway (BNSF)
- Canadian National Railway (CN)
- Canadian Pacific Railway (CP)
- CSX Transportation (CSX)
- GATX Corporation (GATX)
- Greenbrier Companies
- Griffin Wheel, an Amsted Rail Company
- Norfolk Southern Corporation (NS)
- ORX Rail
- Standard Steel
- Transportation Technology Center, Inc. (TTCI)
- Union Tank Car
- Union Pacific Railroad (UP)
- Volpe National Transportation Systems Center

The activities of FRA and the SWG were supported by researchers from ENSCO, Inc. (ENSCO), Railinc (a wholly owned subsidiary of the AAR), and Engineering Systems, Inc. (ESI) during Phase 2.

Results of Phase 1 were documented in late 2017 [1]. Based on the lack of definitive understanding of the formation of VSR failures, Phase 2 activities focused on VSR failures

1.2 Objectives

The objective of Phase 2 of FRA’s Wheel Failure Program was the analysis of industry-collected data and laboratory test results to identify the underlying mechanism(s) for VSRs, and potential solutions and strategies to minimize derailments due to this type of failures.

1.3 Overall Approach

During Phase 2, the research team focused on two approaches to further the investigation of VSR failures:

- The Analysis Working Group (AWG) investigated approaches to analyzing industry data to identify trends in the data that would identify contributions to failures. An investigation of data sources included MD-115 database records, Wheel Impact Load Detector (WILD) history, and wheel profile information and wheel temperature data. This investigation identified several key issues with the data sources that must be overcome to arrive at an analysis plan that is likely to successfully identify contributing factors.
- The Testing Working Group (TWG) conducted laboratory-based tests on eight failed wheels and their mates donated by Class I railroads and industry members. Testing included evaluation of wheel profile contours, out-of-round assessments, microhardness tests, microcleanliness tests, fracture toughness tests and evaluations of residual stress.

1.4 Scope

The scope of Phase 2 of FRA's Wheel Failure Program was:

- The analysis of industry-collected wheel impact and wheel temperature data to identify early indicators of wheels at risk for failure.
- Laboratory testing of failed wheels donated by Class I railroads and industry members.

1.5 Organization of the Report

This report summarizes the results of the efforts conducted by the AWG and TWG through early spring of 2020. The organization of the report is as follows:

- [Section 2](#) summarizes the current knowledge regarding the origin and potential progression of VSR failures.
- [Section 3](#) presents considerations of data made during the preliminary analysis of industry data conducted during this effort.
- [Section 4](#) provides an overview of the laboratory testing conducted under this effort.
- [Section 5](#) summarizes the interim conclusions reached at this stage of the effort and recommendations for next steps.

2. Current Understanding of VSR Wheel Failures

This section summarizes the current understanding of VSR failures determined through data analysis, a review of existing literature, and SWG discussions.

VSRs tend to initiate in connection with shell defects. Typically, an area of delamination occurs approximately 0.20 inches (5 mm) below and parallel to the wheel tread surface, as shown in [Figure 2](#). A vertical crack begins on the delaminated surface which then grows as a vertical crack through the thickness of the wheel rim.

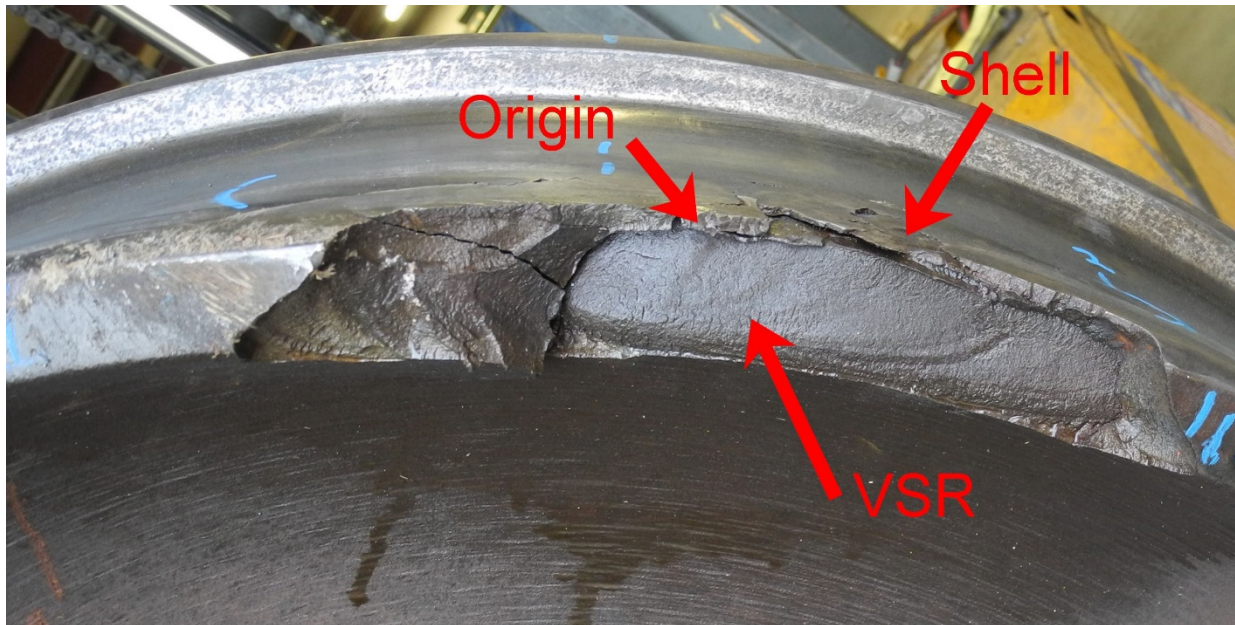


Figure 2. Typical VSR Defect

There are still several competing theories regarding how VSR failures develop. Referring to [Figure 3](#), the questions related to VSR failure can be divided into: 1) how the crack originates and starts propagating transversely (i.e., axially to the wheel), and 2) what drives the crack to turn “downward” radially to the rim surface and grow toward failure. An understanding of how the cracks leading to VSRs are formed and propagate is essential so that improved inspection mitigation practices can be identified and implemented. The expectation is that there is more than one process involved in producing VSR failures, but successful mitigation strategies require that the most prevalent, and their relative influence, be identified.

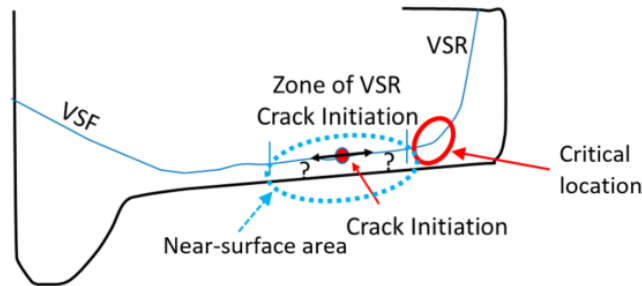


Figure 3. Potential Directions of Propagation from the Zone of Origin for a Subsurface Initiated Crack and Subsequent VSR Failure

Research has established that the crack initiation zone for VSR failures typically extends over the region shown in Figure 3 [2]. A tread surface or subsurface horizontal crack is initiated and grows. The horizontal cracks can be surface initiated (i.e., shelling/spalling/RCF/thermal cracking) or subsurface initiated (i.e., delamination) [1]. The clustering of initiation points on the field side of the treads studied by Cummings (2014) could be due to the low rail in curves contacting the tread in this area and often generating large lateral traction forces and associated rolling contact fatigue (RCF) damage (see Figure 4). Additionally, brake heating predominantly occurs to the field side of the tread which could promote crack initiation and propagation in this region [3].

In the wheels studied by Cummings (2014), the direction of crack growth is usually toward the field side but occasionally it grows toward the flange (see Figure 3). These are both classified as VSR failures, although the failure toward the flange side is sometimes referred to as a vertical split flange (VSF) to distinguish this mode of failure. A broken flange is a separate failure mode with its own Why Made Code⁵ designation where the failure is largely confined to the flange itself.

⁵ Why Made Codes are specific causes established in AAR's Interchange Rules. Why Made Codes are used to record why maintenance or removal was done. WMC66 is for flange cracked or broken.

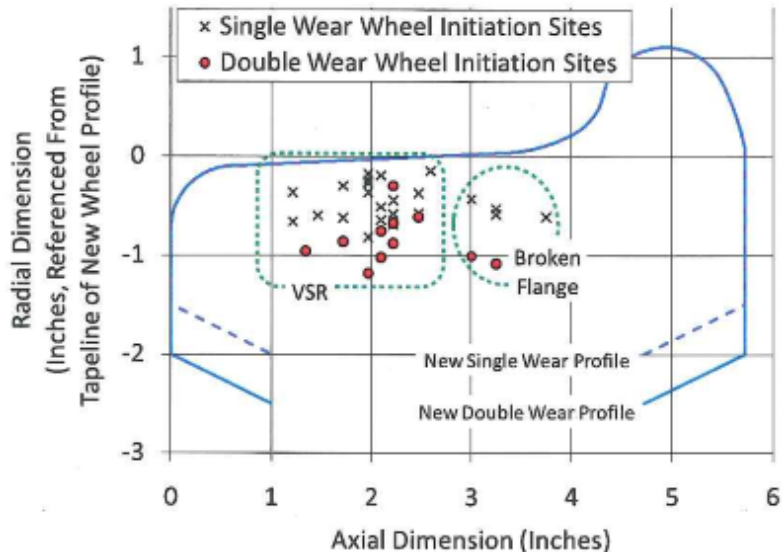


Figure 4. Crack Initiation Locations of Broken Wheels [8]

Berge has suggested that VSR fractures are driven by bending stresses imposed by loading on the tread toward the field side of the rim [2]. Kristan et al. (2004) supported Berge’s proposed mechanism by showing that loading on a false flange and/or low rail curving conditions will provide loading at the front rim [3].

Investigations of the residual stress patterns that develop during the heat-treating process, as well as the alteration of the residual stresses during plastic flow of the tread, each give a stress state that facilitates the formation and growth of VSR cracks [4] [5] [6].

The question of whether most cracks that produce VSR failures originate on or below the tread surface, remains a matter of some debate. A crack that causes a VSR may form at the wheel surface and progress slightly downward before turning laterally (axially) to grow parallel to the tread surface, or it may form slightly below the tread surface and grow axially. Surface originated cracks typically produce tread damage that can be identified by visual inspection and impact loads, while a subsurface-originating crack makes early detection difficult with using common inspection technologies.

The three main types of wheel damage that have the potential to provide cracking that can lead to a VSR are spalling, shelling and delamination. Spalling and shelling both originate and are observable from the tread surface, but delamination is a subsurface phenomenon. Spalling refers to tread damage from heat build-up due to wheel slip from locked brake applications. Spalling typically creates a layer of martensite on the wheel surface due to heat damage which distinguishes it from shelling. Shelling damage results from cracking due to high subsurface stresses from rolling contact. Delamination is a subsurface separation that may remain below the surface or turn upward and terminate at the tread surface. When a delamination breaks out to the tread surface, a shelling defect is created.

Shelling and spalling are often identified as the source of a VSR-initiating crack based only on visual inspection of the tread surface. However, it is possible that a delamination may have produced a crack that led to a VSR while also producing cracks that propagate to the tread surface, producing damage that may lead to mistakenly identifying shelling and spalling as the root cause. Investigation methods such as cutting a cross-section of the failed VSR wheels to

look for delamination can help resolve this question, but without such measures there is the possibility that the cause of VSR failures could be misidentified.

If shelling and spalling are associated with VSR failures without being linked to delamination, then the relative occurrence of all three potential root causes of VSR's, shelling, spalling and delamination, should be determined. Quantifying the causative share of each of these failure modes will lead to better mitigation strategies

2.1 Proposed Mechanism of Delamination

Although the processes that produce spalling and shelling are relatively well understood as described above, the mechanism that causes delamination is not. However, an advancement of some important clues and findings provide a partial answer. The depth of delamination tends to be several millimeters below the tread surface, which is near the depth at which shear stress from rolling contact is maximum. The maximum shear stress can cause a pre-existing crack, or crack initiation at a void, or non-metallic inclusion at this depth, to then propagate both axially and circumferentially.

Crack propagation tends to occur along the axial and hoop planes because this is the path of least resistance for the crack. In the case of delamination, the crack does not allow shear stress from the tread surface to be transmitted across the crack to the material below, and so this stress tends to become tensile in the region at the field side tip of the crack which encourages its continued axial growth toward the field side. It is theorized that as the crack grows axially to the field side, stresses from a large vertical impact load or from brake heating can turn the crack downward, away from the tread surface. Once a crack "turns downward" its propagation rate may then increase due to the crack tip encountering the residual tensile stress region where the tensile stress increases with depth.

2.2 Interpretation of the Cause of VSR Failures

Although it has been difficult to establish whether spalling, shelling or delamination is the most common cause of VSR failures to date, wheel impact load measurement (see [Section 3](#)), has been thought to provide some indication. Dick et al. (2017) showed that VSRs most often occurred in wheels that had been subjected to elevated impact loads. A neural network analysis of 81 VSR wheels and 48 non-VSR wheels predicted the occurrence of high impacts as an effect in 84 percent of the wheels, while age, location in car and ambient temperature were not significant [7]. However, it remains uncertain if impacts contribute to the formation of VSRs, or if the presence of the VSR causes the wheel to produce impacts. Wheel impact was not a reliable precursor to identifying VSR wheel failures (see [Section 3](#)).

A definitive conclusion on the influence of car type or train operations has not been established by researchers [1]. However, once a conclusion on the driving factors for wheel damage that leads to VSRs is established, it may be possible to identify cars or operations that are at higher risk for VSR failures. Some car types will be in unit train operation and experience more heat input from tread braking at higher speeds and therefore are more prone to shelling, while other car types routinely move between train consists and are subject to hand brake operations than others and have excess tendencies to form spalling damage. More specifically, cars in intermodal operation are more prone to thermal and mechanical shelling due to higher amounts of brake heating, while freight cars in mixed consists tend to exhibit more spalling due to occasional unreleased hand brakes.

3. Considerations of Industry Data

The information contained in this section describes industry data considered during Phase 2 activities.

3.1 WILD Data as an Indicator of Impending VSR Failure

Some industry members have hypothesized that WILD measurements have the potential to be used to identify wheels that are developing VSR failures. Increasing impact loads associated with increasing tread damage has been thought by some to be able to serve as an early warning of propagating cracks before they can develop into a VSR failure. Past investigations of WILD data preceding a VSR failure have not revealed a unique trend that can be associated with a VSR that is easily distinguishable from impact load trends for the general population of wheels that do not develop VSR failures. Given that WILD data is readily available to the industry and has been considered in the past, researchers attempted to revisit the suitability of WILD data as a practical means to identify wheels at risk for VSR failures.

During Phase 2, Railinc personnel provided the research team with WILD data histories for a set of 21 failed wheels. Eleven of the wheels were identified as VSRs failures, 8 were identified as broken flange failures and 2 wheels failed from cracked plates. Of the 11 VSR wheels, 7 exhibited increasing impact loads towards the end of the wheel data history. Four of the VSR wheels did not exhibit any appreciable change in WILD impact data throughout the impact history. Figure 5 through Figure 8 shows four examples of VSR wheels with uniformly small impact loads.

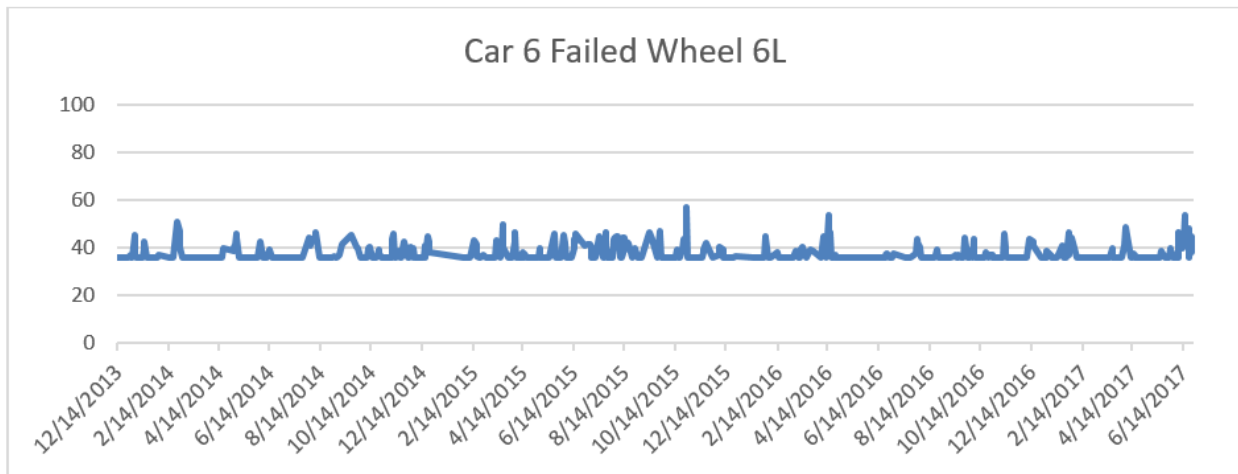


Figure 5. Example of WILD Data for VSR Failure with Small Impact Loads—Car 6

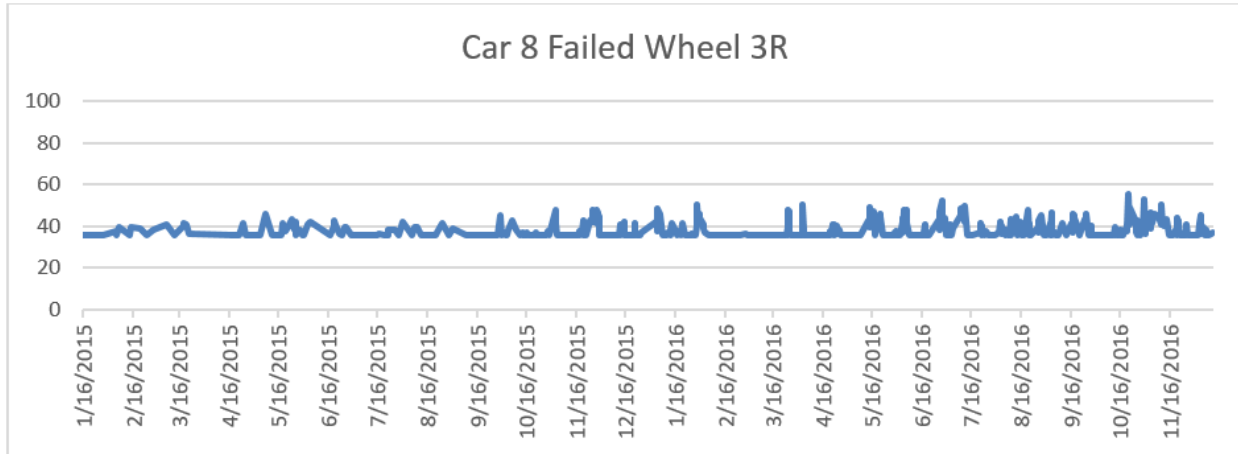


Figure 6. Example of WILD Data for VSR Failure with Small Impact Loads—Car 8

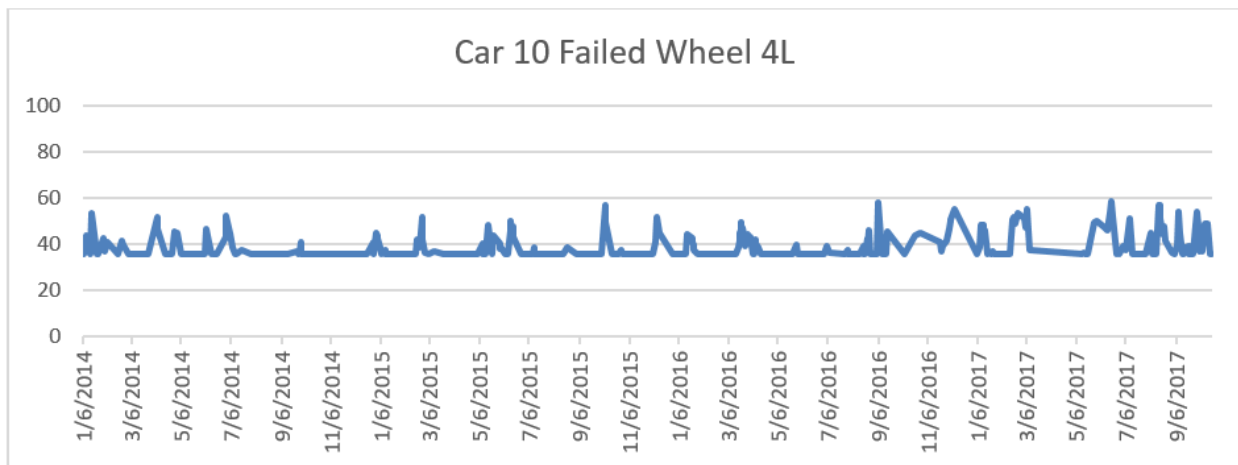


Figure 7. Example of WILD Data for VSR Failure with Small Impact Loads—Car 10

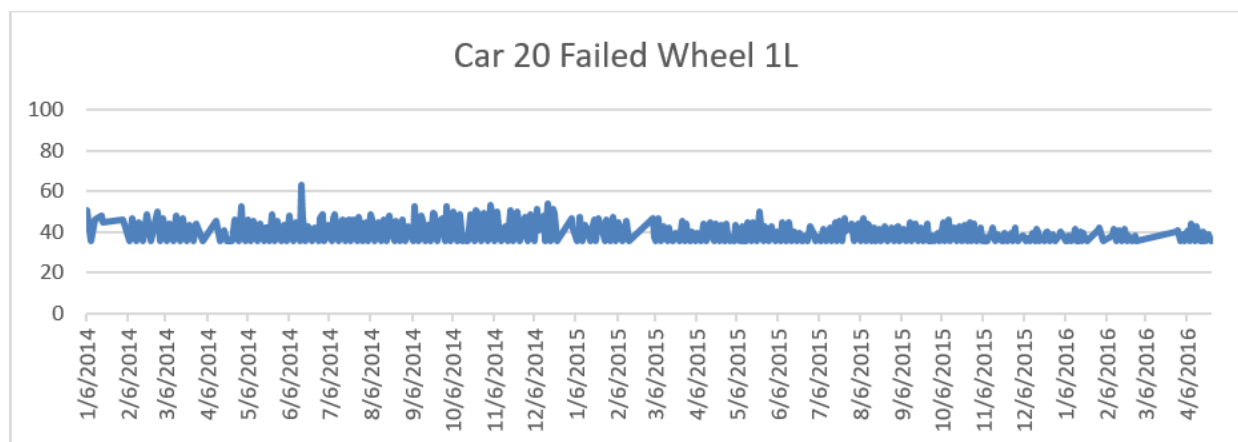


Figure 8. Example of WILD Data for VSR Failure with Small Impact Loads—Car 20

There are several reasons for the difficulty in determining an identifiable trend in impact loads:

- 1) Impact loads provide an indirect and approximate measure of the severity of wheel tread surface damage.
- 2) VSRs caused by cracks propagating below the tread surface might not produce the wheel surface damage needed for detection by impact load.
- 3) The damaged location that produces a VSR may be toward the field side of tread which mostly contacts the rail in curves but seldom in tangents where WILDs are typically located.

Thus, WILD data history considering only the impact loads as collected from the sites is not a reliable indicator of the imminence of a VSR. Efforts employing WILD data may be warranted if they reduce at least a portion of these failures. However, when considering WILD data, care must be taken to understand the limitations in the data prior to drawing erroneous conclusions.

One way to account for the cumulative damage from impact loads is to review the impact load history of a failed wheel to find the increasing peak loads and the number of days between successive peaks prior to failure. This can potentially identify trends that can be used to find at-risk wheels before failure. Impact loads that result from tread damage would tend to follow the monotonically increasing trend illustrated in Figure 9. Impact loads due to crack growth may increase, slow down and perhaps be arrested for a time, but not reverse their trends. WILD data typically shows individual or clusters of data points that appear to be non-monotonic due to variable static vertical wheel loads and variable speeds. However, if all impact data could be normalized or corrected for speed and static loading, the overall trend may tend to be monotonically increasing loads with increasing tread damage. Some researchers have investigated the use of successive peak loads to identify an overall trend.

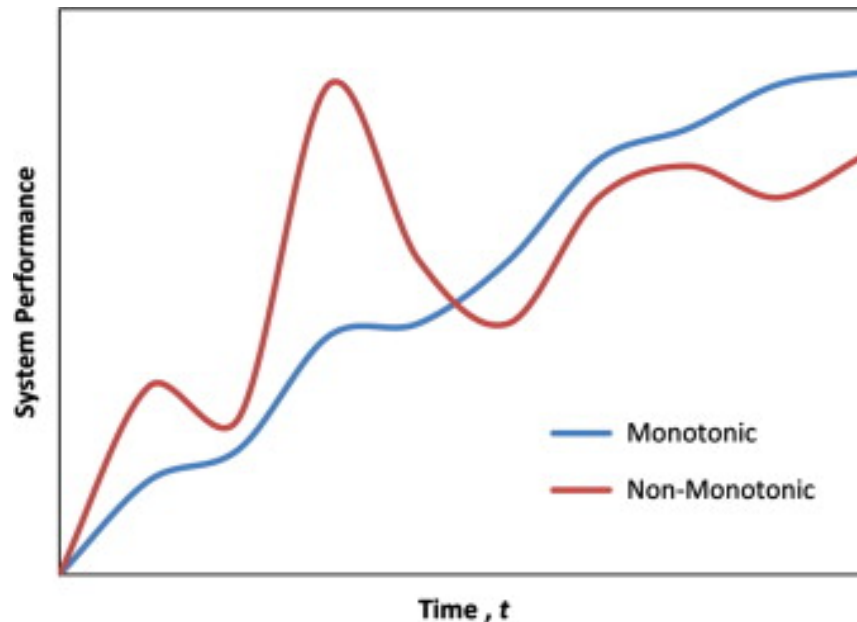


Figure 9. Illustration of Monotonically Increasing and Non-Monotonically Increasing Data Trends

3.1.1 WILD Data and Cumulative Impact Loading in “kip-days”

For a wheel with increasing impact loads, Cummings recommends representing the cumulative damage as the cumulative sum of each increasing impact load magnitude, in kips, multiplied by the number of days until the next higher impact load occurs [2]. The result is a value of “kip-days.” Figure 10 and Figure 11 show example calculations of kip-days for a VSR failed wheel using data that was anonymized by Railinc as part of a preliminary consideration of WILD data for this study. Figure 10 shows only the impact load above the static vertical nominal wheel load, or dynamic augment, to illustrate the increasing trend of impact load for a fully loaded 110-ton car.

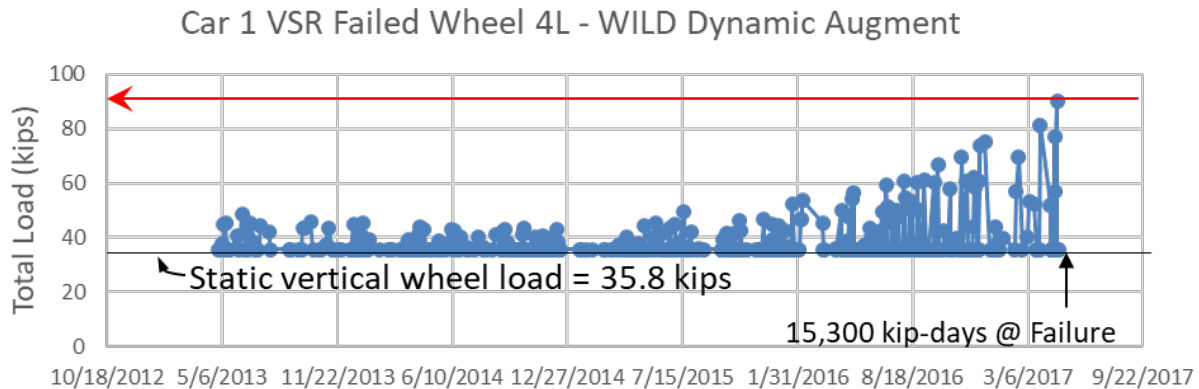


Figure 10. Example of WILD Data for a VSR Failed Wheel Showing Increasing Dynamic Augment

According to the method described by Cummings (2014), the counting of kip-days should start at the first impact load greater than 30 kips plus the static vertical wheel load. This corresponds to 65.8 kips for the wheel impact history shown in Figure 11. The first total impact load, which equals static load plus dynamic augment, above this threshold is 66.6 kips; there are 42 days until the next higher load of 69.7 kips. Therefore, the incremental kip-days for the 66.6 kips load is 66.6×42 , or 2,797 kip-days. This is rounded to the nearest hundred days to 2,800 kip-days, as are the other values of kip-days in Table 1 calculated for the example shown in Figure 11. The counting starts again for the next higher load of 69.7 kips for 32 days and the cumulative sum is calculated until wheel failure, as indicated by an impact load of 90 kips,⁶ is reached at a total of 15,300 kips-days.

⁶ 2015 Field Manual of the AAR Interchange Rules. AAR guidance (Rule 41) states that when a freight car's wheel registers a WILD impact of 65 kips or more, that the car's owner receives notification of that reading. When a wheel registers from 80 to 89 kips on a WILD, that wheel is condemnable and may be replaced when the car is on a shop or repair track for any other reason. Any wheel that registers over 90 kips is condemnable and may be replaced at any time.

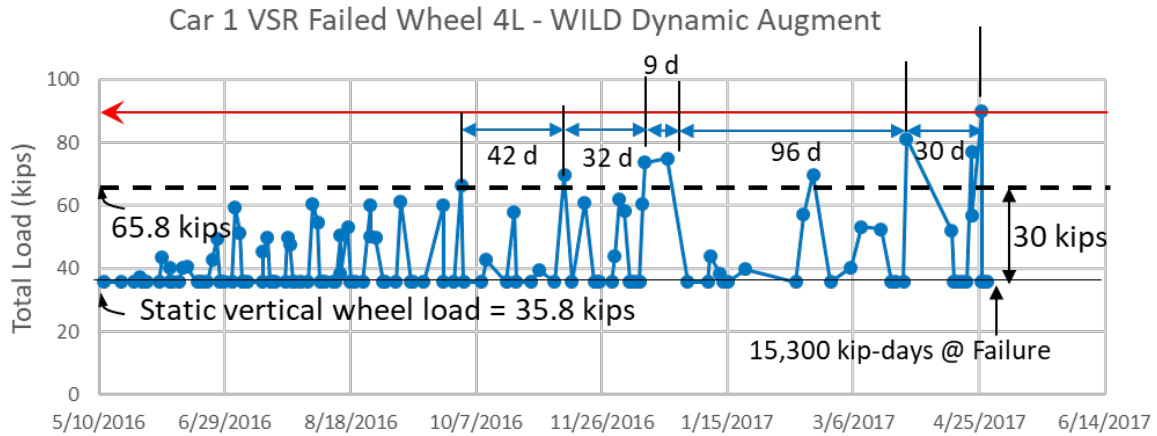


Figure 11. Example Calculation of “kip-days” at Time of VSR Failure

Table 1. “Kip-days” Calculations for Wheel History Shown in Figure 11

Kip Load	Days	Kip Days = Kip Load*Days	Cumulative Kip Days
66.6	42	2,800	2,800
69.7	32	2,200	5,000
73.8	9	700	5,700
75	96	7,200	12,900
81.2	30	2,400	15,300
89.9	Fail	----	----

Cummings suggests a possible limiting threshold value of 11,000 kip-days to prevent a VSR failure based on his research [8]. Using this criterion, the wheel would have been removed from service before the 81.2-kip impact load event, approximately 2 months before failure. Figure 12 shows two additional examples of wheels, using the 11,000-kip days limit, that would have been removed from service before failure at 12,700 and 13,100-kip days, respectively.

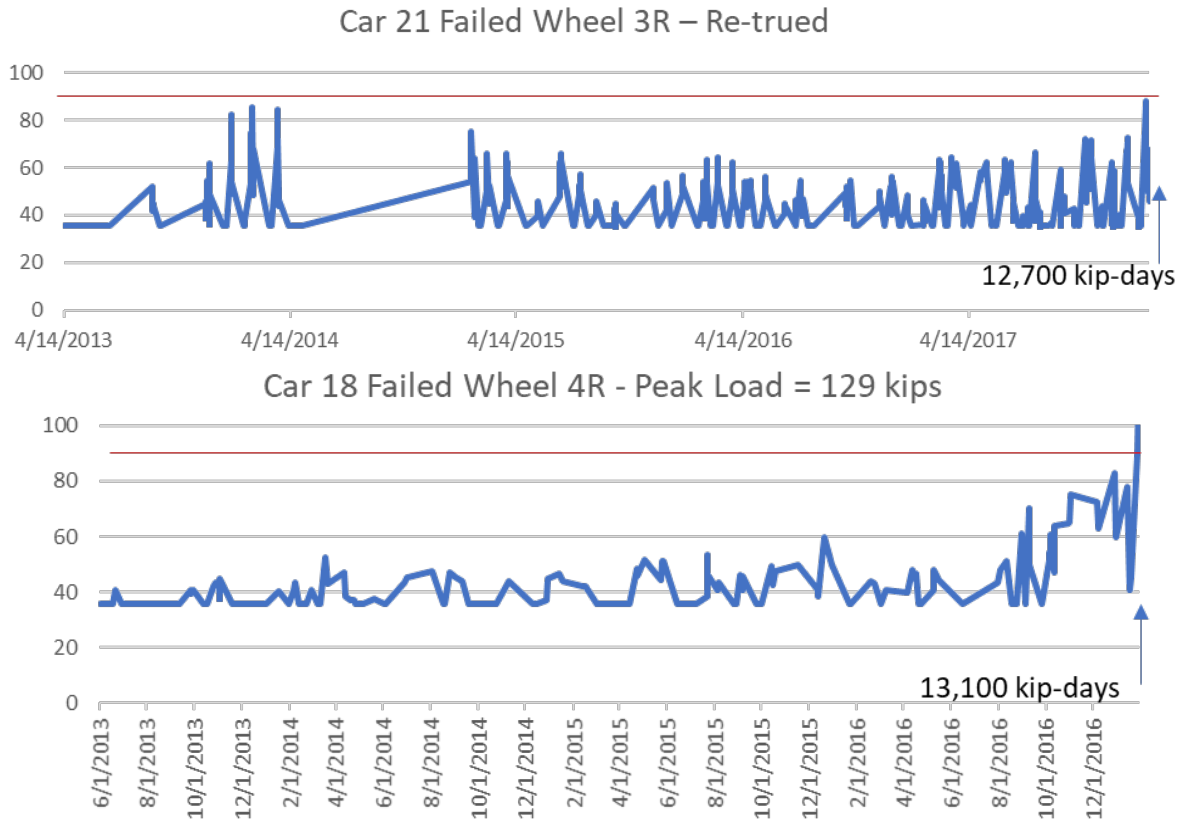


Figure 12. Further Examples Showing Number of Kip-Days at VSR Failure

However, further review of WILD data yields examples of VSR failures well before 11,000-kip days have elapsed; [Figure 13](#) shows three examples.

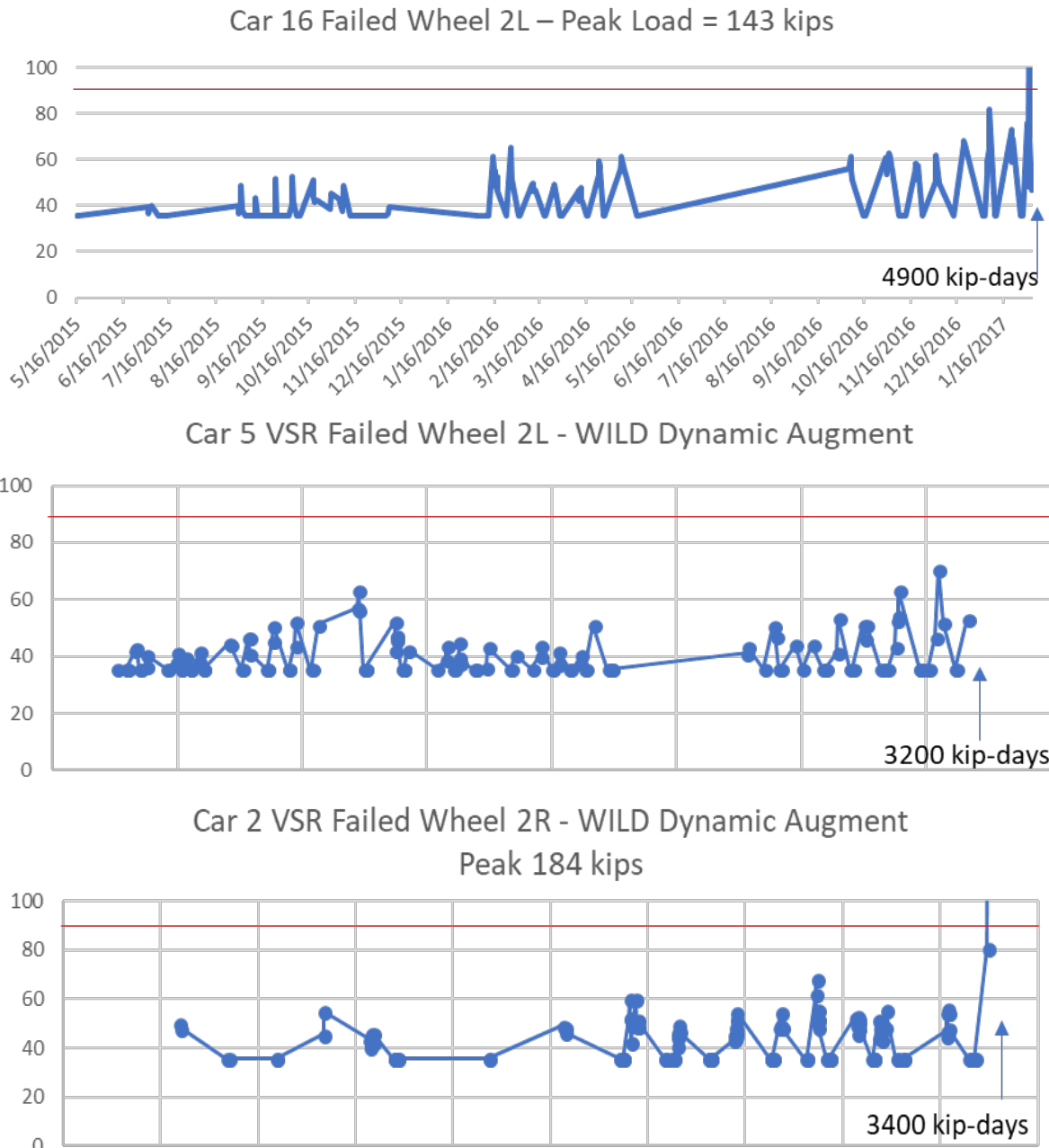


Figure 13. Examples of VSR Failure Well Before Suggested 11,000 Kip-Days Limiting Criterion

Further investigation of available WILD data from VSR failed wheels and non-failed wheels should be reviewed to determine if a variation of the measure of kip-days can provide a reliable indication of pending VSR failure. In addition to reliably predicting VSR's, any predictive method must also not falsely indicate a pending VSR failure, (i.e., a false positive). The economic impact of replacing wheels that exceed the kip-days limit but do not develop VSR failures would be unsustainable. If the criterion of kip-days is used as a basis for removing wheels from service to prevent VSR failure, more research is needed to establish a limiting value that accounts for the tradeoff between safety and economics.

3.1.2 Use of WILD Data to Characterize Rapid Rise in Impact Load Before VSR Failure

It is possible that the kip-day criterion is not sufficiently different for VSR failed wheels and wheels that do not develop VSRs. Researchers evaluated an alternate indicator of impending VSR failure that comes from more directly characterizing the rate of impact load increase. Because fatigue crack growth often displays a very non-linear, exponential increase before failure, it is worth considering if it is more effective to select a measured output that better reflects this sudden increase. An example of such an approach will be discussed.

Figure 14 shows impact data for a wheel that failed due to a VSR when the impact load increased suddenly after April 12, 2004 [9]. However, the sustained increase in impact loads over the prior year, from March 12, 2003, to March 12, 2004, would not necessarily be distinguishable from other wheels that have increasing impact loads yet do not fail. The feature that seems to indicate imminent failure is the exponential increase in impact load toward the end of the wheel life. Figure 14 provides an example of a rapid increase to VSR failure when the impact loads prior to the exponential increase are already relatively large [9]. Figure 15 shows an example of a VSR failure where the rate of increase in impact loads prior to failure is much lower [9], but the sudden increase has the same characteristic as in Figure 14. Note that the rates of increase in impact load in Figure 14 and Figure 15 are similar to the characteristic curve for the increasing size of a fatigue crack in a rail before failure shown in Figure 16 [10]. It is expected that crack growth rates in the wheel would display similar trends observed in the rail, with slow initial growth followed by rapid growth to failure.

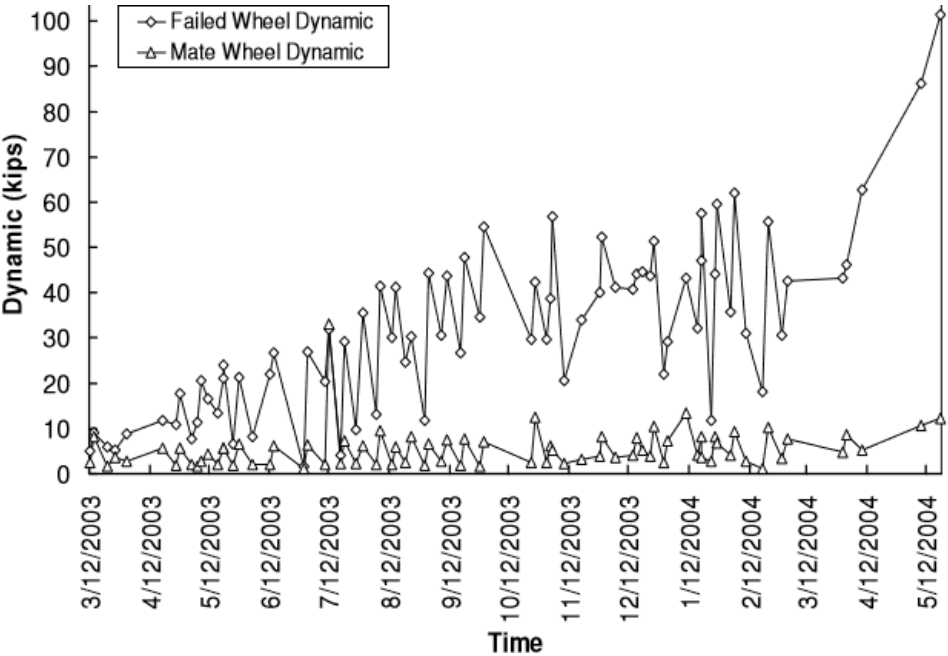


Figure 14. WILD Data for a VSR Wheel with a Large Impact Load Before Failure [9]

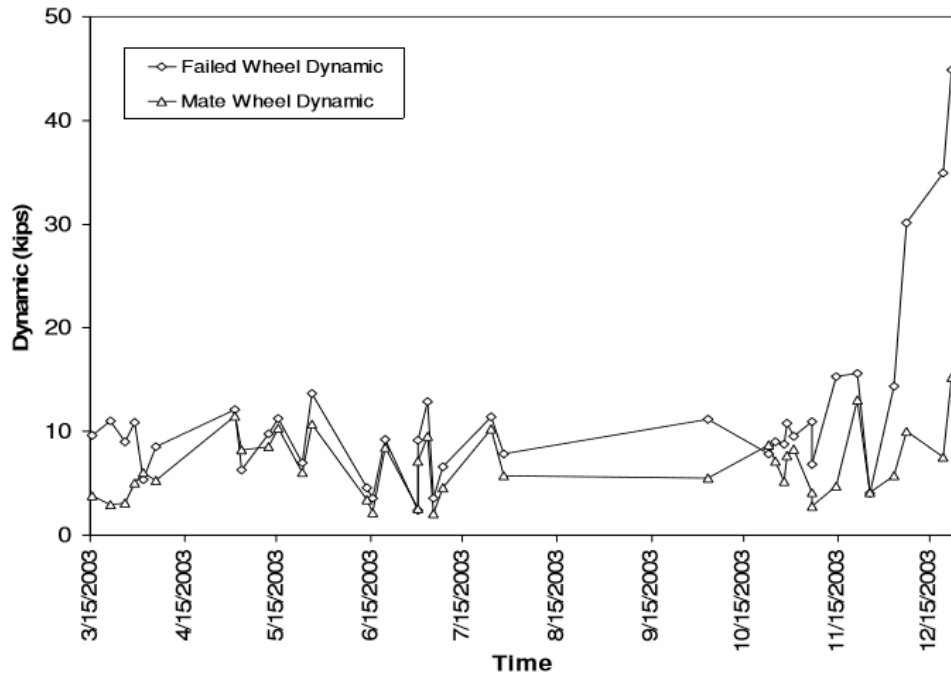


Figure 15. WILD Data for a VSR Wheel with a Small to Moderate Impact Load Before Failure [9]

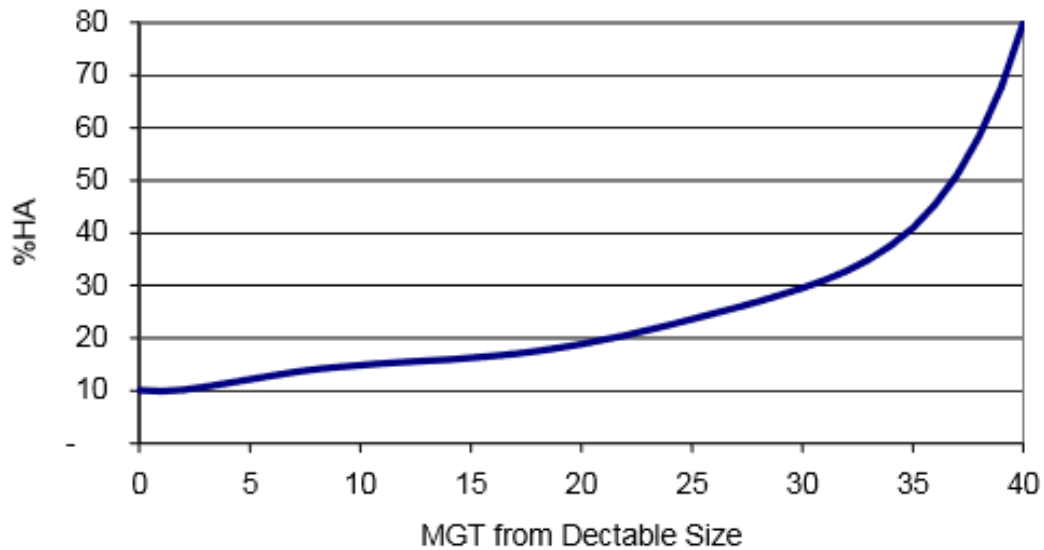


Figure 16. Example of Fatigue Crack Growth Rate in Rail [11]

Figure 17 shows actual measured data of the rate of increase in the size of a rail fatigue crack in terms of percent of the rail Head Area (HA) occupied by the crack preceding failure with an even more rapid rise in defect size than the general characteristic rate in Figure 16 [12]. For a rail or wheel with the rate of crack growth in Figure 17, intervention to avoid a broken wheel or rail will have to occur very quickly following measurement of the last data point on the trend line.

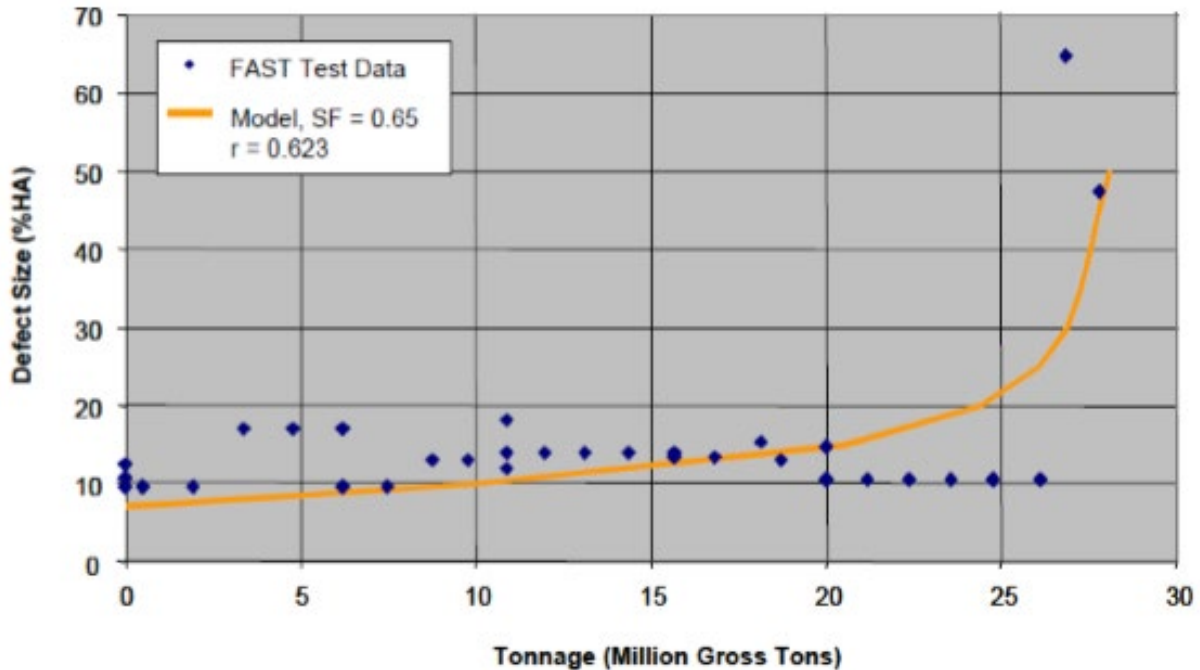


Figure 17. Measured Increase in Rail Fatigue Crack Size with Cumulative Tonnage [12]

To allow for timely intervention, monitoring of WILD data for each wheel must determine if there is a pattern of increasing loads in the most recent values. The rate of increase in impact loads would have to be compared to a to-be-established threshold criterion to determine the level of severity and need for action.

Figure 18 shows a proposed method of calculating the rate of increase in impact loads. The most recent peak load (P_2) is compared with the one before that (P_1) and if $P_2 > P_1$ the amount of increase is calculated as $P_1 * (P_2 - P_1)$. This multiplicative “ $P * \Delta$ ” form of the data is weighted appropriately to produce a higher, more critical value for larger impact loads (P) and for larger increases (Δ) above that impact load. Assuming a threshold $P * \Delta$ value of 1,000 is found to indicate pending failure, the wheel with the $P * \Delta$ of 1,344 in Figure 8 would be pulled from service based on the incremental increase in impact load from 64 kips to 85 kips.

If the value of $P_1 * (P_2 - P_1)$ was less than the assumed threshold value of 1,000, the calculation would continue if the impact load prior to P_1 was less than 64 kips which indicates a trend of increasing impact load over at least three data points. Continuing backward in this fashion allows identification of a rapid increase in the data. Quantifying the rate of increase as described here provides a severity ranking when it is compared to an established threshold. For the case in Figure 18, there is an impact load data point on the upward trend line of less than 64 kips, which would require the calculation to continue. Because the $P * \Delta$ of the first analyzed segment from 64 to 85 kips exceeded 1,000, the limiting criterion is already exceeded and there is no need to go further.

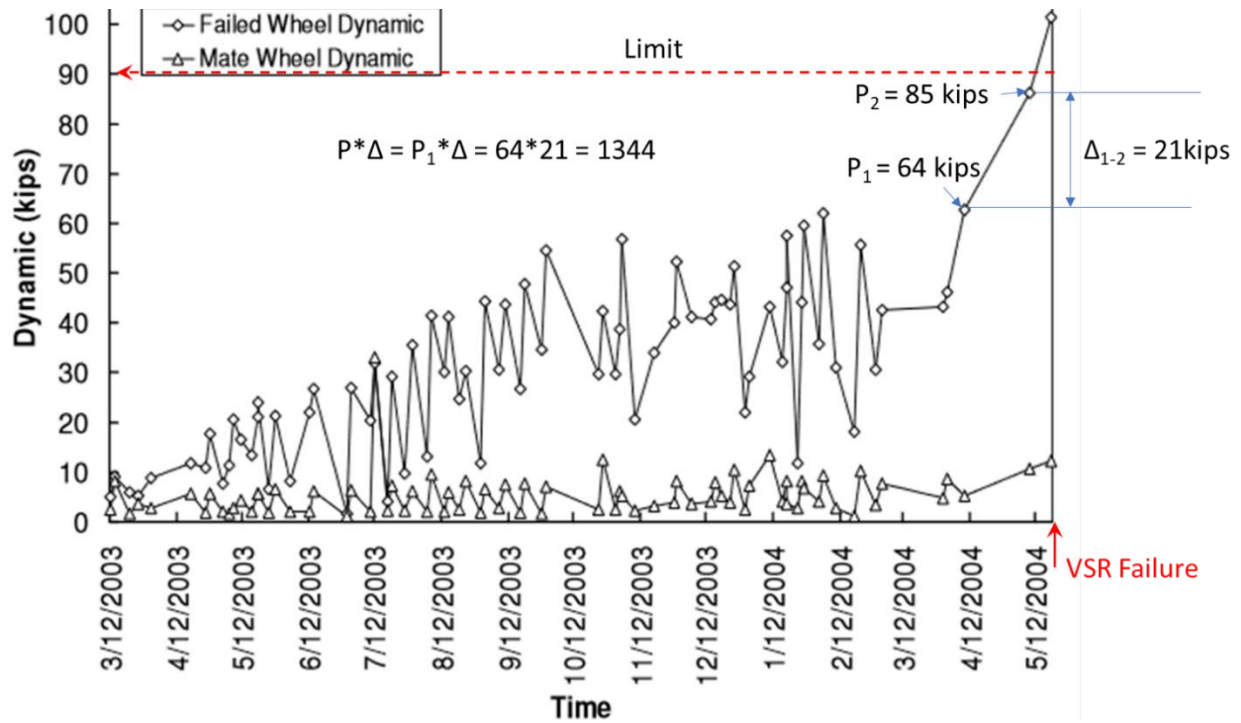


Figure 18. Example Calculation of $P^*\Delta$ for Rapid Increase of Initially Large Impact Load

Figure 19 through Figure 21 show examples where the calculation must proceed to three data points to quantify the upward trend of impact $P^*\Delta$ load to determine if the sudden increase poses a danger [9].

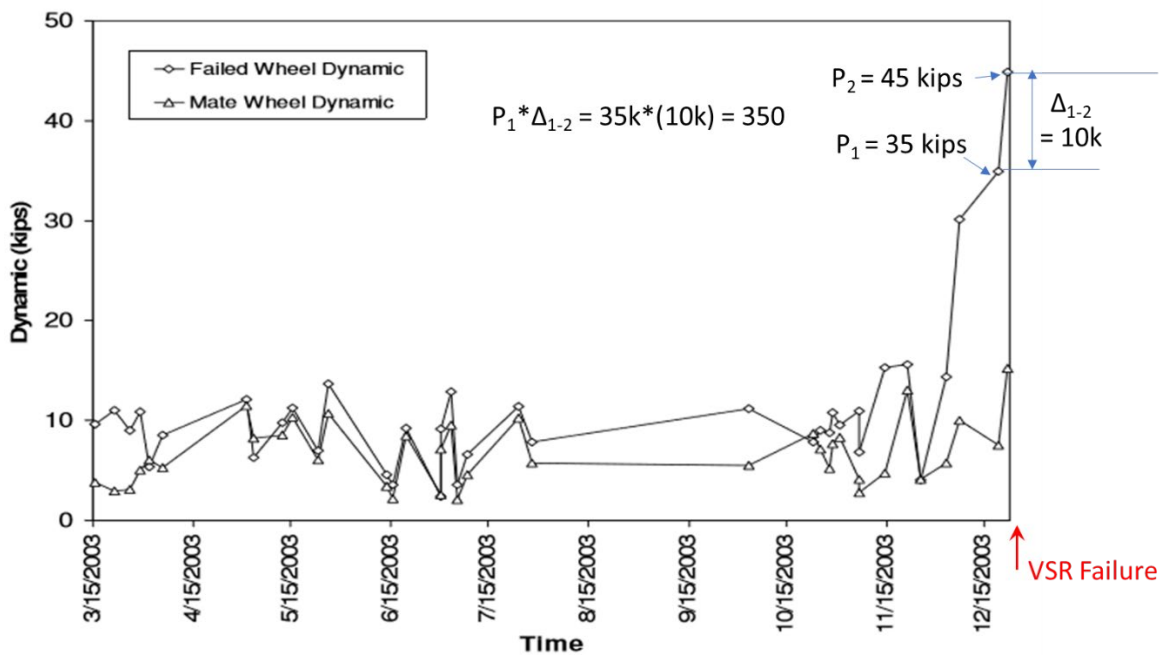


Figure 19. Example Calculation 1 of $P^*\Delta$ for Rapid Increase of Initially Small Impact Load

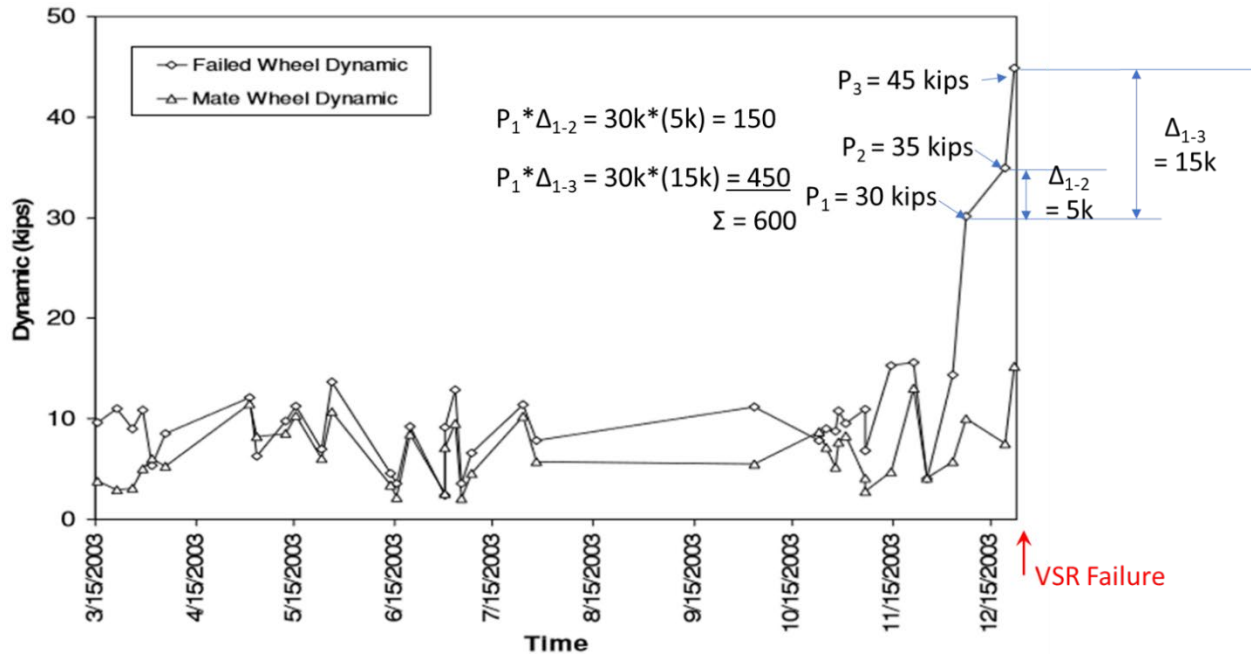


Figure 20. Example Calculation 2 of $P * \Delta$ for Rapid Increase of Initially Small Impact Load

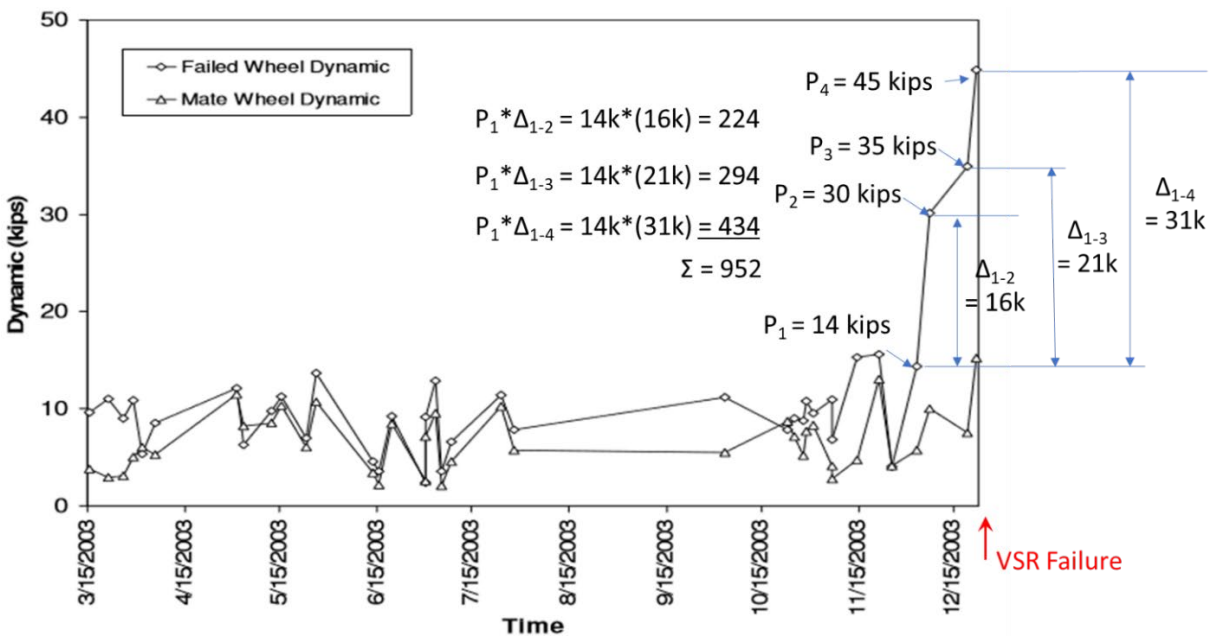


Figure 21. Example Calculation 3 of $P * \Delta$ for Rapid Increase of Initially Small Impact Load

If the $P * \Delta$ value of 952 is rounded to the nearest hundred, this rapid increase of impact load is correctly identified as a wheel that requires removal from service to avoid a VSR failure.

3.1.3 Comparing Kip-Days to $P * \Delta$ Rating of Incipient VSR Failure

The two criteria of kip-days and $P * \Delta$, with their respective proposed limits, are compared to determine their ability to indicate a wheel that develops a VSR. Figure 22 through Figure 24 show three cases where both rating methods correctly predicted wheel failure, and Figure 25

through Figure 27 show three cases where the P*Δ method predicted failure but kip-days did not. Further exploration of the P*Δ method may be warranted.

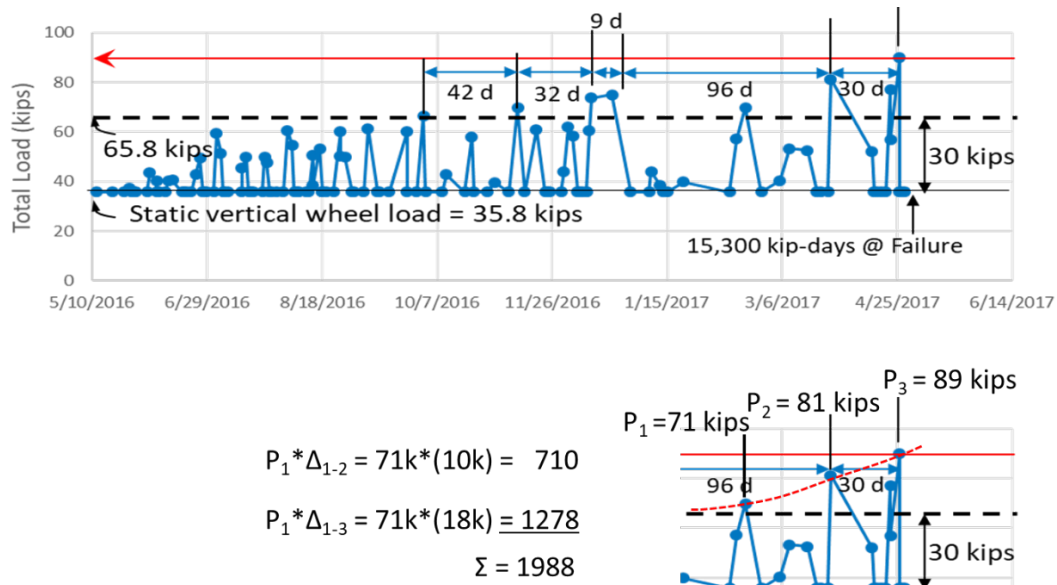


Figure 22. Comparing Kip-Days with P*Δ for a VSR Failed Wheel for Car 1

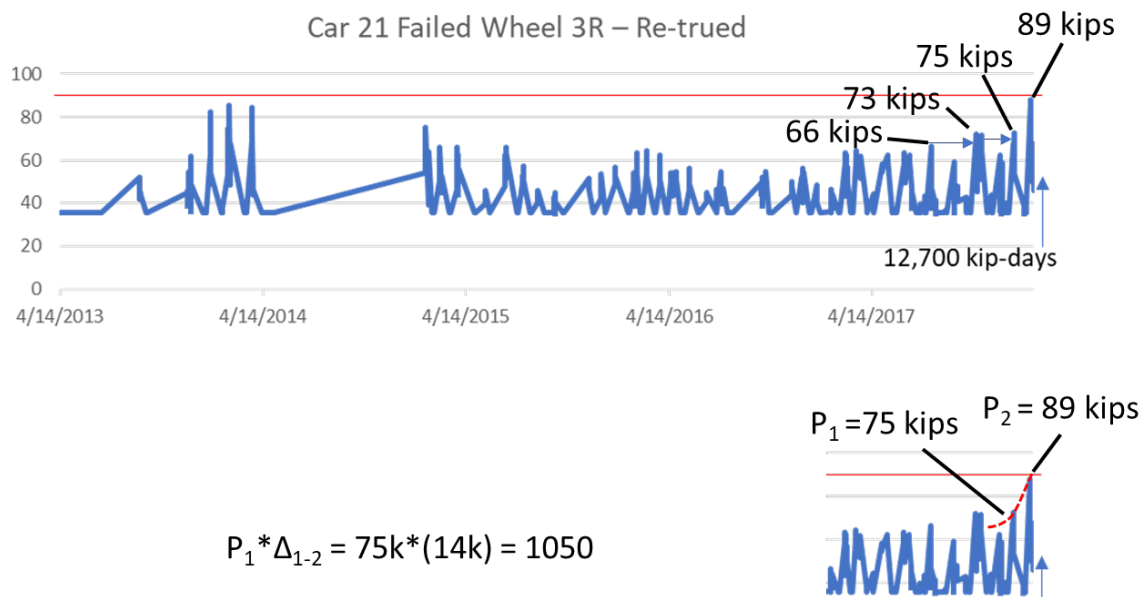


Figure 23. Comparing Kip-Days with P*Δ for a VSR Failed Wheel for Car 21

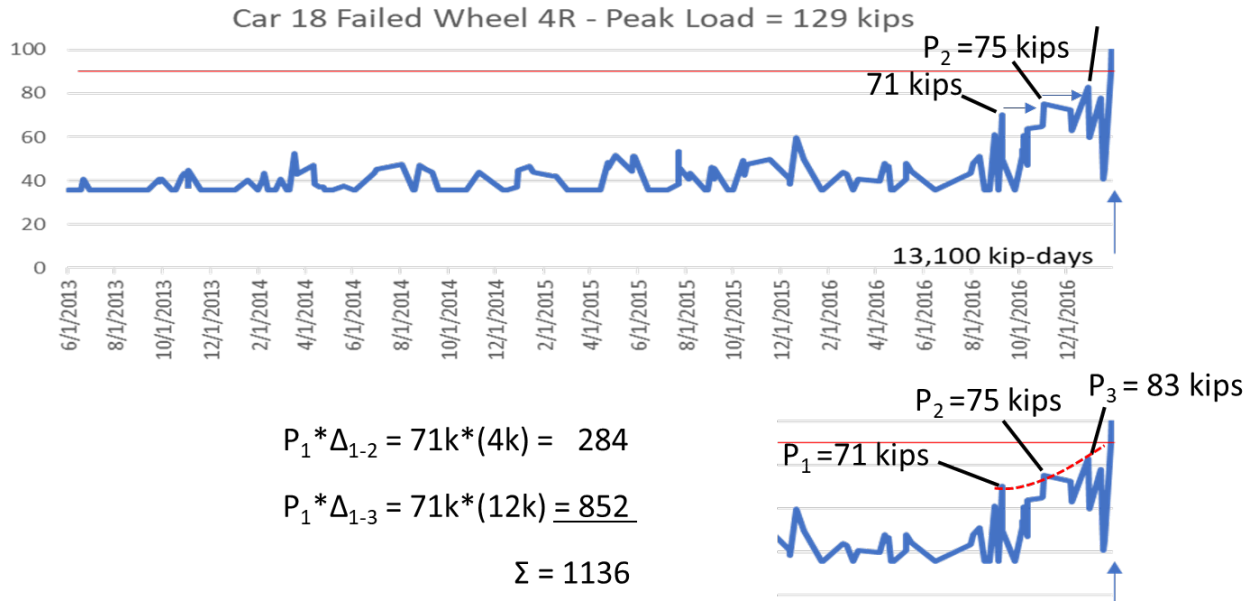


Figure 24. Comparing Kip-Days with $P * \Delta$ for a VSR Failed Wheel for Car 18

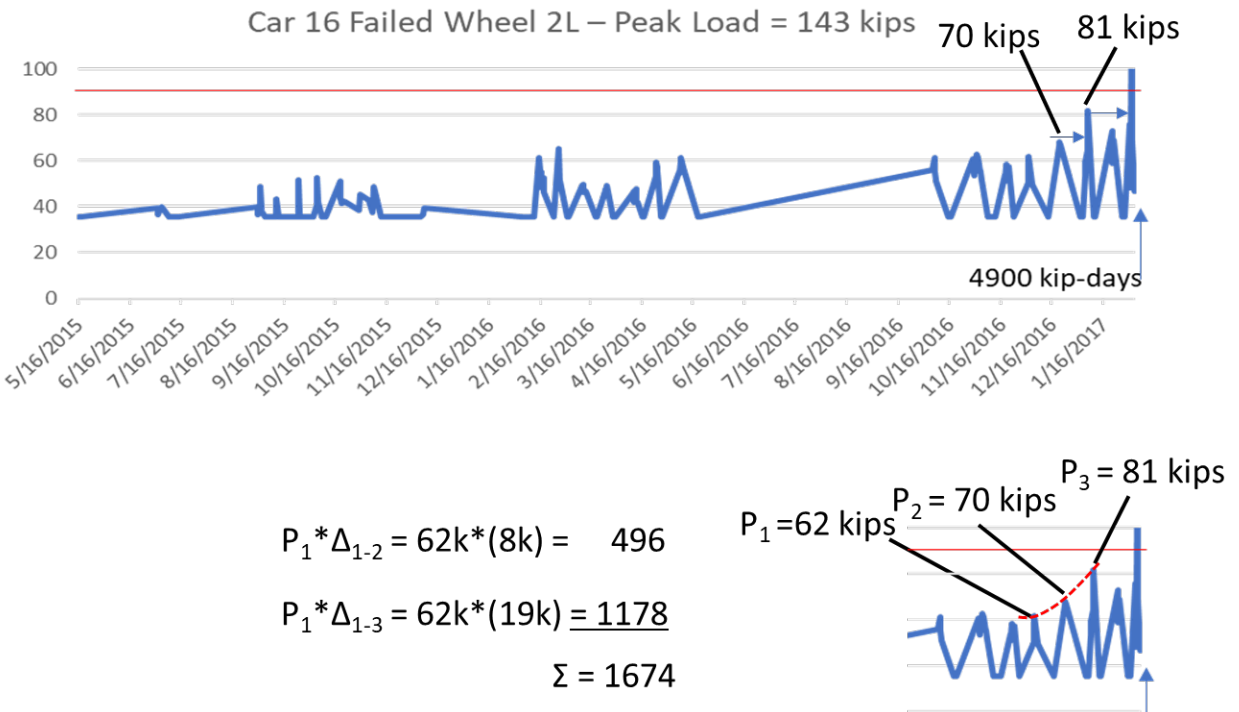


Figure 25. Comparing Kip-Days with $P * \Delta$ for a VSR Failed Wheel for Car 16

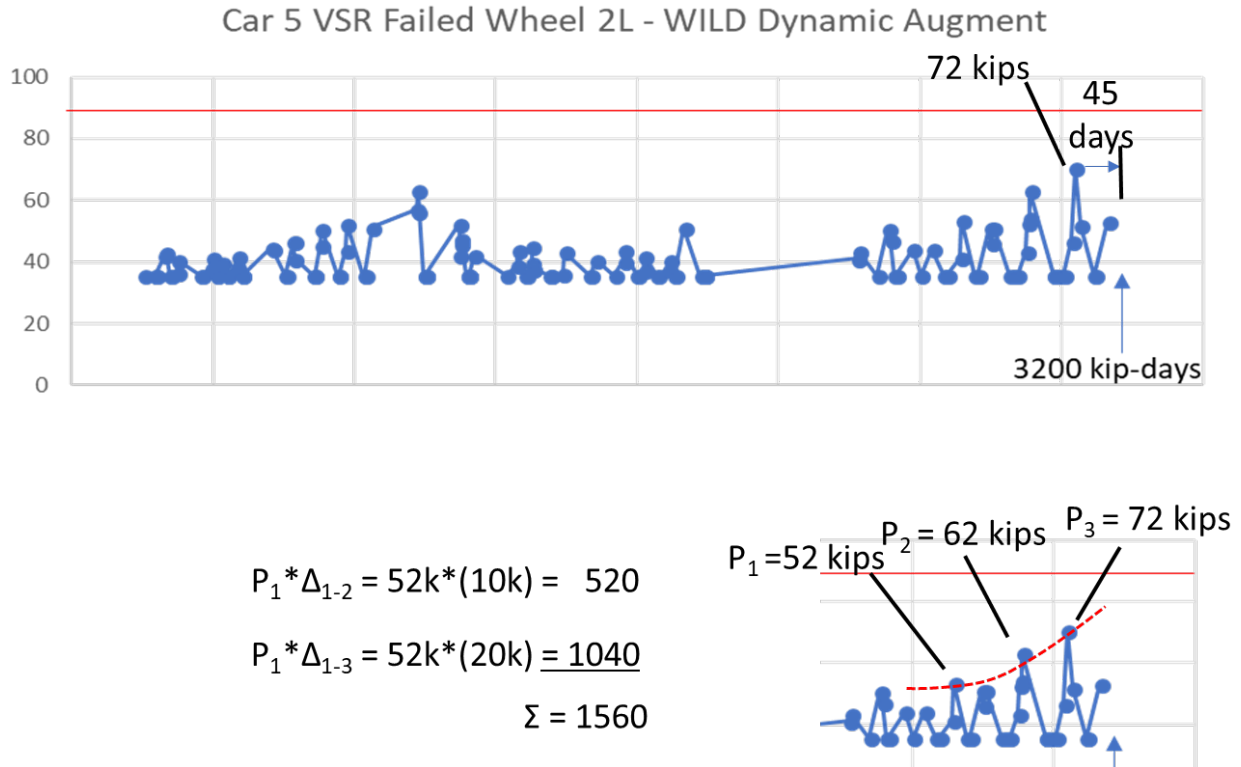


Figure 26. Comparing Kip-Days with P*Δ for a VSR Failed Wheel for Car 5

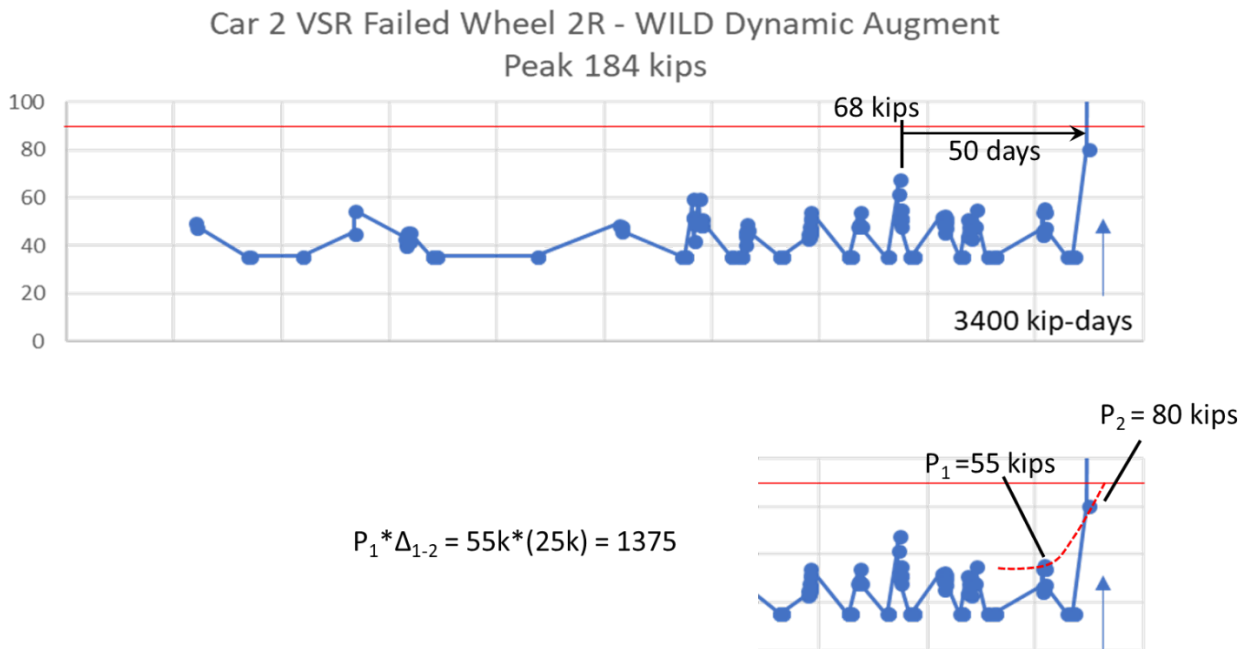


Figure 27. Comparing Kip-Days with P*Δ for a VSR Failed Wheel for Car 2

3.2 Wheel Temperature Data and VSR Failures

A feature routinely reported with VSR failures is evidence of excessive heating from on-tread braking. Dedmon et al. (2016) 14 notes that “Oxidation associated with brake heating of VSR cracked wheels appears much greater than has been reported from hot wheel detectors.” Dedmon found visual evidence of oxidation and discolored fracture surfaces on 32 of the 35 VSR failed wheels in the study [13].

The maximum temperature that a wheel has been exposed can indicate the severity of damage. Moderately elevated tread temperatures due to brake heating may provide some benefits. For example, an increased tread hardness can result when rolling contact is combined with braking that produces tread temperatures of approximately 450 °F [14] These beneficial effects could be offset by increases in subsurface residual stresses, which can promote subsurface crack initiations. However, tread temperatures well above this level and approaching 1,000 °F are more commonly associated with excessive heat that produces reduced resistance to fatigue, degradation of steel properties, and a reduction in beneficial compressive hoop stresses. Further, Lonsdale et al. (2011) four found that high tread temperatures can generate large residual axial tensile stress in the wheel. Lonsdale also found that brake heating may influence residual stress by moving the axial tensile stress zone closer to the tread surface which could promote crack growth.

Due to the potential importance of heat damage in contributing to VSR failures, Hot Wheel Detector (HWD) data was reviewed for a sample of wheels with VSR failures to determine if high temperature damage had a role in the failure and if HWD data could be used as an indicator for wheels that are at risk for VSR. HWD data is comprised of measured wheel tread temperatures. HWD does not generally contain any information regarding heat damage to wheels.

A review of a small sample of HWD data provided for preliminary analysis by Railinc found that some VSR failed wheels had histories of maximum tread temperatures in the moderate range of 500 to 600 °F (above-ambient) while others had maximum measured temperatures less than 100 °F.⁷ The maximum measured wheel temperatures from various HWD sites for the 11 VSR failures and 8 broken flange failures provided by Railinc for this study are shown in [Table 2](#). [Figure 28](#) shows the wheel temperature history for the VSR wheel with the highest measured wheel temperature above ambient. No trend is apparent in either dataset.

⁷ Stewart, M. F., Flynn, E., Marquis, B., & Sharma, 2019, “[An Implementation Guide for Wayside Detector Systems](#).” Report No. DTFR53-12-D-0004, Washington, DC: U.S. Department of Transportation, Federal Railroad Administration. This study presents levels for HWD readings: X<500 °F for level 1, X<650 °F for level 2, X>650 °F for level 3. Remedial action depends on specific railroad rules.

Table 2. Maximum Measured Wheel Temperature and Wheel Failure Mode for Sample Failed Wheel Dataset

Max Wheel Temp Above Ambient (°F)	Failure Mode	Max Wheel Temp Above Ambient (°F)	Failure Mode
900	Broken Flange	430	Broken Flange
882	Broken Flange	404	VSR
868	Broken Flange	300	VSR
635	Broken Flange	270	Broken Flange
582	Broken Flange	97	VSR
568	VSR	90	VSR
554	VSR	70	VSR
480	VSR	38	VSR
448	VSR	30	VSR
434	Broken Flange		

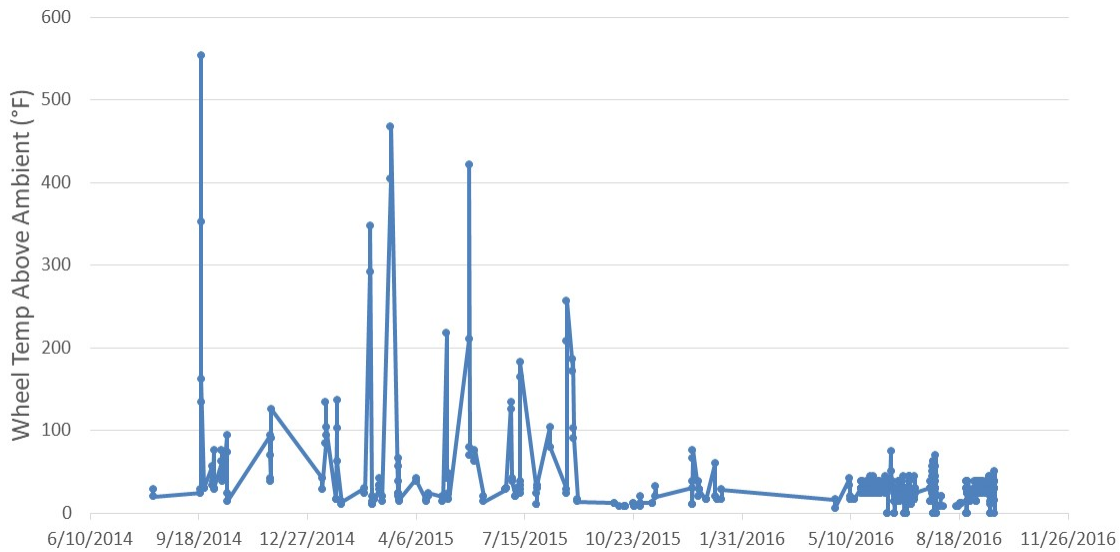


Figure 28. Wheel Temperature Above Ambient History for Sample VSR Failed Wheel

Despite the expected strong correlation between elevated wheel temperatures and VSR formation, the data observed did not support such a conclusion. Dedmon’s observation that heat damage on VSR wheels is much more common than indicated by HWDs may support the contention that HWDs are under-reporting high temperature events [15]. This under-reporting may be due, in part, to the fact that railroad employ different practices in placing HWD throughout their systems.

The probability of measuring wheels with elevated temperatures increases with the placement of detectors at strategic locations such as near the end of a downgrade where brakes would tend to be applied. Since railroads follow different practices for HWD placement, agreement between railroads may be lacking over which wheels “run hot” and the maximum temperature to which a wheel has been exposed. Added to this difficulty in wheel temperature measurement is the transient nature of heating as opposed to impact loading which is more sustained. For these reasons, the available temperature data for VSR wheels appears to be unreliable as a predictor of failure or of the amount of heat damage a wheel has experienced. Temperature remains an important consideration in preventing VSRs and means to reduce this damage will provide benefits. However, the HWD data reviewed in this study does not lend itself to being used alone to serve as a predictor of VSR failures.

4. Laboratory Testing

This section describes procedures and results from laboratory testing of failed wheels conducted during Phase 2 activities. ESI staff conducted detailed metallurgical analysis of eight wheels that failed due to VSR and the mating wheels donated by three railroads and one car owner.

Experimental residual stress analysis was conducted on two of the wheels with VSRs and their mates. The eight failed wheels were designated as UP1, PR2, BNSF3, BNSF4, BNSF6, BNSF7, CSX8, and UP9. Details of the consideration of the failed wheels and their mates are provided in [Appendix A](#).

4.1 Test Wheels

BNSF6 and its mate were two-wear, 36-inch diameter wheels. The other seven failed wheels and their mates were one-wear, 36-inch diameter wheels. [Table 3](#) shows the rim thickness, flange thickness, flange heights and amount of tread hollowing measured using a LazerView® system for each failed wheel. Six of the wheels had flange heights exceeding the FRA maximum; these values are indicated with red, underlined values.

Table 3. Tread Geometry for Phase 2 Failed Wheels Using LazerView® Measurements

Wear Measurements	FRA/AAR Required (1/16ths)	UP1	PR2	BNSF3	BNSF4	BNSF6	BNSF7	CSX8	UP9
Flange Height, 1/16-in.	24.0 Max	20.25	<u>30.87</u>	<u>28.57</u>	<u>31.44</u>	<u>28.24</u>	<u>29.20</u>	<u>32.17</u>	18.52
Flange Thickness, 1/16-in.	14.0 Min	23.66	35.43	32.08	34.79	33.04	33.01	36.61	22.66
Rim Thickness, 1/16-in.	12.0 Min	25.60	41.41	30.41	46.58	33.31	28.24	28.79	17.97
Tread Hollow*, 1/16-in.	2.67 Max ⁸	1.07	1.09	0.19	0.19	1.19	0.54	0.64	0.62

*AAR Requirement

The degree of out-of-roundness was measured on failed wheels for which sufficient material was available. In addition, the most recent wheel impact loads on the failed wheels recorded by WILDs were obtained. These results are shown in [Table 4](#). Three wheels showed various degrees of out-of-roundness but only one of these exceeded AAR limits for interchange service. Three of the five wheels for which impact loads were available had produced loads that were in excess of the levels for condemning per AAR Interchange Rule 41.1.r.

⁸ AAR requirement is established as 4.0 mm = 5/32-in. = 2.667/16-in. For consistency of the table, the requirement is expressed in 1/16ths of an inch.

Table 4. Available Impact and Out-of-Round Measurements for Failed Wheels Considered in Phase 2

	AAR Requirement	UP1	PR2	BNSF3	BNSF4	BNSF6	BNSF7	CSX8	UP9
Impact Load (Kips)	90	N/A	N/A	64	97	120	97	N/A	N/A
Out-of-Round (Inches)	0.070	0.040	N/A	N/A	0.068	N/A	N/A	N/A	0.080

4.2 Metallurgical Analysis

The chemical composition of each of the wheels was determined and compared to the requirements of AAR Specification M-107/M-208, as shown in Table 5. Values in excess of applicable requirements are indicated with red, underlined values.

Table 5. Chemical Composition Determined by Check Analysis for Wheels Tested in Phase 2

Element	AAR Specification M-107/M-208	Wheel								Avg.
		UP1	PR2	BNSF3	BNSF4	BNSF6	BNSF7	CSX8	UP9	
Carbon	0.67-0.77	0.74	0.72	0.74	0.77	0.73	0.73	0.77	<u>0.79</u>	0.75
Manganese	0.60-0.90	0.83	0.76	0.74	0.69	0.77	0.75	0.75	0.81	0.76
Phosphorus	0.030 Max.	0.022	0.025	0.022	0.014	0.025	0.016	0.015	<u>0.034</u>	0.022
Sulfur	0.005-0.040	0.027	0.036	0.029	0.009	0.022	0.025	0.020	0.021	0.023
Silicon	0.15-1.00	0.44	0.24	0.35	0.50	0.46	0.45	0.27	0.49	0.40
Residual Elements										
Nickel	0.25 Max.	0.07	0.09	0.07	0.06	0.06	0.07	0.05	0.11	0.07
Chromium	0.25 Max.	0.10	0.13	0.12	0.12	0.12	0.09	0.07	0.01	0.10
Molybdenum	0.10 Max.	0.02	0.02	0.02	0.04	0.01	0.02	0.01	0.05	0.02
Vanadium	0.040 Max.	0.009	0.009	0.008	0.000	0.002	0.002	0.001	0.004	0.004
Copper	0.35 Max.	0.20	0.23	0.17	0.20	0.08	0.15	0.09	0.11	0.14
Aluminum	0.060 Max.	0.007	0.006	0.006	0.007	0.008	0.007	0.005	0.008	0.006
Titanium	0.03 Max.	0.00	0.02	0.01	0.00	0.00	0.00	0.00	0.00	0.00
Columbium/ Niobium	0.05 Max.	0.00	0.00	0.00	0.00	0.00	0.00	0.00	0.00	0.00

The microcleanliness was determined in accordance with the American Society for Testing and Materials (ASTM) Standard Practice E1245 using six specimens prepared in accordance with Section 9.2 of AAR M107/M208. As a result of tread wear, the specimen location was below that specified in the standard. The microcleanliness results are shown in Table 6. The results show that the average areas of voids plus oxides and the area of the worst sulfide field are within the specified requirements, while the void plus oxide worst field area is above the required level in three of the wheels. These values are indicated with red, underlined values.

Scanning electron microscope images of wheels UP1 (Appendix A, Figure A-8) and UP9 (Appendix A, Figure A-59) show the presence of axial cracks on the shelled surfaces. These cracks are likely nucleation sites for VSRs that did not progress to fracture.

Table 6. Microcleanliness Ratings of Failed Wheels Considered in Phase 2

	Required	UP1	PR2	BNSF3	BNSF4	BNSF6	BNSF7	CSX8	UP9
Voids + Oxides									
% Area, Average	<0.100	0.075	0.025	0.069	0.040	0.051	0.029	0.039	0.058
% Area Worst Field	<0.750	<u>1.051</u>	0.229	0.335	0.299	0.597	<u>0.941</u>	0.351	<u>1.063</u>
Sulfides									
% Area Worst Field	<0.750	0.473	0.479	0.424	0.184	0.438	0.324	0.411	0.325

Based on results contained in [Appendix A](#), all the shelling cracks and VSR crack surfaces were coated with a layer of iron oxide. Based on previous research [15], this is typical of the presence of a temperature in excess of 750 °F. Additionally, wheels UP1 ([Appendix A](#), Section A.1) and BNSF7 ([Appendix A](#), Section A.6) had a surface layer of martensite, indicating exposure to a temperature in excess of 1,350 °F.

4.3 Residual Stress

All the VSRs considered in this phase of the study initiated from a delamination that typically formed 1/8 to 3/16 of an inch (3 to 5 mm) below the surface. Previous work has shown the development of tensile residual stress in the plane of VSR crack growth [4] [5] [6]. The residual stress state was determined on radial sections of Wheels BNSF7, UP9 and their mates at a depth of a quarter of an inch (6.4 mm) below the tread surface and 1 inch (25.4 mm) from the front rim face by x-ray diffraction according to ASTM Standard E915.

The results are shown in [Table 7](#). The stress component of primary interest is the axial stress, which is perpendicular to the crack plane propagated by unstable crack growth. In general, the stress component in the plane perpendicular to the crack has the greatest effect on the crack with the exception being when the wheel has a stress gradient field. The axial residual stresses at the location considered have either lowered to near-zero ksi or developed a low level of tension. These axial residual stresses are relatively low, therefore, having a small effect on any axial tensile stress that would result from service loading. The results indicate that there was relatively little tensile residual stress in the axial direction that could be considered a driving factor in VSR. Maximum, minimum, and angle are calculated using Mohr's circle.

Table 7. Residual Stress States in Failed Wheels BNSF7 and UP9 and Their Mates

	Axial Stress (ksi)	Radial Stress (ksi)	Maximum Stress (ksi)	Minimum Stress (ksi)	Maximum Stress Variation from Radial
BNSF7 (Failed)	-1.2	-41.9	-0.1	-43.1	80.1°
BNSF7 Mate	1.2	-30.5	2.4	-31.7	79.2°
UP9 (Failed)	-7.4	-38.0	-7.4	-38.0	79.2°
UP9 Mate	-2.7	-10.7	7.5	-20.9	53.2°

4.4 Observations and Conclusions from Laboratory Testing

The following observations and conclusions are based on information summarized in this section and detailed in [Appendix A](#) as well as prior education, training, testing, engineering analysis, and experience:

- Six of the eight wheels tested exhibited flange heights in excess of the FRA maximum, while all wheels had acceptable flange and rim thickness. All the wheels showed minor levels of tread hollowing but were well below the 4-mm AAR permitted hollowing.
- The wheel impact loads of three of the four wheels where data were available exceeded the 90-kip impact levels that are cause for removal. These data agree with those reported in a previous study [9]. However, it is uncertain whether the high impact loads are the result of the presence of the VSR or are the driving force of the VSR occurrence.
- All the wheels tested met the chemical composition requirements for AAR Grade C steel.
- The results of the microcleanliness evaluations show that the average areas of voids-plus-oxides and the area of the worst-sulfide-field are within the specified requirements, while the void-plus-oxide-worst-field-area is above the required level in three of the wheels. However, because of tread wear, the specimen location was below that specified in the testing standard. This out-of-specification results is not considered to be a contributor to the failure mode.
- The measured fracture toughness for the analyzed wheels (see [Appendix A](#), Section A.6, and Section A.8) values do not appear to affect ultimate wheel fracture.
- Once formed, VSRs appear to grow by either quasi-cleavage or rapid fatigue crack growth. The mode of crack growth may be irrelevant as previous research has shown that the stress intensity associated with a VSR crack is sufficient to cause a fatigue crack to grow to a full VSR in less than 100 miles [19] [20].
- All the shelling cracks and VSR crack surfaces were coated with a layer of iron oxide, typical of the presence of a temperature in excess of 750 °F [15]. Additionally, wheels UP1 and BNSF7 had a surface layer of martensite, indicating exposure to a temperature in excess of 1,350 °F.
- All the VSRs considered in this phase of the study started from delamination that typically formed 1/8 to 3/16 of an inch (3 to 5 mm) below the surface. Previous work showed the development of tensile residual stress in the plane of VSR crack growth [4], [5], [6]. Residual stress measurements of wheels BNSF7 and UP9 show that the axial residual stresses a quarter of an inch (6.4 mm) below the tread surface have either lowered to near-zero ksi or developed a low level of tension.
- Scanning electron microscope images of wheels UP1 ([Appendix A](#), Figure A-8) and UP9 ([Appendix A](#), Figure A-59) show the presence of axial cracks on the shelled surfaces. These cracks are likely nucleation sites for VSRs that did not progress to fracture.

In conclusion, the initiation of VSR failures appears to be the result of a combination of factors. These factors are likely RCF, moderate-to-high heat inputs from on-tread braking, and, possibly, impact loads that altered the beneficial residual stress state that was imparted during heat-treatment.

5. Conclusion

A summary of conclusions based on activities conducted during Phase 2 of the wheel failure study is provided in this section. This also presents recommendations for investigations in a subsequent phase of the study.

The following are conclusions drawn from the efforts conducted under Phase 2 and prior research activities:

1. Investigations using WILD data collected prior to a VSR failure have not revealed a unique, definitive trend that can be reliably used to identify wheels that will experience a VSR. Impact load trends for VSR wheels can be indistinguishable from impact load data for the general population of wheels that do not develop VSRs. There are several reasons for the difficulty in finding an identifiable trend:
 - The interval between WILD detections may not be frequent enough to be able to identify, isolate and remove a potential VSR from service.
 - Impact loads provide an indirect and approximate measure of the severity of wheel tread surface damage
 - VSRs caused by cracks propagating below the tread surface might not produce the wheel surface damage needed for detection by impact load
 - The damaged location that produces a VSR may be to the field side of tread which is only in rail contact in curves and not in tangents where WILDs are typically located.
 - Investigation of the practicality of WILDs in curves may be warranted. WILDs deployed in curved track may help identify wheels at risk for potential VSR failures of wheels with tread surface damage well to the field side amongst other potential benefits.
2. WILD data collected on wheels prior to VSR failure may contain information that could provide an early indication of a wheel that is at risk for failure. One method that shows promise, based on a very small sampling of VSR wheels, identifies and quantifies a sudden upward trend in impact load before failure and is recommended for further investigation. The method(s) considered must be able to identify known VSR wheels with very few false positives when applied to a wider population of wheels.
3. Based on a limited sampling of VSR wheels, the reliability of wheel temperature data from existing wayside measurement systems as an indicator of damage and VSR failure is questionable. This is due to large differences in maximum recorded temperatures between wheels. The large variability is due to temperature measurements being very sensitive to the location of HWD within the network and varying practices regarding placement of HWD.
4. A new approach to analysis of industry-provided data needs to be formulated to identify contributing factors to VSR failures. WILD and HWD data on their own did not exhibit the expected trends.
5. Regarding the eight wheels with VSR failures subjected to laboratory testing and previous history analysis during this phase of the study:

- The wheel impact loads of three of the four wheels where data were available exceeded the 90-kip impact level that is cause for removal. However, it is uncertain whether the high impact loads are the result of the presence of the VSR or are the driving force of the VSR occurrence.
 - All the wheels tested met the chemical composition requirements for AAR Grade C steel. The results of the microcleanliness evaluations show that the average areas of voids-plus- oxides and the area of the worst-sulfide-field are within the specified requirements, while the void-plus-oxide-worst-field-area is above the required level in three of the wheels. However, because of tread wear, the specimen location was below that specified in the testing standard. This out-of-specification result is not considered to be a contributor to the failure mode.
 - All the shelling cracks and VSR crack surfaces were coated with a layer of iron oxide, typical of the presence of a temperature in excess of 750 °F. Two of the wheels studied exhibited evidence of exposure to a temperature in excess of 1,350 °F.
 - All the VSRs considered in this phase of the study initiated from a delamination that typically formed 1/8 to 3/16 of an inch (3 to 5 mm) below the surface. Residual stress measurements made on two of the failed wheels show that the axial residual stresses a quarter of an inch (6.4 mm) below the tread surface have either lowered to near-zero ksi or developed a low level of tension. In a defect-free wheel, this zone has typically high compressive hoop and axial stresses
6. Initiation of VSR failures appears to be the result of a combination of factors. These factors are likely RCF, moderate-to-high heat inputs from on-tread braking, and, possibly, impact loads that altered the beneficial residual stress state that was imparted during heat-treatment.

This research group recommends that a parametric study using finite element analysis (FEA) be conducted to identify the relative contributions of factors that can directly contribute to VSR failures. The FEA should answer the following questions:

- What are the major factors that cause the subsurface crack to turn towards the surface of the rim?
- What is the relative role of contact mechanics and operating conditions including the development of thermal stresses in the wheel that will lead to the development of VSR?
- Given what is learned from this FEA and historical research, what information collected by industry, either presently or in the future, can identify conditions that could be indicators of at-risk wheels?

The FEA-based approach should consider the following in a manner that allows for the assessment of the result of each factor as well as the combined effect of the factors:

- Mechanical loading resulting from revenue service operations
- Routine and excessive braking
- Wheel wear

6. References

- [1] Dick, M., Sundaram, N., and Sherrock, E., "[Wheel Failure Investigation Program: Phase 1](#)," U.S. Department of Transportation, Federal Railroad Administration, Technical Report No. DOT/FRA/ORD-21/04, Washington, DC, 2021.
- [2] Berge, S., "Spall/Shell Basics," BNSF Wheel Defect Meeting, May 2001.
- [3] Kristan, J., Stone, D., and Elkins, J., "[Effect of Wheel Loading on the Occurrence of Vertical Split Rim Wheel Failures](#)," in *Proceedings of the 2004 ASME International Mechanical Engineering Congress and Exposition*, Report No. IMECE2004-59049, Anaheim, California, November 13–20, 2004.
- [4] Lonsdale, C., and Oliver, J., "Wheel Rim Axial Residual Stress and a Proposed Mechanism for Vertical Split Rim Formation," in *Proceedings of the ASME 2011 Rail Transportation Division Fall Technical Conference*, 2011.
- [5] Lonsdale, C., and Oliver, J., "Further Research into Wheel Rim Axial Residual Stresses and Vertical Split Rim Wheel Failures," in *Proceedings of the 2012 Joint Rail Conference*, Report No. JRC2012-74010, Philadelphia, PA, April 17–19, 2012.
- [6] Lonsdale, C., Oliver, J., Bitner, A., and Guzel, H., "Vertical Split Rim Wheel Failures and the Role of Axial Residual Stress," in *Proceedings of the 17th International Wheelset Congress*, Kiev, Ukraine, 2013.
- [7] Stone, D. H., and Meddah, A., "A Neural Network Analysis of the Causes of Vertical Split Rim Wheel Failure," in *Proceedings of the 17th International Wheelset Congress*, Kiev, Ukraine, 2013.
- [8] Cummings, S., "[Broken Rims in Railroad Wheels](#)," U.S. Department of Transportation, Federal Railroad Administration, Technical Report No. DOT/FRA/ORD-14/41, Washington, DC, 2014.
- [9] Stratman, B., Liu, Y., and Mahadevan, S., "Structural Health Monitoring of Railroad Wheels Using Wheel Impact Load Detectors," *Journal of Failure Analytics and Prevention*, vol. 7, no. 3, p. 218–225, 2007.
- [10] Dick, M., Iwand, H., McConnell, D., Magner, J., and Snyder, T., "Characterization of Vertical Split Rim Failures," BNSF Wheel Defect Meeting, May 2008.
- [11] Palese, J., and Wright T. W., "Risk-Based Ultrasonic Rail Test Scheduling on Burlington Northern Santa Fe," in *American Railway Engineering Maintenance Association Annual Technical Conference*, Dallas, TX, 2000.
- [12] Eadie, D., "[Rail integrity: what really matters, and what can be done about it?](#)" in *Heavy Haul Seminar, Wheel-Rail Interaction Conference*, 2016.

- [13] Dedmon, S., Pilch, J., Hiramatsu, S., Yamamoto, Y., and Kato, T., "Finite Element Analyses of Vertical Split Rim Cracks and Prediction of Failure Mode(s)," in *World Congress on Railway Research*, Milan, Italy, 2016.
- [14] Dedmon, S., Kato, T., and Pilch, J., "Effect of Temperature on Hardening and Residual Stress Development During Wheel/Rail Rolling Contact," in *Proceedings of the 2016 Joint Rail Conference*, Report No. JRC2016-5815, Columbia, SC, April 12–15, 2016.
- [15] Dedmon, S. L., "The Role of Oxidation in Railroad Wheels," in *Proceedings of the ASME/ASCE/IEEE 2012 Joint Rail Conference*, Paper No. JRC2012-74124, Philadelphia, PA, April 17–19, 2012.
- [16] Stone, D. H., Marich, S., and Rimnac, C. M., "Deformation Behavior of Rail Steels," *Transportation Research Record*, no. 744, p. 16–21, 1980.
- [17] Stone, D. H., and Park, Y. J., "Cyclic Plasticity of Class A and B Heat-Treated Wheel Steels," in *Winter Annual Meeting of the American Society of Mechanical Engineer*, Chicago, IL, November 16–21, 1980.
- [18] Kato, T., Yamamoto, Y., Kato, H., Dedmon, S., and Pilch, J., "Effect of fracture toughness on vertical split rim failure in railway wheels," *Engineering Fracture Mechanics*, vol. 186, p. 255–267, 2017.

Appendix A.

Results of Laboratory Testing of Individual Failed Wheels

A.1 Wheel UP1

The wheel was removed due to a VSR which originated from shelling on the tread surface of the wheel. A secondary shattered rim fracture was also present. Figure A-1 shows the wheel set in the as-received condition. Figure A-2 shows that the fracture is approximately 8 inches long. An area of shelling on the tread surface was approximately 2 1/2 inches in diameter.

Additionally, a separate shattered rim developed from the VSR, 1 1/4 inches directly below the shelled area, Figure A-3.



Figure A-1. Overall View of Wheelset, as Received



Figure A-2. Overall View of Fractured Portion

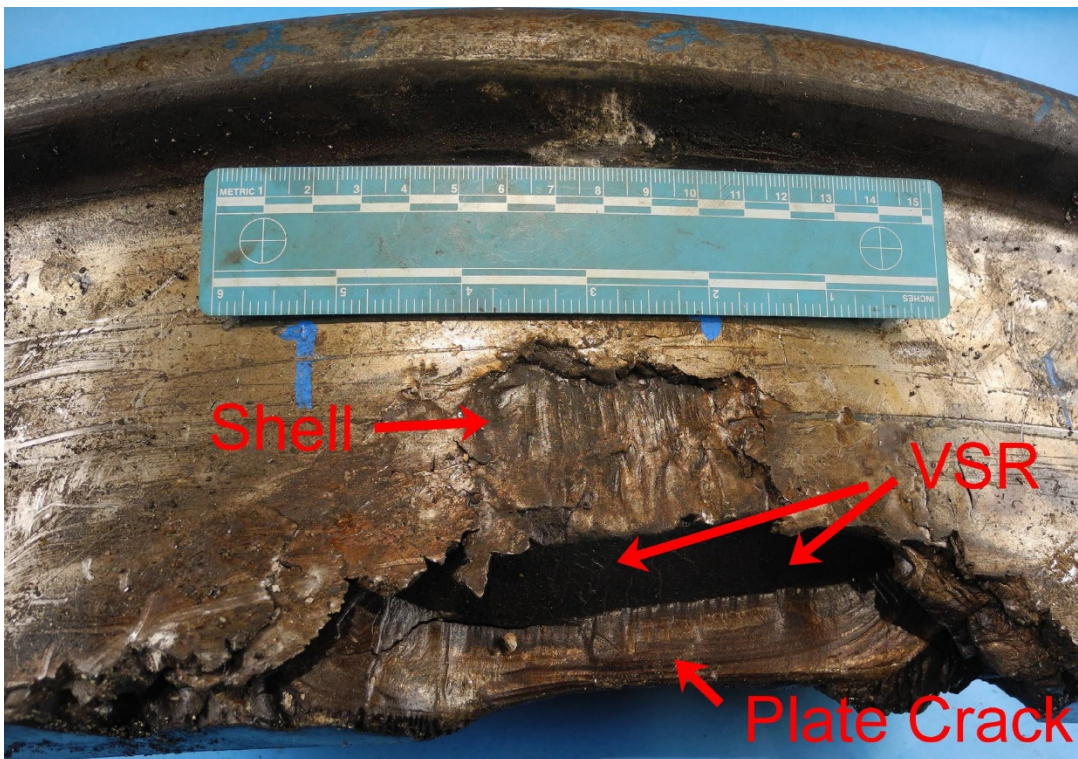


Figure A-3. Detailed View of Fractured Areas with Tread Shelling at the Origin of the Rim

The vertical split rim initiated under the tread shell and grew by low cycle fatigue through the thickness of the rim, as seen in Figure A-3. At some point the VSR initiated a plate formed a plate crack, also seen in Figure A-3.

Microhardness measurements were made on a specimen cut adjacent to the fractured area in the radial direction from the surface to a depth of 1/2 an inch. The results of the hardness measurements versus depth shown in Figure A-4 suggest the possible presence of an area of work softening.

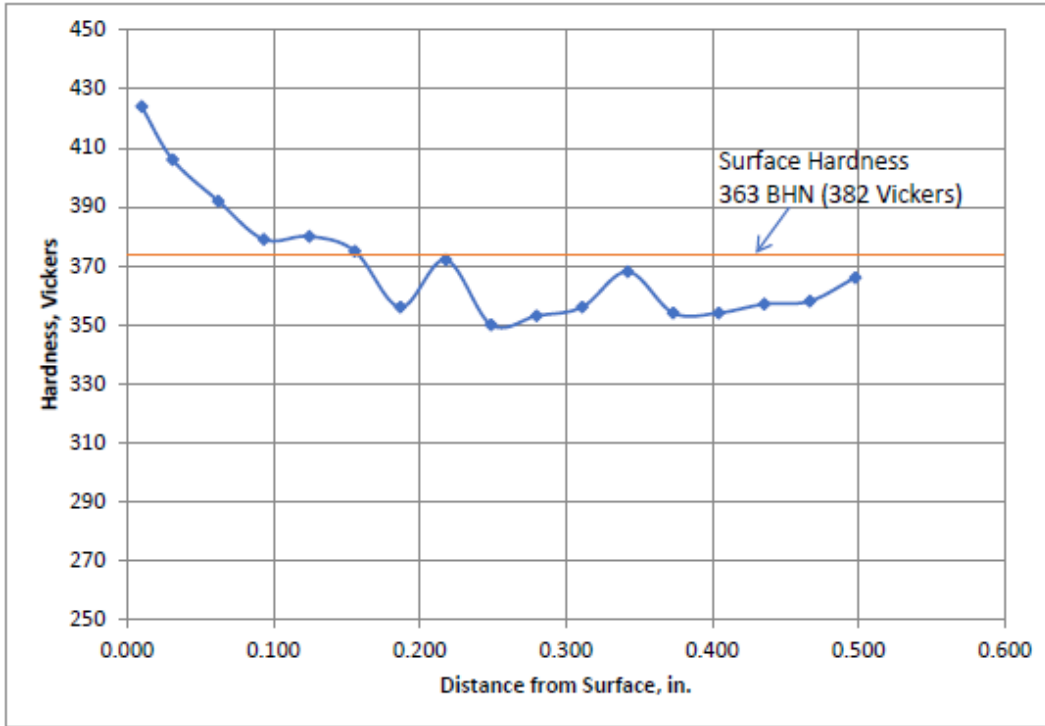


Figure A-4. Microhardness Traverse of Wheel UP1

Previous work on rail steel has shown a zone of work softening that develops at the boundary between the line affected by plastic flow and unaffected base material, as shown in Figure A-5 [16]. If VSR wheel defects are analogous to detail fractures in rail, then this effect is of interest, because the softened area is the location of detail fracture initiation in rails. Figure A-6 shows this effect clearly during reversed cyclic loading of wheel steel specimens [17].

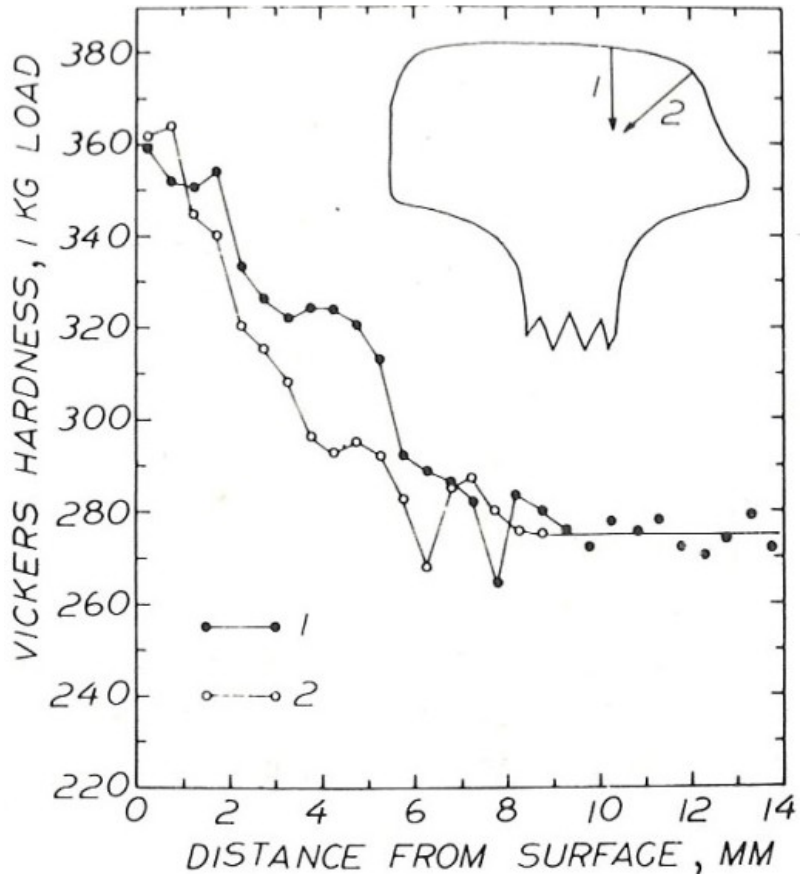


Figure A-5. Microhardness Traverses of Used Rail

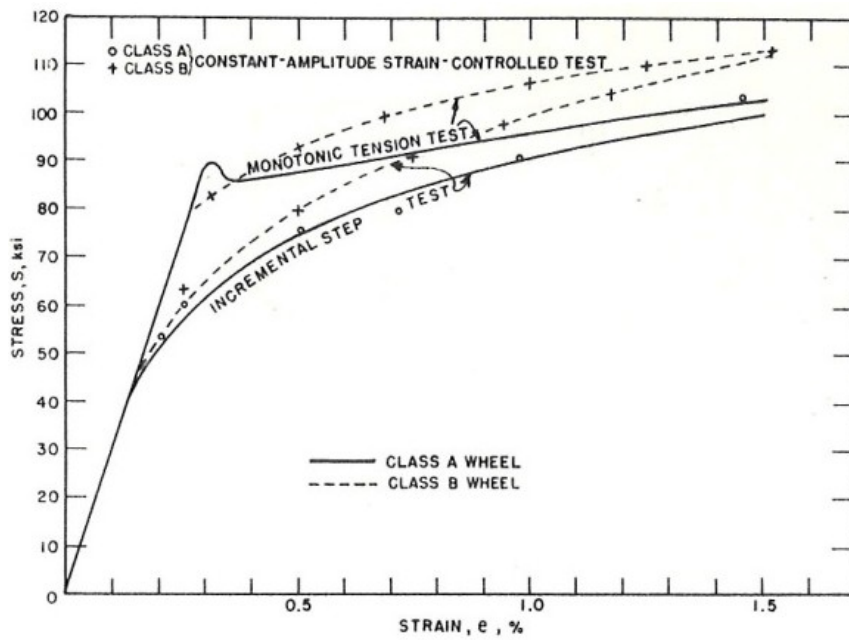


Figure A-6. Work Softening of Wheel Steel During Strain-Based Fatigue Loading

Metallographic analysis of the shell surface, Figure A-7, shows a layer of white etching material on the shell surface. The nature of white etching zones is not well understood. Some researchers suggest that they are the result of dissolved carbides, while others suggest that they are the result of martensite formation. However, both mechanisms involve heating. Additionally, several short axial cracks have developed from the surface.

The fracture surfaces of the shell area and the VSR surface were examined by scanning electron microscopy. In Figure A-8, the shelled surface has the appearance of repeated shear with a vertical crack that has formed within one of the shear bands that could be the nucleation point of a VSR. The VSR surface shown in Figure A-9 has quasi-cleavage facets that are typical of brittle fracture.

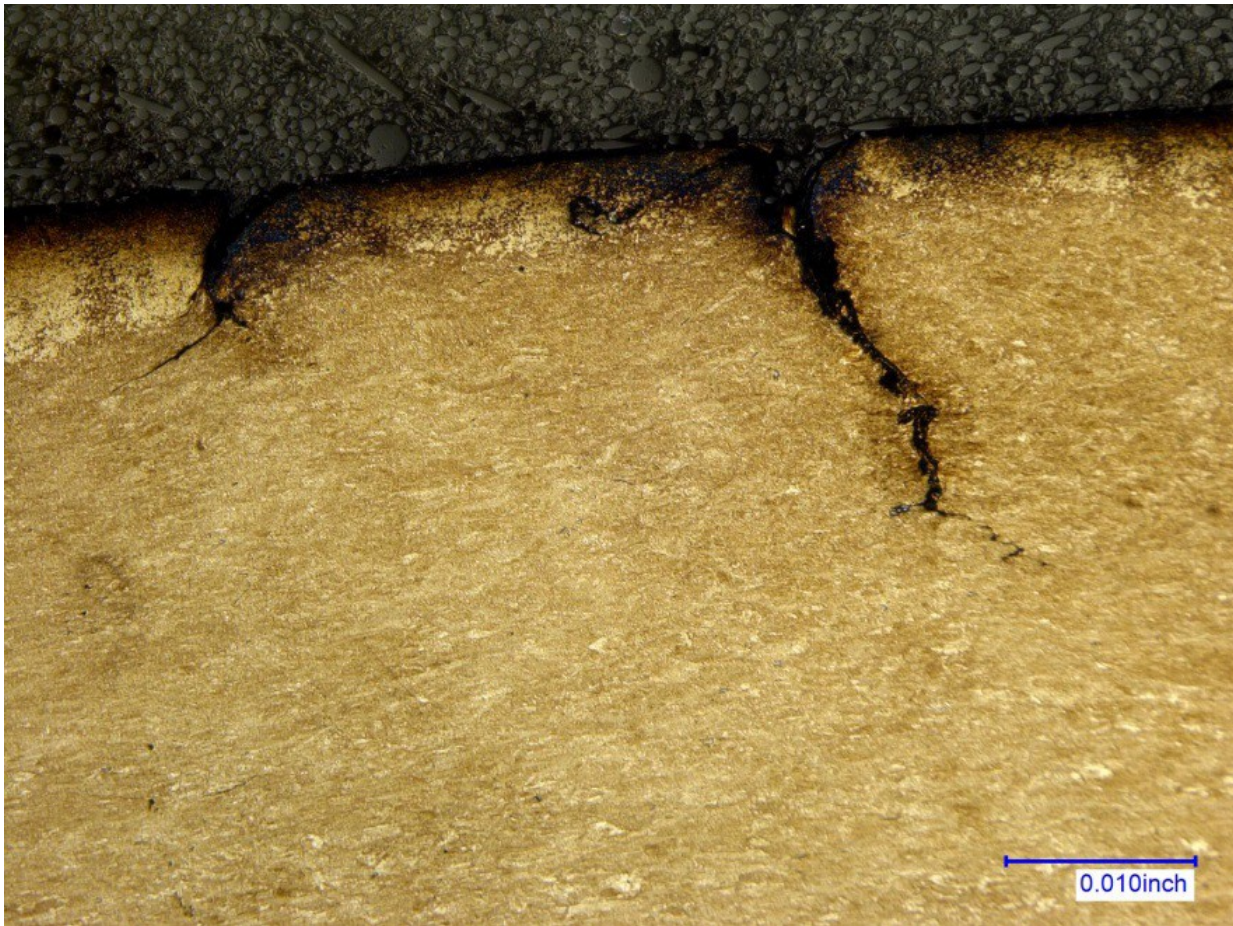


Figure A-7. UP1 Microstructure at Shell Surface, Original Magnification x200, Nital Etch

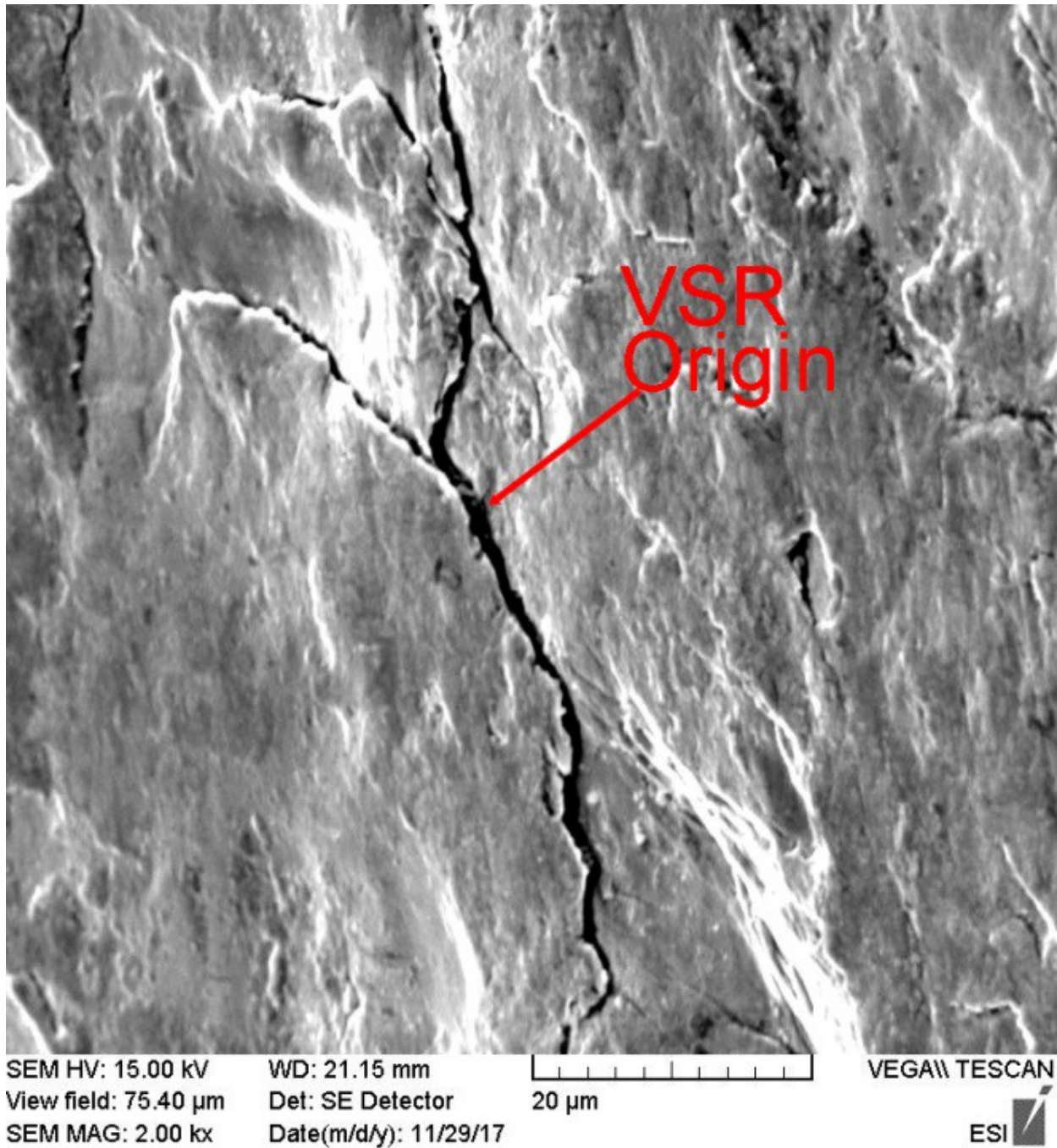
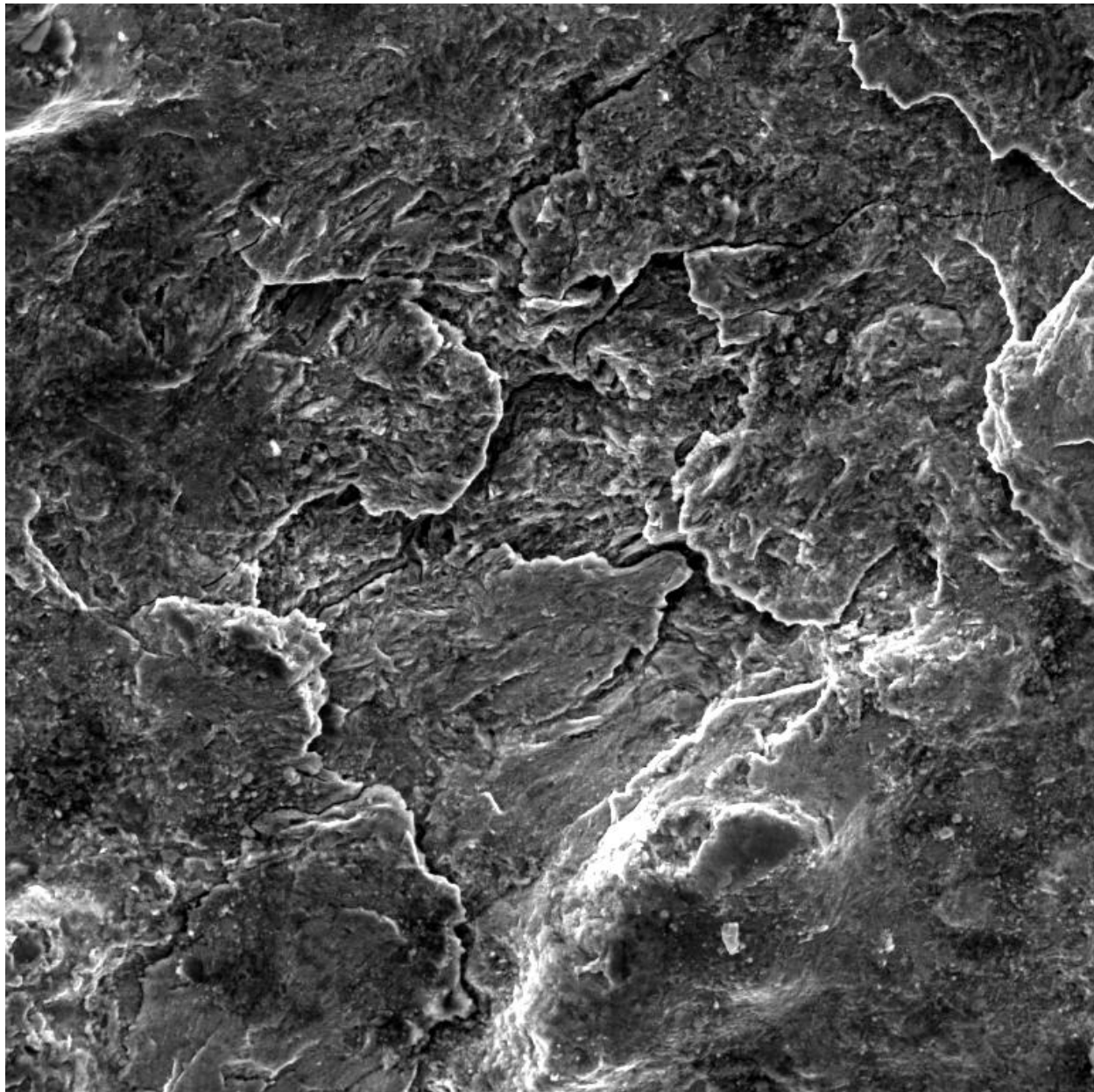


Figure A-8. Scanning Electron Microscope Image of UP1 Shell Fracture Surface, Original Magnification x2,000



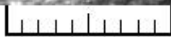

SEM HV: 15.00 kV WD: 19.22 mm  VEGA\\ TESCAN
View field: 150.8 μm Det: SE Detector 20 μm
SEM MAG: 1.00 kx Date(m/d/y): 11/29/17 ESI 

Figure A-9. Scanning Electron Microscope Image of UP1 VSR Fracture Surface, Original Magnification x1,000

A.2 Wheel PR2

The wheel contained a VSR that had not separated, as shown in Figure A-10 and Figure A-11. The failure occurred in two steps. First, a large shell defect grew approximately 3/16 of an inch below the tread surface and formed an initial VSR that grew from the tread shell, as shown in Figure A-12. The fatigue crack then initiated the remainder of the VSR by a quasi-cleavage rupture, Figure A-13.



Figure A-10. Cracking on Tread of Wheel PR2



Figure A-11. Termination of VSR at Rim-Plate Fillet

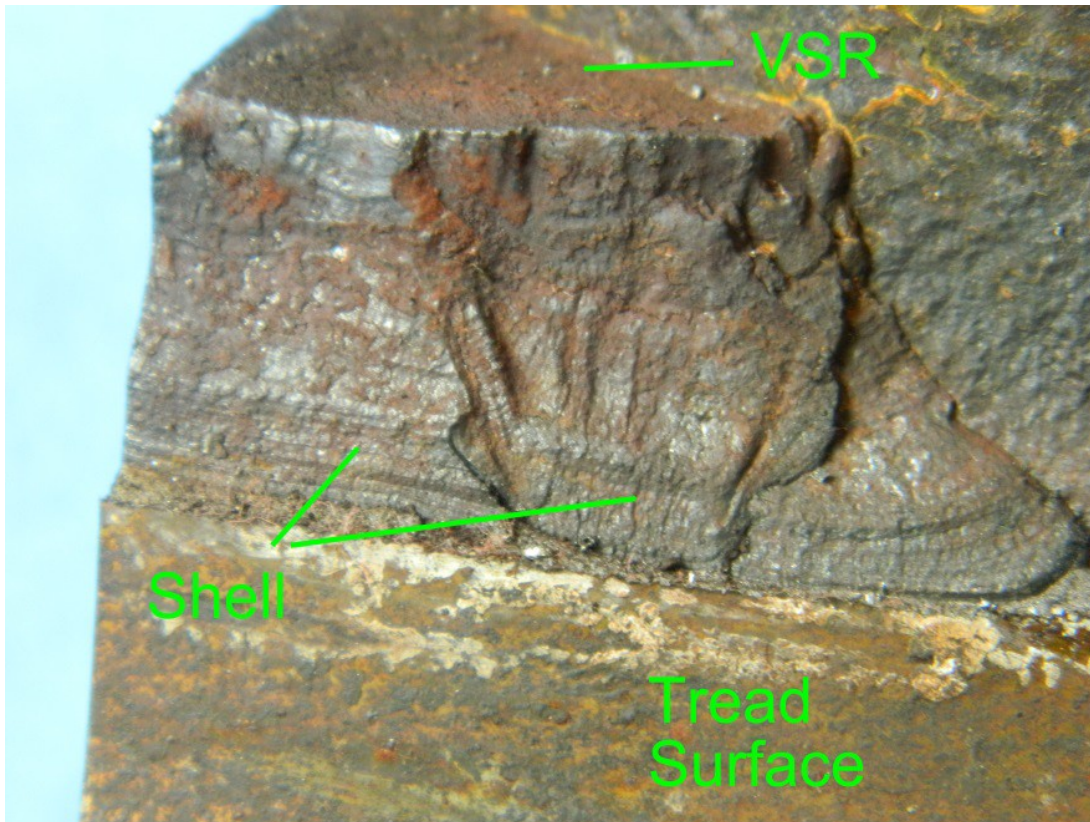


Figure A-12. Initial Fracture Location on Wheel PR2



Figure A-13. Transition of Shell to VSR on Wheel PR2

Microhardness measurements were made on a specimen cut adjacent to the fractured area in the radial direction from the surface to a depth of 1/2 inch. The results of the measurements versus depth of hardening suggest the possible presence of an area of work softening, shown in Figure A-14.

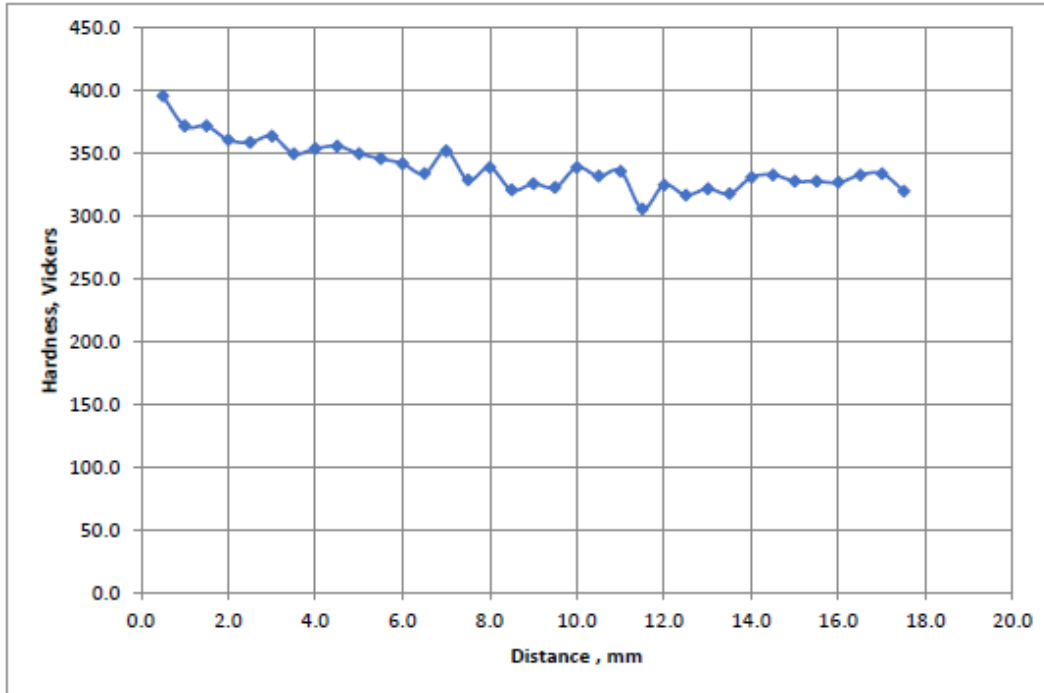


Figure A-14. Microhardness from Wheel PR2 Tread Surface in Axial Direction

Metallographic analysis of the areas above the shell crack shows flowed and deformed grains, while the area below the crack appears unaffected, shown in Figure A-15. However, this wheel did not show any evidence of martensite or oxide on the crack surfaces, that would have been the result of brake heating, as was the case with all the other wheels.



Figure A-15. Microstructure Above and Below PR2 Shell Crack, Original Magnification x1,000, Nital Etch

A.3 Wheel BNSF3

The majority of VSRs fracture along the front rim face (field side) of the wheel, while a smaller number of VSR fractures break away the back rim face (gauge side) of the wheel. Wheel BNSF3 is unusual in that VSRs were identified on the back rim face and the front rim face. Figure A-16 shows the front face VSR, and Figure A-17 shows the back rim face VSR. The relative locations of the two VSRs are seen in Figure A-18. Sectioning of the rim between the two VSRs demonstrated that the two failures were not continuous or connected.



Figure A-16. VSR on Front Face of Wheel BNSF3



Figure A-17. VSR on Flange Side of Wheel BNSF3



Figure A-18. Location of VSRs on Front and Rear Wheel BNSF3

The back rim face fracture surface was coated with a layer of rust, while the front rim face fracture was not, indicating that the back rim face VSR occurred at some time before the VSR on the front face. The microstructures of the surface shelled area and VSR initiation surface were evaluated and are shown in Figure A-19 and Figure A-20. Figure A-19 shows that a surface layer of martensite had developed, indicating application of an unusually high brake shoe force or wheel slide. Figure A-20 shows that the subsurface cracks are coated with a high temperature oxide that is typical of most of the other VSR and shell cracks that have been observed. However, an approximately 0.003-mm diameter, non-metallic inclusion is present at the shell-VSR transition. Analysis of the inclusion indicated that it was iron oxide (i.e., rust).

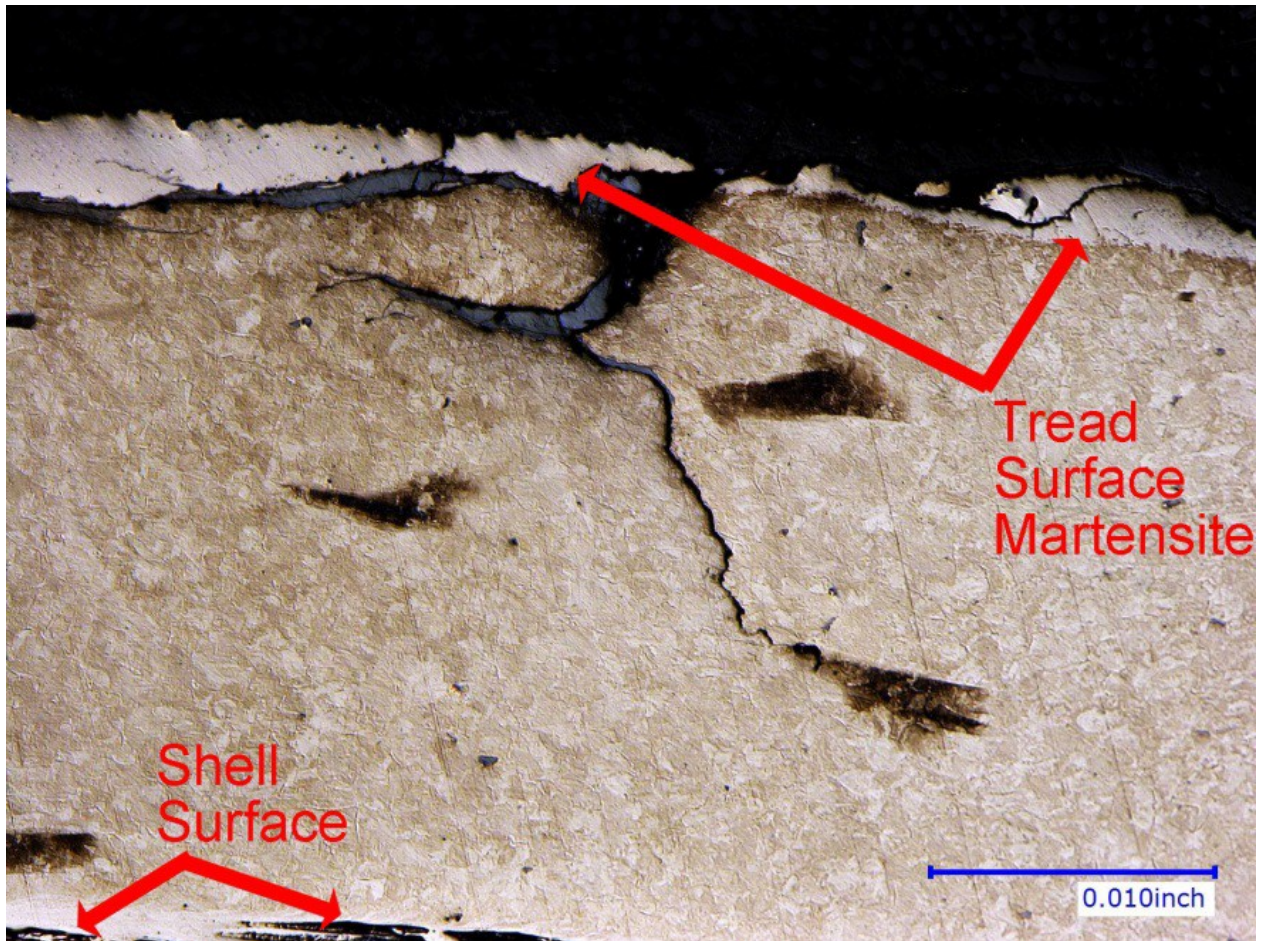


Figure A-19. BNSF3 Microstructure at Surface of Back Face VSR, Original Magnification x200, Nital Etch

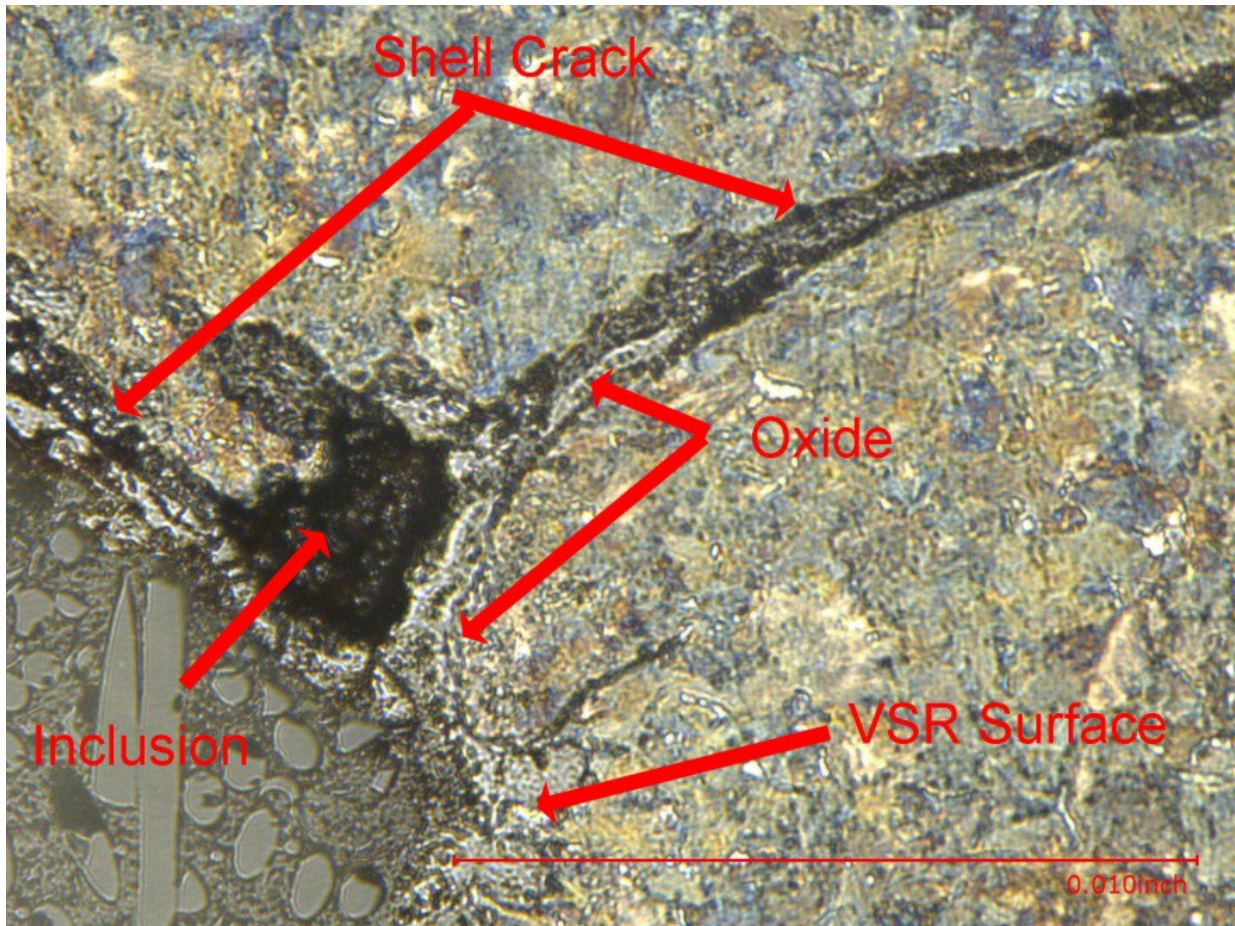


Figure A-20. BNSF3 Microstructure at Shell-VSR Boundary, Original Magnification x700, Nital Etch

Microhardness measurements were performed on a specimen cut adjacent to the fractured area, in the radial direction from the surface to a depth of half an inch. The results of the measurements of hardness versus depth suggest in Figure A-21 the possible presence of an area of work softening.

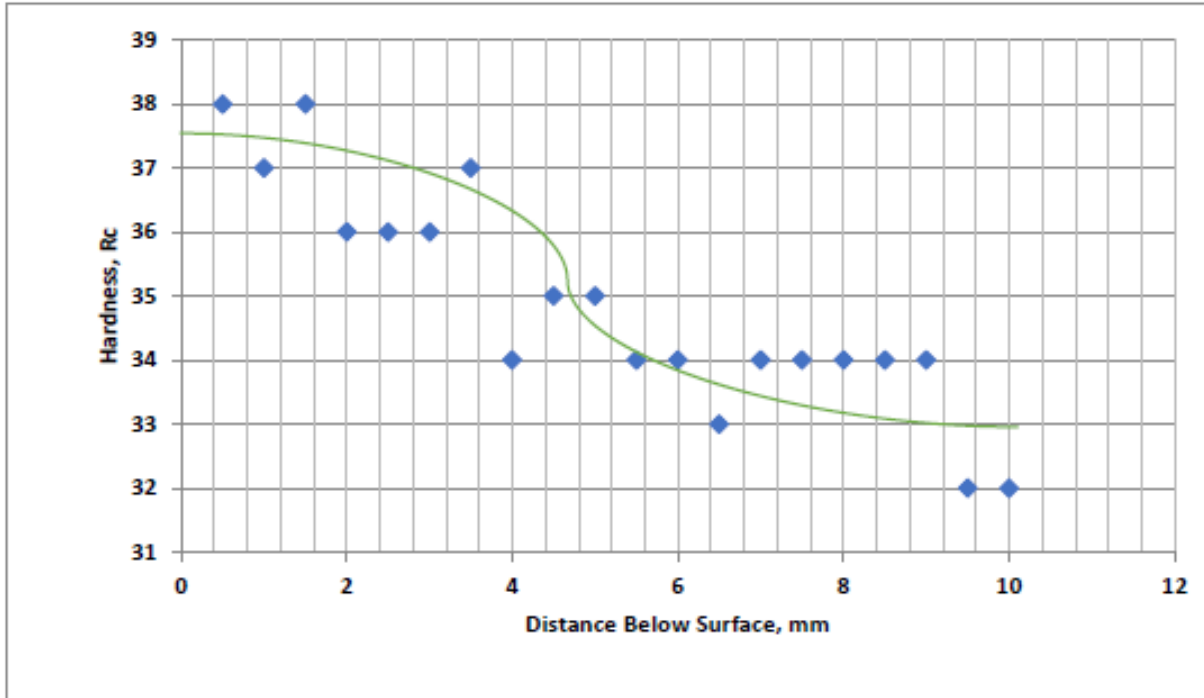


Figure A-21. BNSF3 Microhardness Variation from Surface, Shell Crack Depth is Between 3.5 and 4 mm

A.4 Wheel BNSF4

The wheel contained a VSR that had not separated, as shown in Figure A-22 and Figure A-23. The failure occurred in two steps. First, a large shell or delamination defect grew approximately a quarter of an inch below the tread surface and formed an VSR that grew from the tread shell, as shown in Figure A-24. The transition from delamination to VSR shows that the delamination was formed from multiple fatigue cracks, Figure A-25.



Figure A-22. Tread Crack in Wheel BNSF4



Figure A-23. VSR Crack in Wheel BNSF4 that Extended into Plate

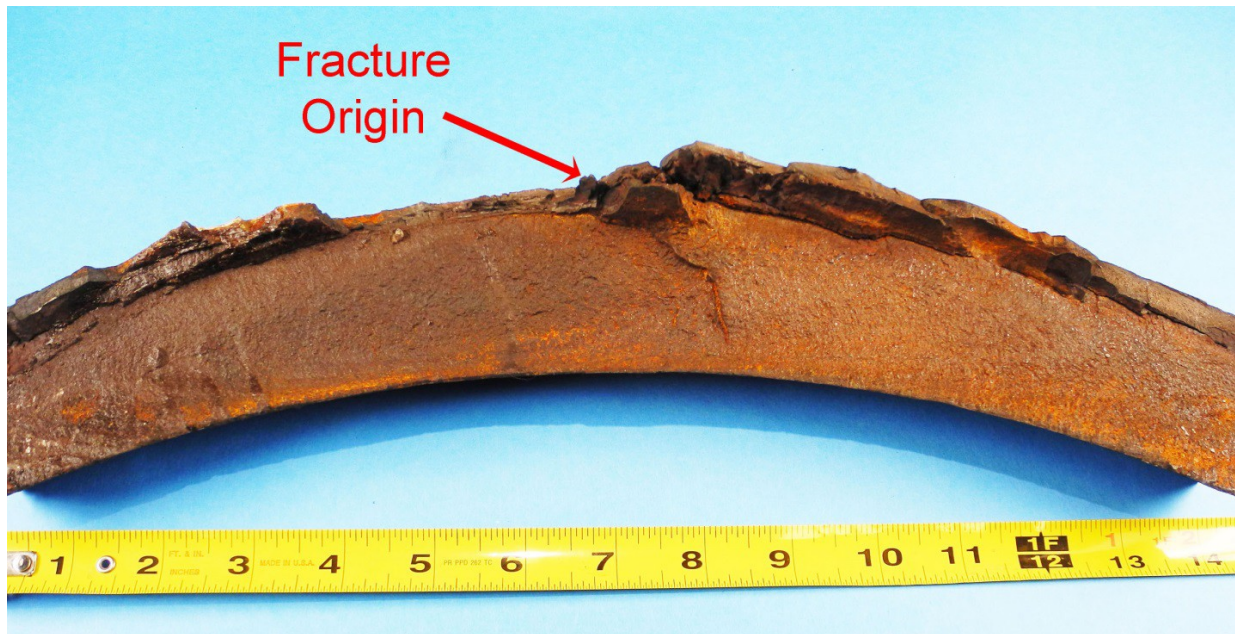


Figure A-24. Initial Fracture Location on Wheel BNSF4

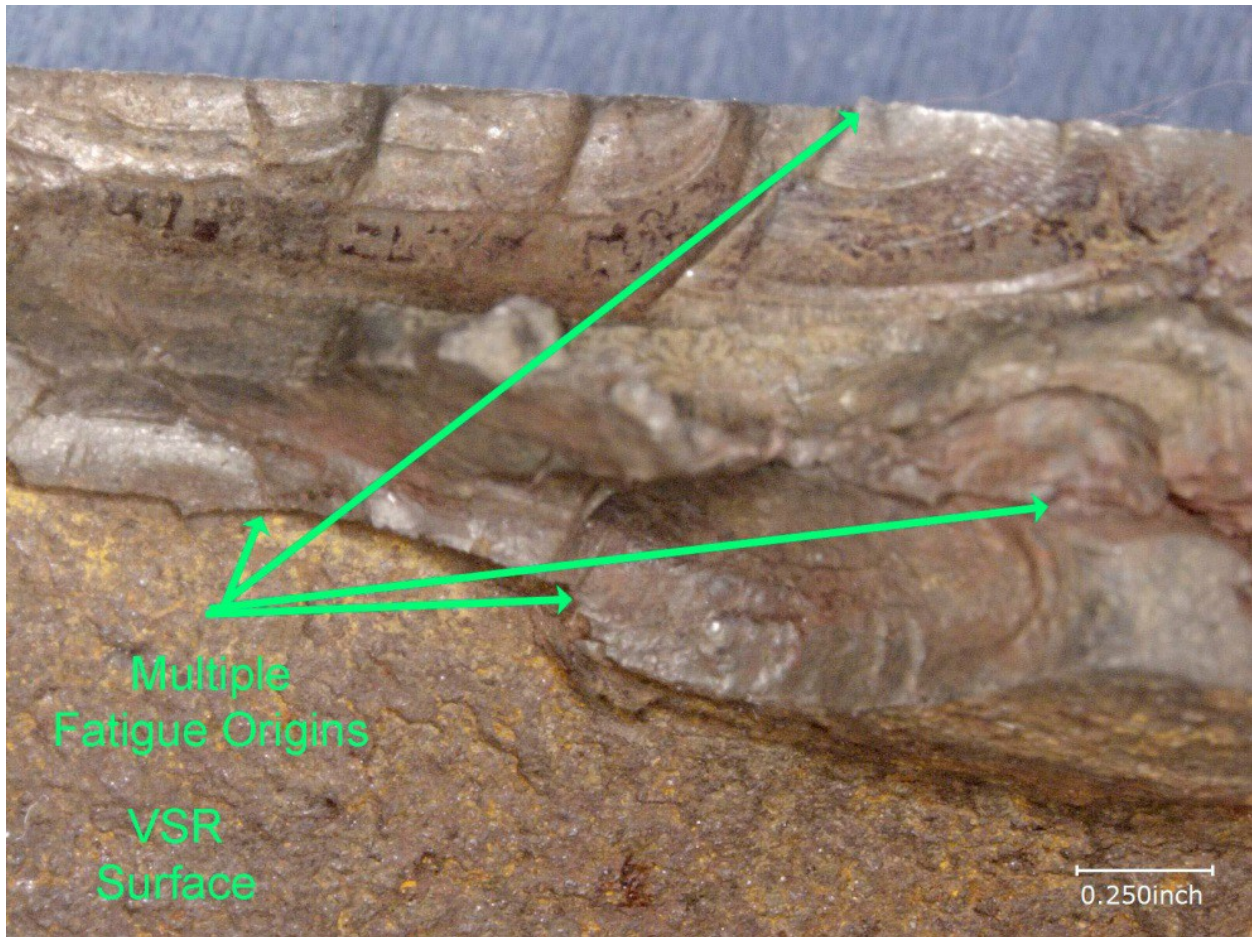


Figure A-25. Oblique View of Delamination and VSR on BNSF4, Original Magnification x10

Microhardness measurements were performed on a specimen cut adjacent to the fractured area, in the radial direction from the surface to a depth of half of an inch. The results of the measurements versus depth shown in Figure A-26 suggest the possible presence of an area of work softening.

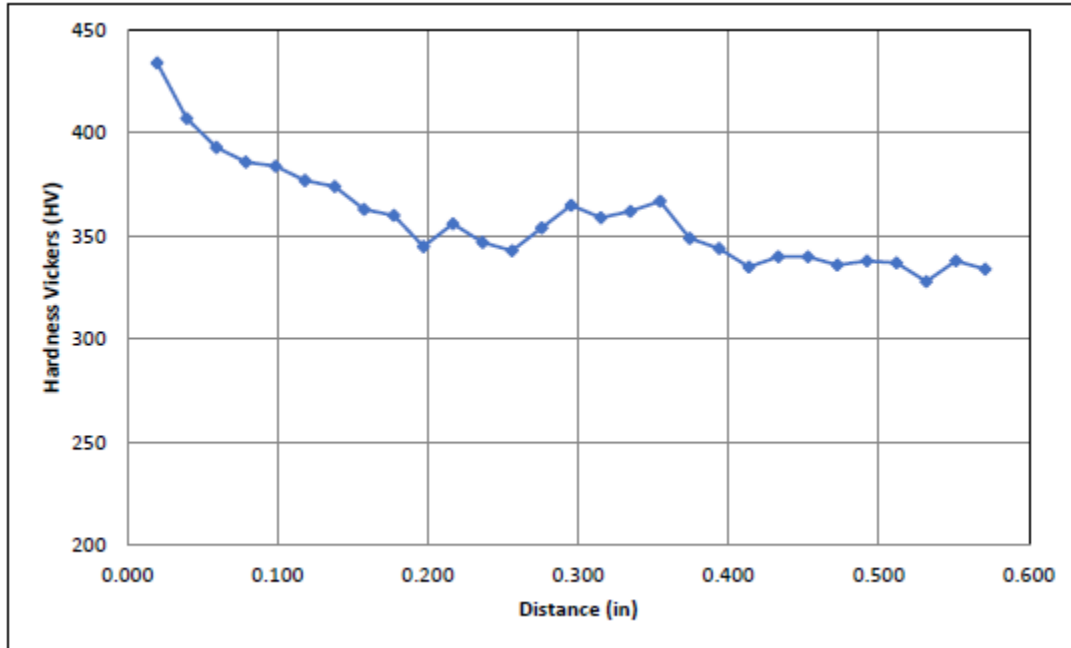


Figure A-26. BNSF4 Microhardness Variation from Surface

Metallographic analysis of the areas above the shell crack cast structure shows dissolved proeutectoid ferrite and almost complete spheroidization of the pearlitic structure. These changes, shown in Figure A-27, indicate a short time exposure of temperatures in the range of 1,400 °F. In Figure A-28, the area below the shell crack has retained its normal dendritic structure. The microstructure at the transition from shelling or delamination in Figure A-29 shows that the crack surfaces contain a grey oxide coating, indicating exposure greater than 1,000 °F.

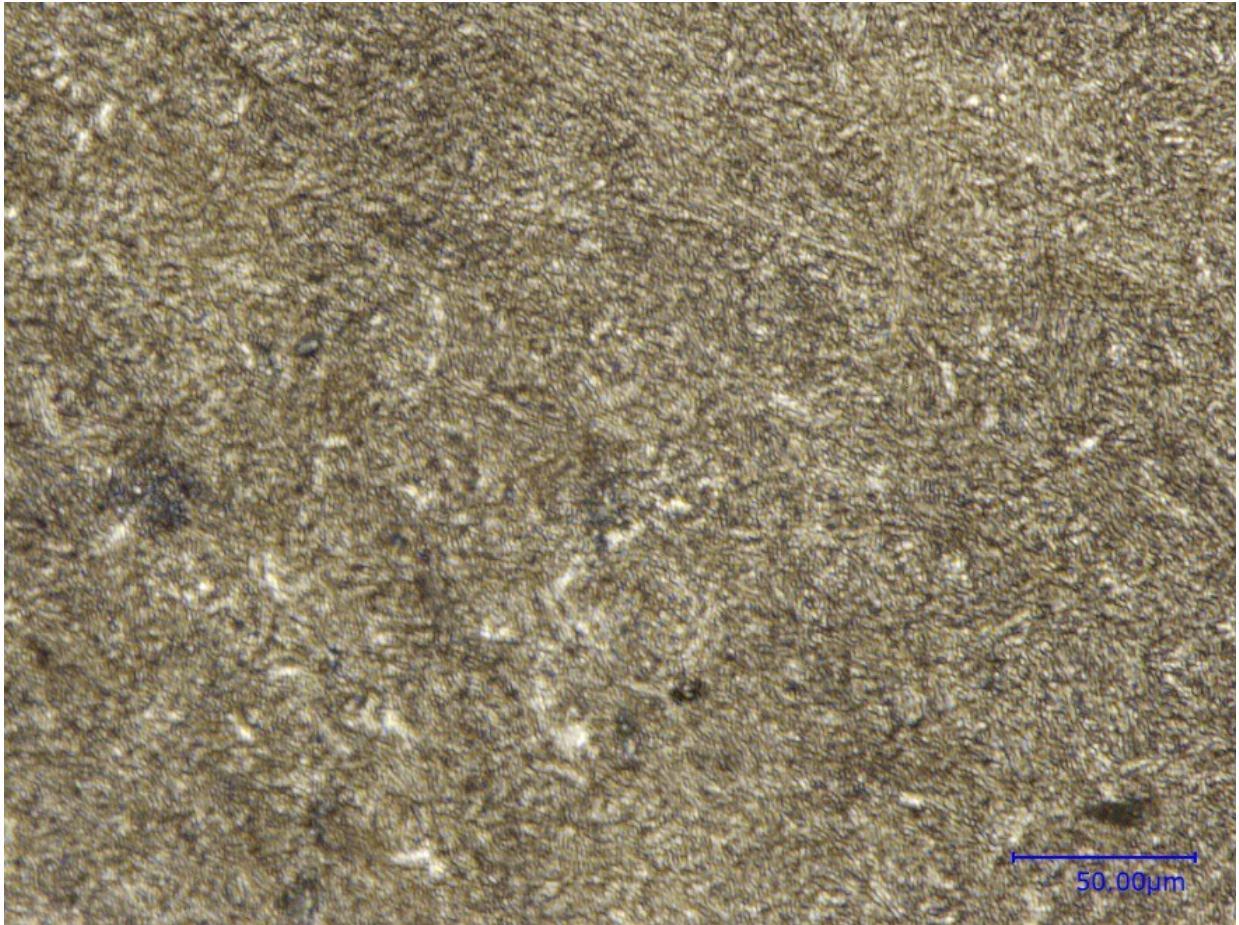


Figure A-27. BNSF4 Microstructure Above Shell Crack, Original Magnification x1,000, Nital Etch

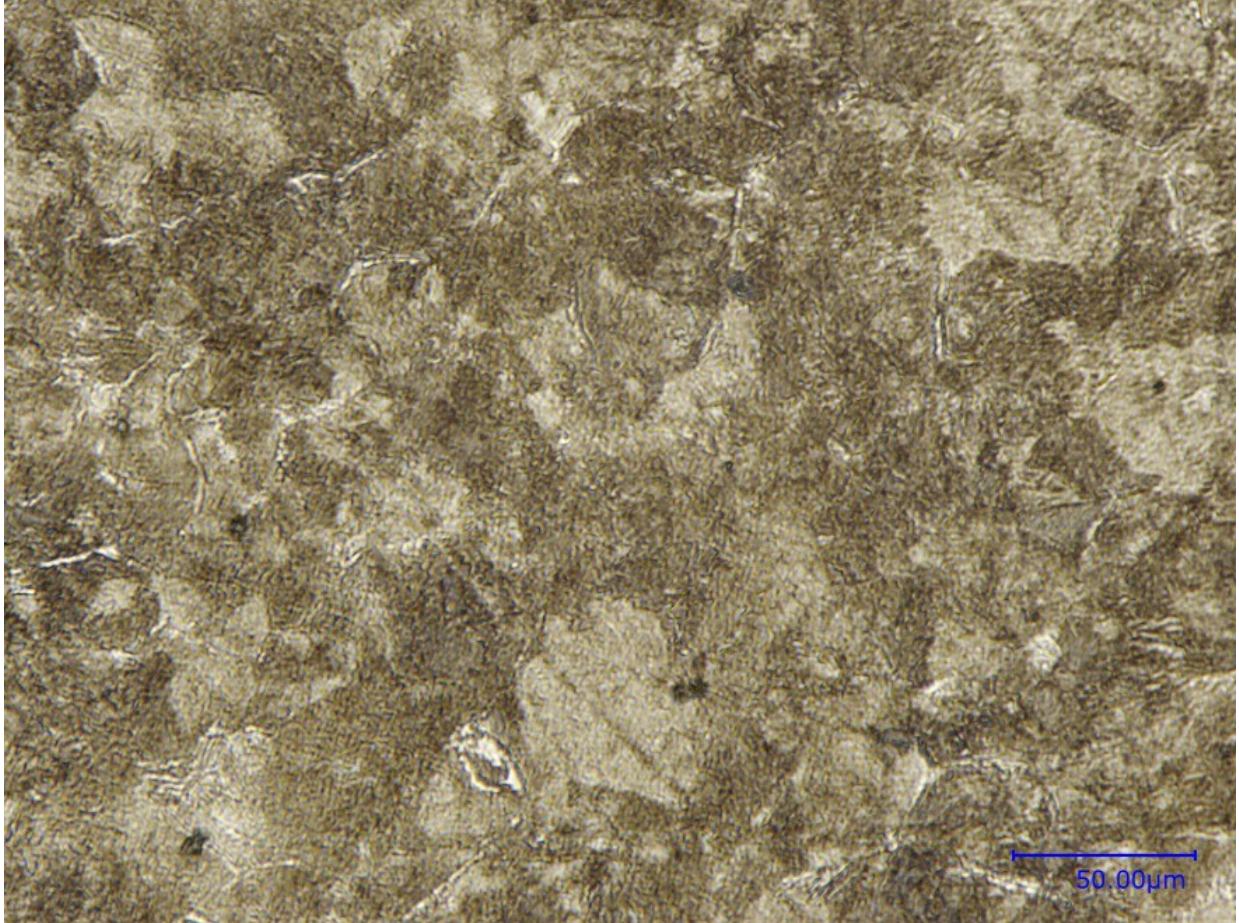


Figure A-28. BNSF4 Microstructure Below Shell Crack Showing Typical Grain Structure, Original Magnification x1,000

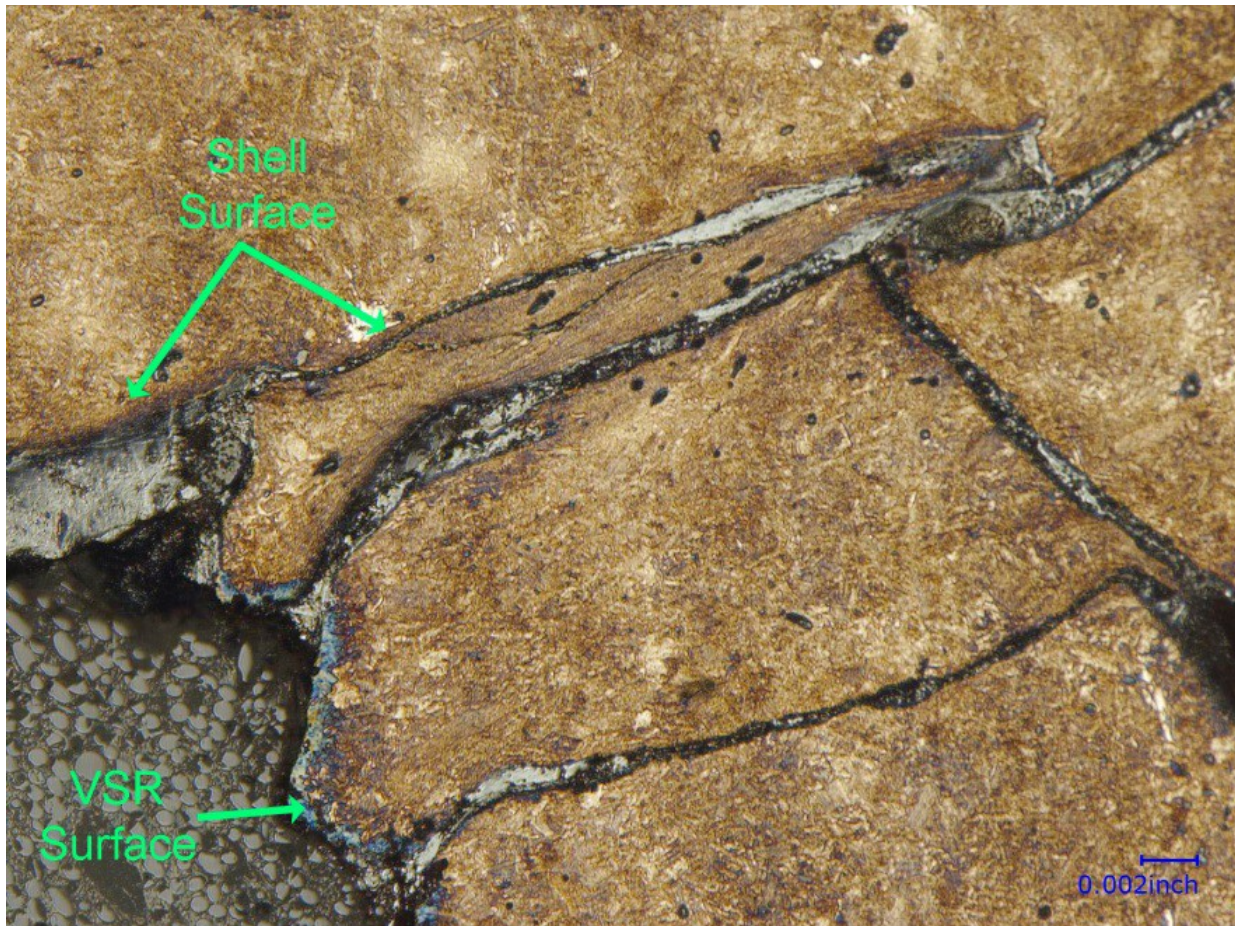


Figure A-29. Transition from Shell Crack to VSR on BNSF4 with Oxidized Crack Surfaces, Original Magnification x300, Nital Etch

A.5 Wheel BNSF6

The front rim VSR had separated, as shown in Figure A-30 and Figure A-31. The failure occurred in two steps. First, a large shell defect grew approximately 1/8 of an inch below the tread surface and formed a VSR that grew from the tread shell, as shown in Figure A-31. Metallographic analysis of the areas above and below the shell crack shows flowed and deformed grains, while the area below the crack appears unaffected with a layer of high-temperature oxide within the crack (Figure A-32). Figure A-33 shows the surface of the VSR origin with oxide in secondary cracking.



Figure A-30. Cracking on Tread of Wheel BNSF6



Figure A-31. Termination of VSR on BNSF6 at Rim Plate Fillet

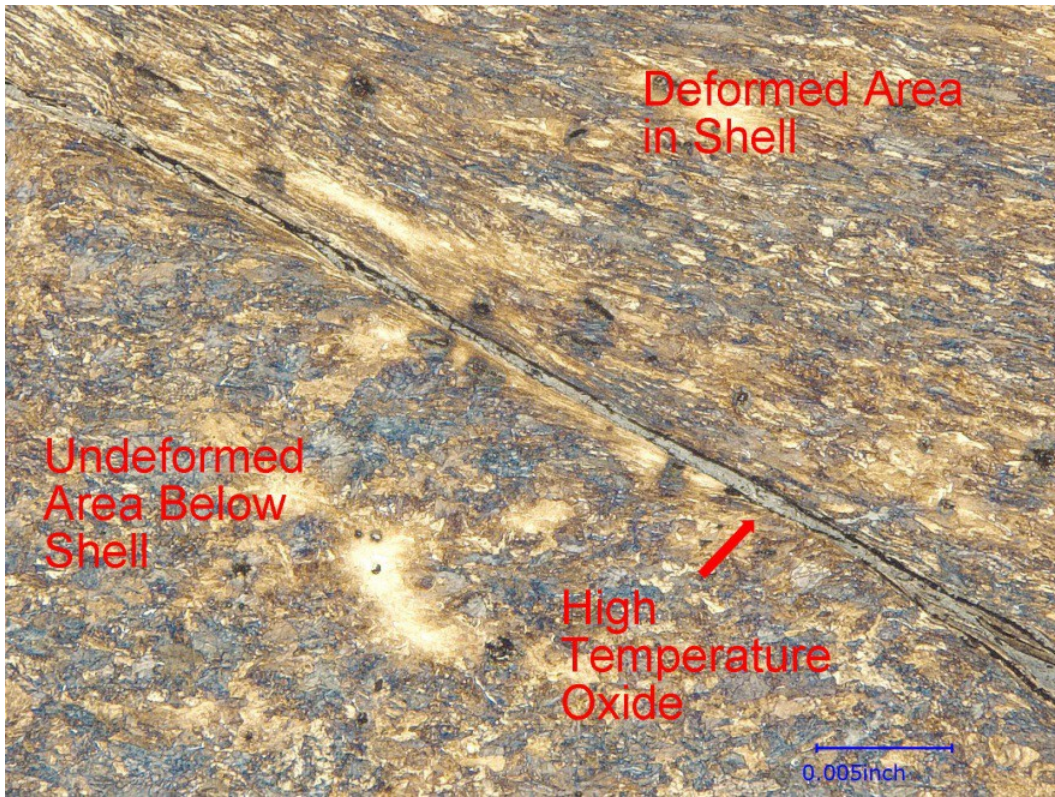


Figure A-32. BNSF6 Microstructure Above and Below Shell Crack, Original Magnification x200, Nital Etch



Figure A-33. Secondary Crack from BNSF6 VSR Face with Oxide, Original Magnification x200, Nital Etch

Microhardness measurements were made on a specimen cut adjacent to fractured area in the radial direction from the tread surface to a depth of 1/2 of an inch. The results of the measurements versus depth suggest the possible presence of an area work softening, Figure A-34.

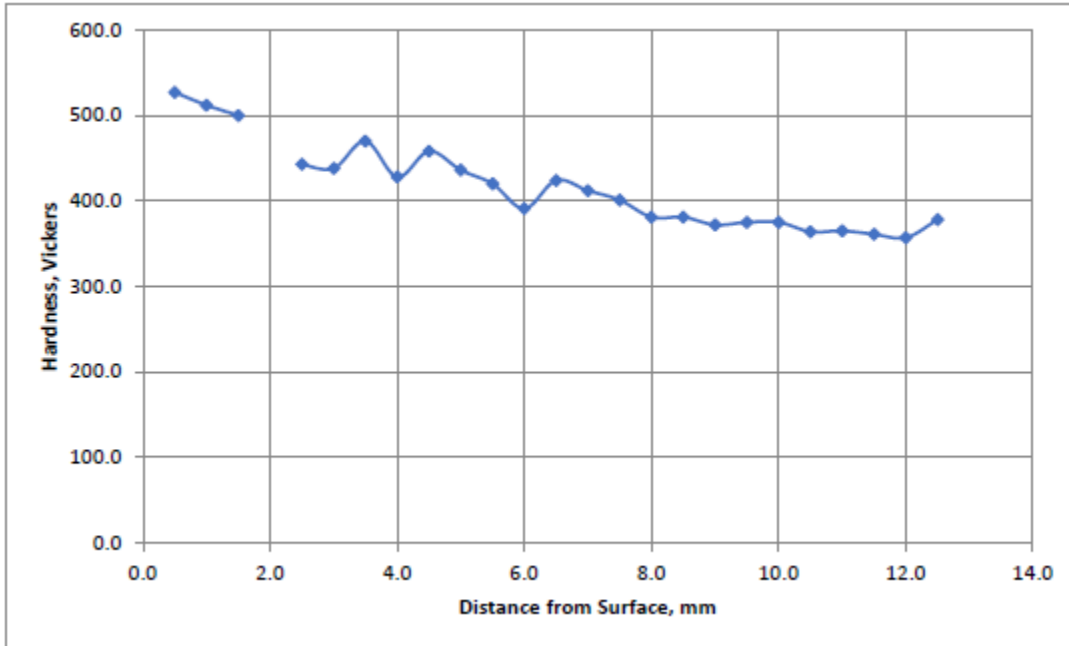


Figure A-34. BNSF6 Microhardness vs. Depth, Discontinuity is Location of Crack

A.6 Wheel BNSF7

The wheel contained a VSR that had developed for a distance of approximately 10 inches around the tread toward the front rim face of the wheel, as shown in Figure A-35. The VSR had extended completely through the rim, Figure A-36. The wheel tread contained discontinuous shelling around the circumference. Figure A-37 shows the fracture surface of the VSR after numerous attempts to remove the as-received rust layer.



Figure A-35. VSR on Tread of Wheel BNSF7, BNSF Tread Photograph



Figure A-36. Wheel BNSF7 VSR on Rim Plate Fillet



Figure A-37. Fracture Face of Wheel BNSF7 VSR

Metallographic analysis of the areas above and below the shell crack (Figure A-38) shows flowed and deformed grains, while the area below the crack appears unaffected with a layer of high temperature oxide within the crack. Figure A-39 shows the surface of the VSR origin with oxide in secondary cracking.

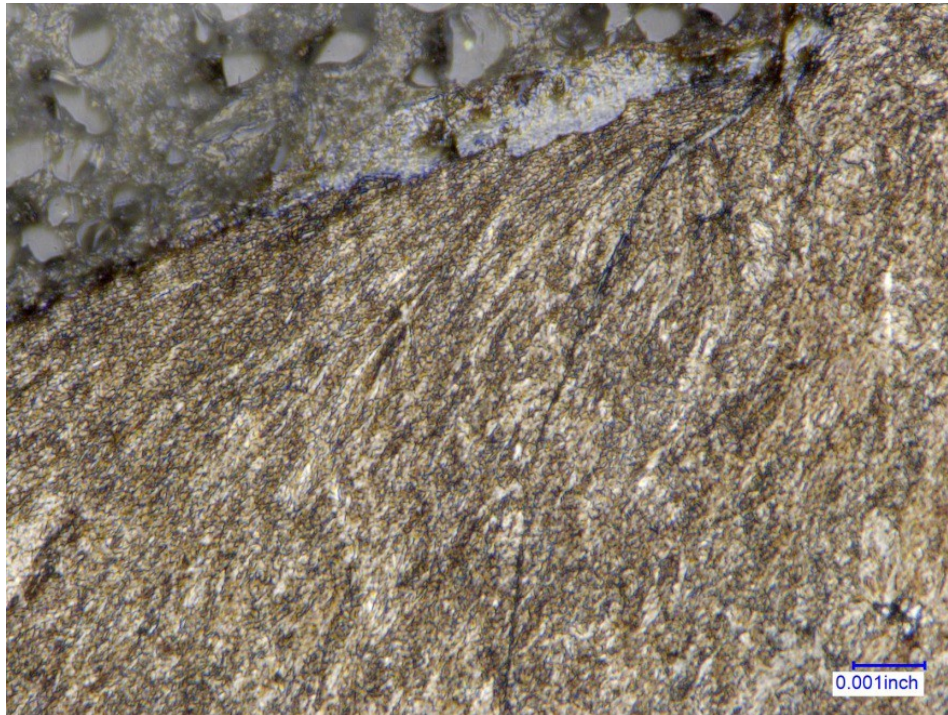


Figure A-38. Microstructure at Tread Surface of Wheel BNSF7 with Crack in Flowed Structure, Original Magnification x1,000, Nital Etch



Figure A-39. Crack from Shelling in Wheel BNSF7, Original Magnification x100, Nital Etch

The fracture toughness of the failed and mate wheels was determined according to ASTM Standard Method E399. The failed wheel had a plane-strain fracture toughness, K_{Ic} , of 41.8 $\text{ksi}\sqrt{\text{in}}$, while the mate wheel K_{Ic} was 50.3 $\text{ksi}\sqrt{\text{in}}$. These values are similar to that of 53.3 $\text{ksi}\sqrt{\text{in}}$ reported for a forged wheel in an earlier study of wheel fracture properties[18].

Microhardness measurements were made on a specimen cut adjacent to the fractured area in the radial direction from the surface to a depth of half of an inch. The results of hardness to depth suggest the possible presence of an area work softening, Figure A-41.

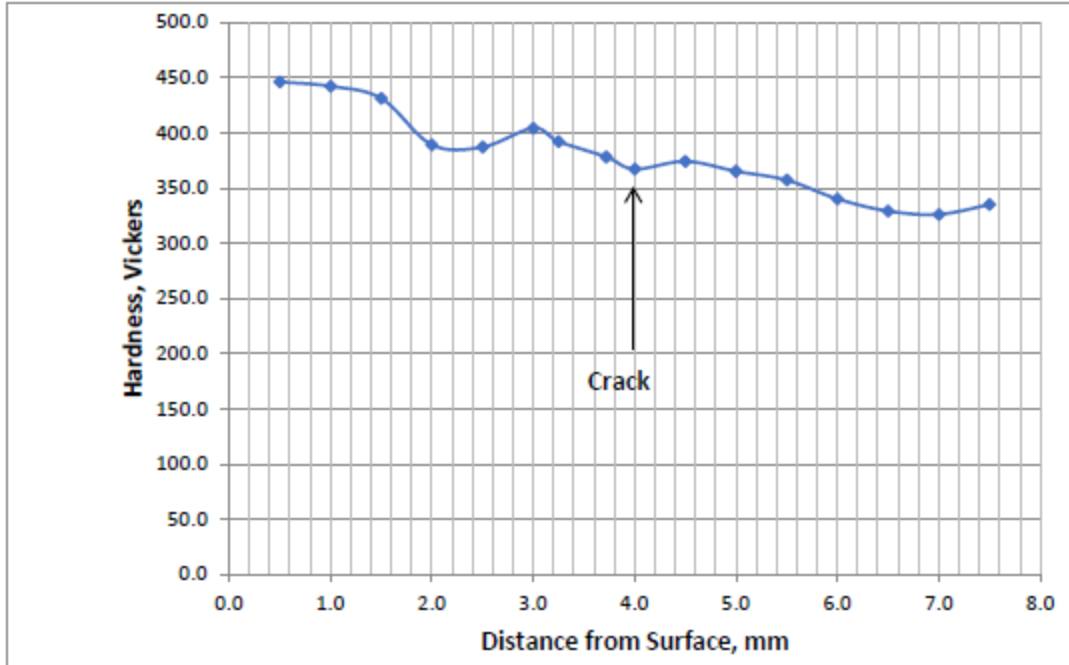


Figure A-40. BNSF7 Microhardness Variation from Surface

A.7 Wheel CSX8

The wheel fractured due to a VSR that lost a section of the rim at least four feet long by three inches wide. The as-received wheelset and an approximately 4-foot long section of the tread are shown in Figure A-41 and Figure A-43, respectively. The fracture, shown in Figure A-43 and Figure A-44, was atypical of most VSR failures because of the absence of extensive tread shelling.

The suspected origin of the VSR with associated tread delamination is shown in Figure A-46 and appears to be a quarter of an inch-deep fatigue crack. The remainder of the VSR fracture is unstable crack growth.



Figure A-41. Fractured Wheel CSX8, as Received



Figure A-42. Front Rim Section that Separated from Wheel CSX8



Figure A-43. Field Side Section of CSX8 Tread without Surface Shelling

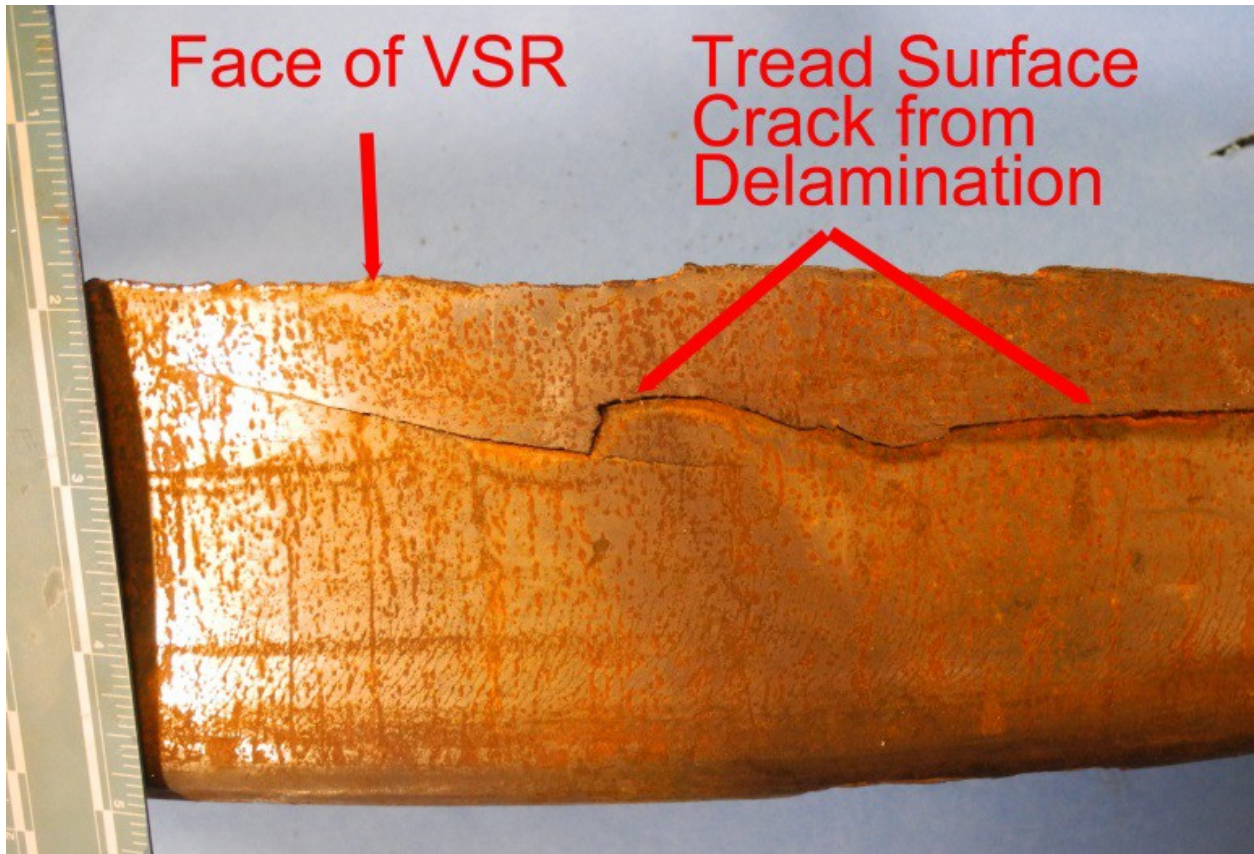


Figure A-44. CSX8 Tread Surface Exit Crack from Delamination

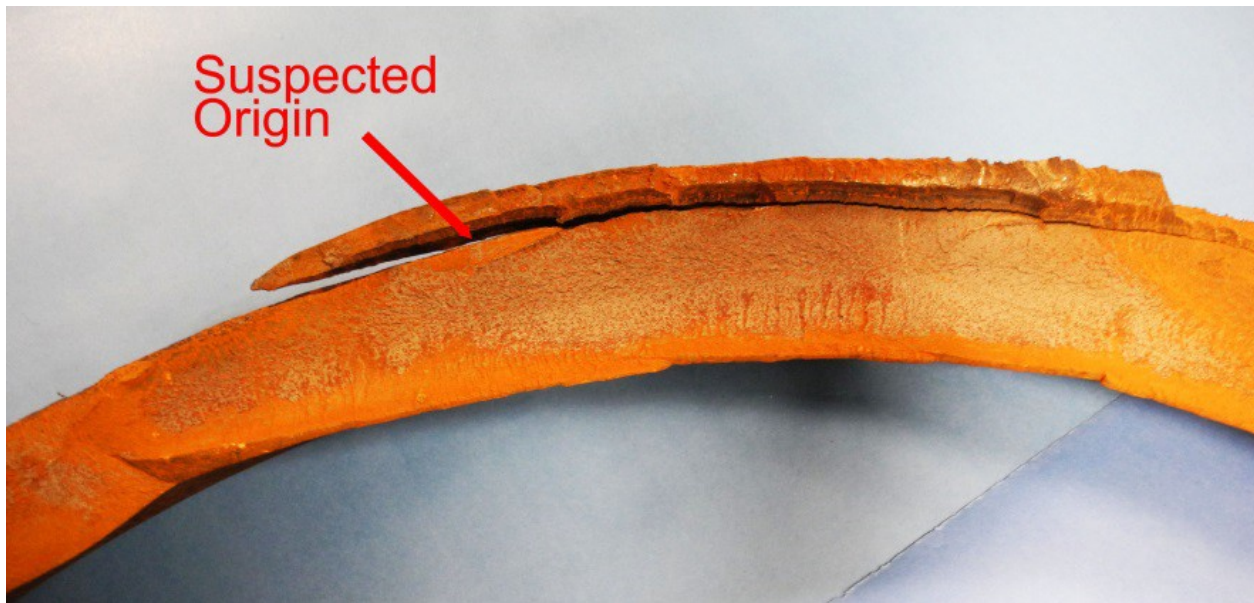


Figure A-45. Fracture Surface of CSX8 VSR with Suspected Origin

A specimen was cut axially through suspected origin that includes the tread surface, the shell surface, and the VSR surface, as shown in Figure A-46. The fracture surfaces were then examined with a scanning electron microscope.

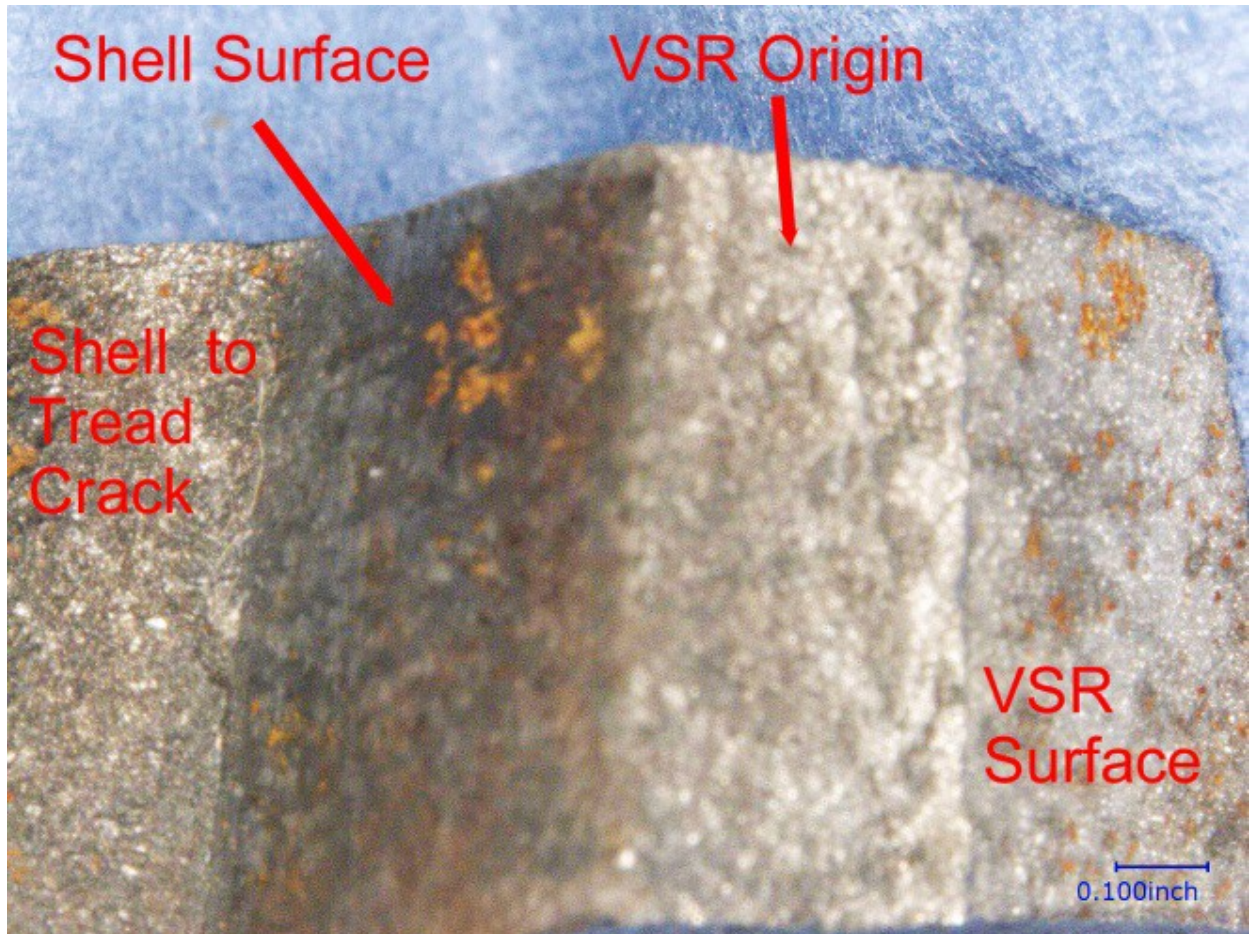
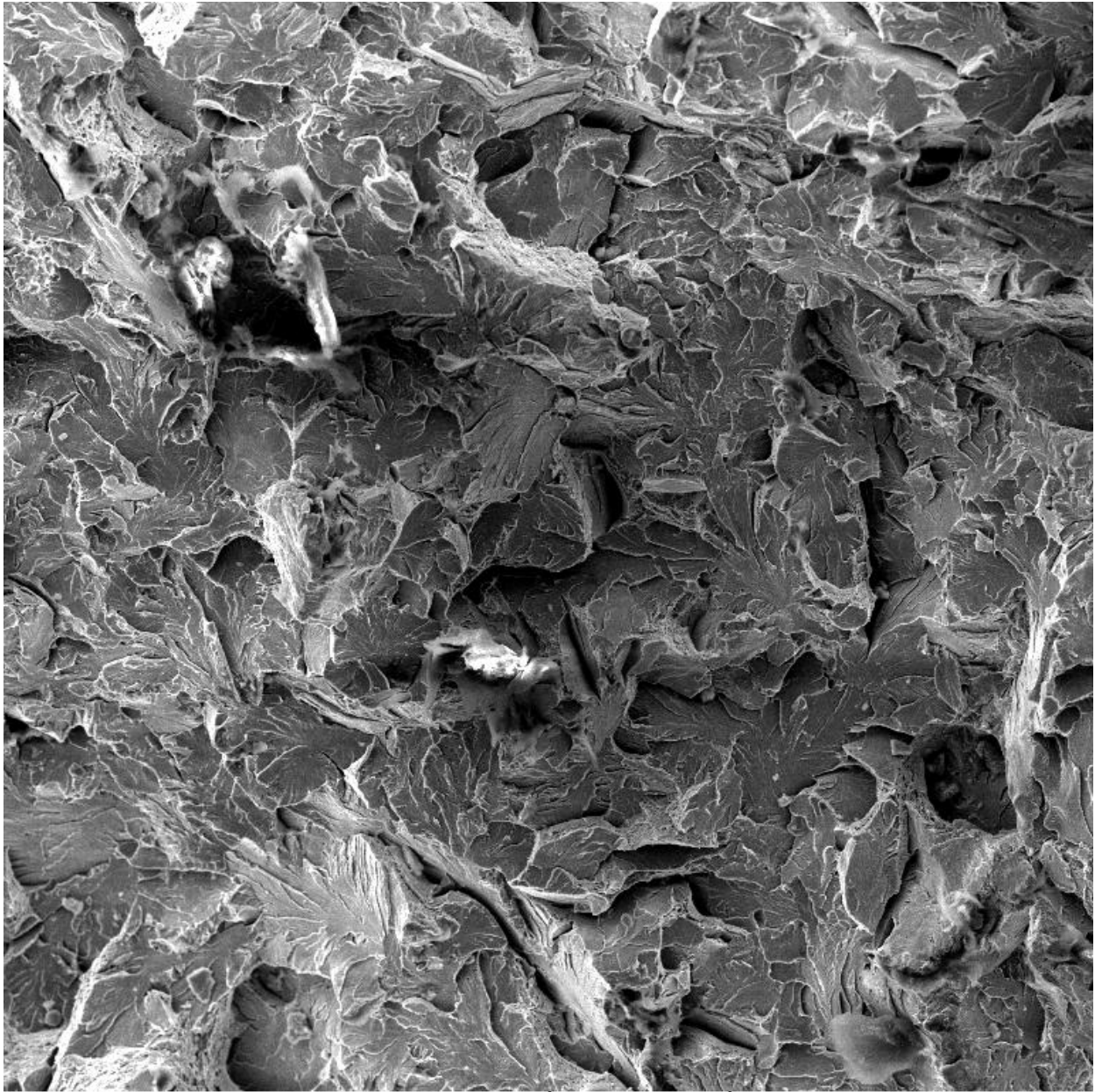


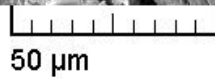
Figure A-46. Fracture Surfaces of CSX8 Through Shelling, VSR Origin, and VSR, Original Magnification x15

The fracture surface of the VSR is typical of rapid or overload fractures (quasi-cleavage), Figure A-47. The VSR origin fracture surface shown in Figure A-48 also shows rapid fracture. The transition of the shell fracture surface to the VSR origin is shown in Figure A-49.



SEM HV: 15.00 kV
View field: 301.6 μ m
SEM MAG: 500 x

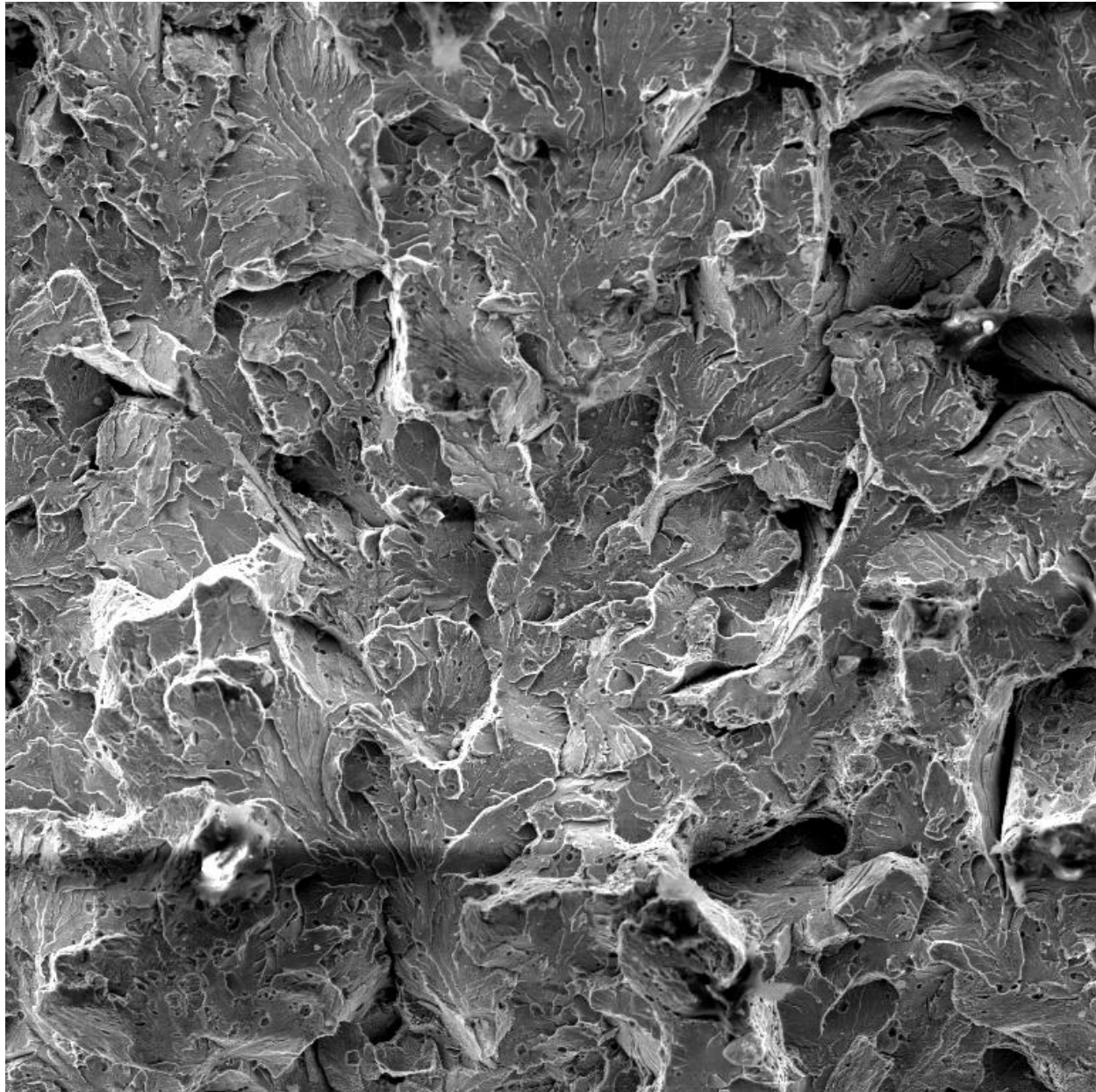
WD: 13.26 mm
Det: SE Detector
Date(m/d/y): 02/26/18



VEGA\\ TESCAN



Figure A-47. Scanning Electron Microscope Image of CSX8 VSR Fracture Surface, Original Magnification x500



SEM HV: 15.00 kV

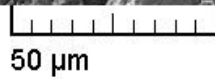
WD: 10.47 mm

View field: 301.6 μ m

Det: SE Detector

SEM MAG: 500 x

Date(m/d/y): 02/26/18



VEGA\\ TESCAN



Figure A-48. Scanning Electron Microscope Image of CSX8 VSR Origin Fracture Surface, Original Magnification x500

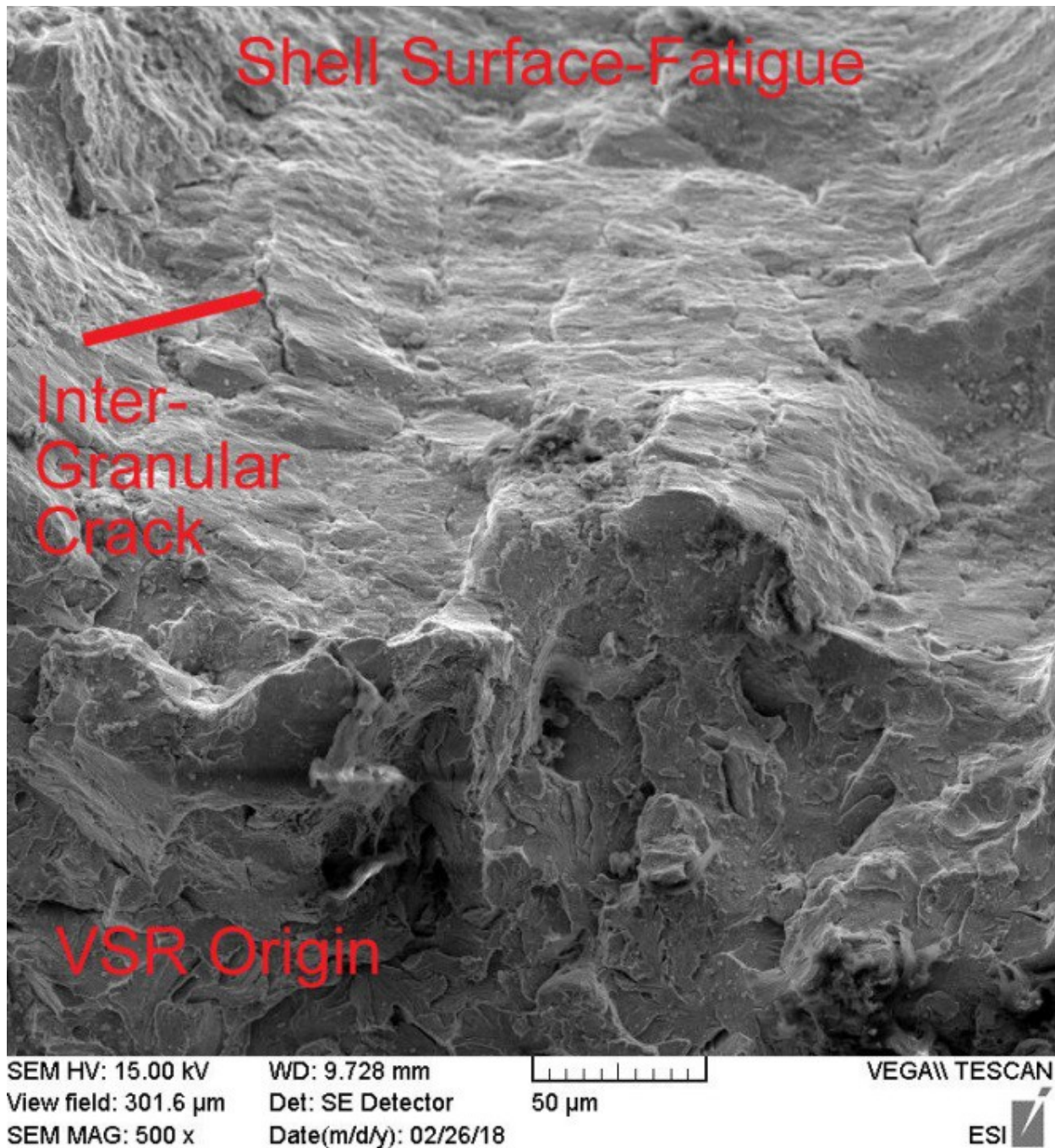


Figure A-49. Transition from Shell Surface Fatigue to CSX8 VSR Initiation, Original Magnification x500

The sectioned surface of the specimen shown in Figure A-46 was polished, etched, and examined with the Keyence microscope system. A layer of martensite was observed on the tread surface, Figure A-50, indicating that the wheel had been subject to an unusual level of brake shoe heating or a wheel slide.

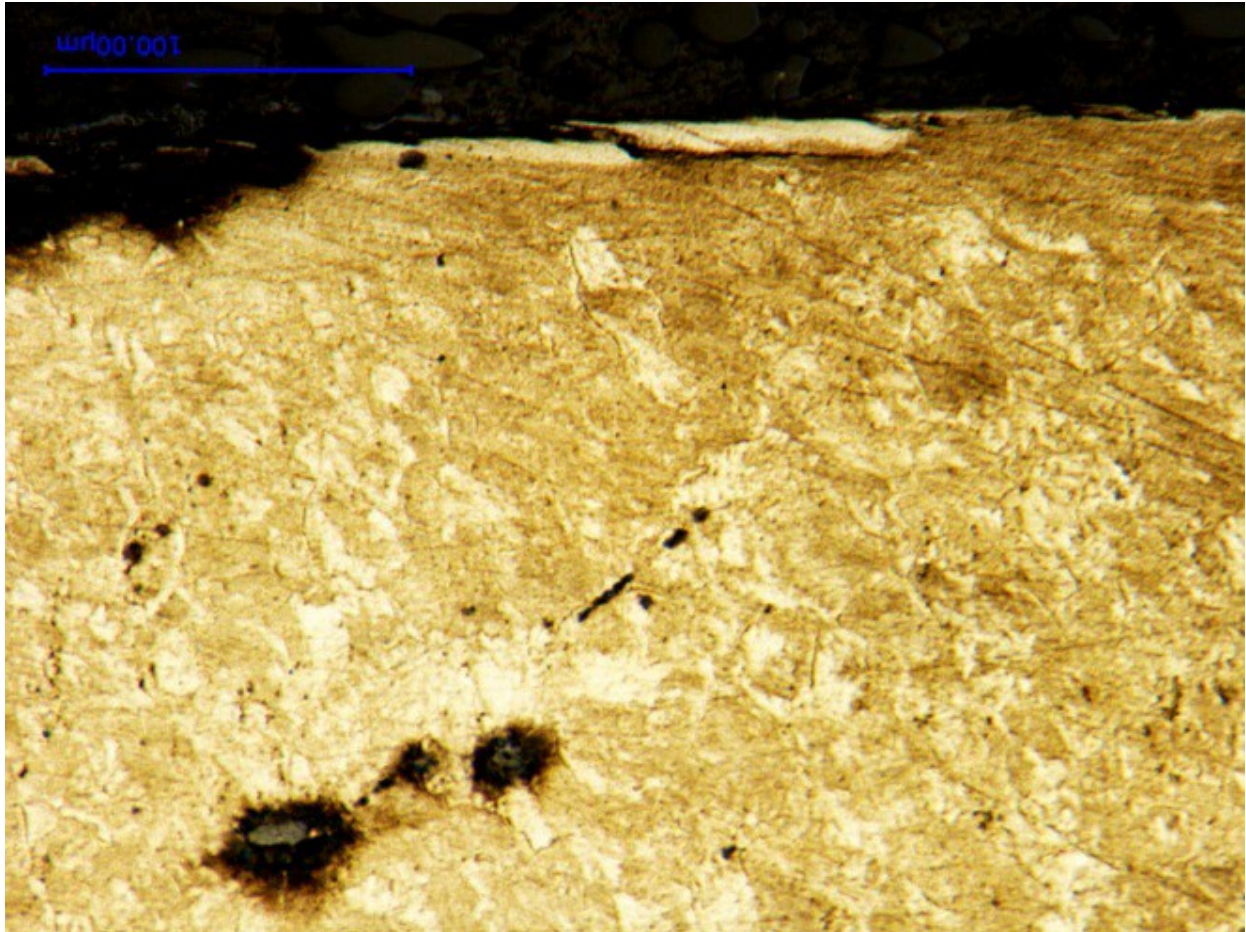


Figure A-50. Microstructure of CSX8 Tread Surface with Martensite Layer, Nital Etch, Original Magnification x1,000

Microhardness measurements were performed on a specimen cut adjacent to the fractured area, the in the radial direction from the surface to a depth of half of an inch. The results of the measurements versus depth in Figure A-51 suggest the possible presence of an area of work softening.

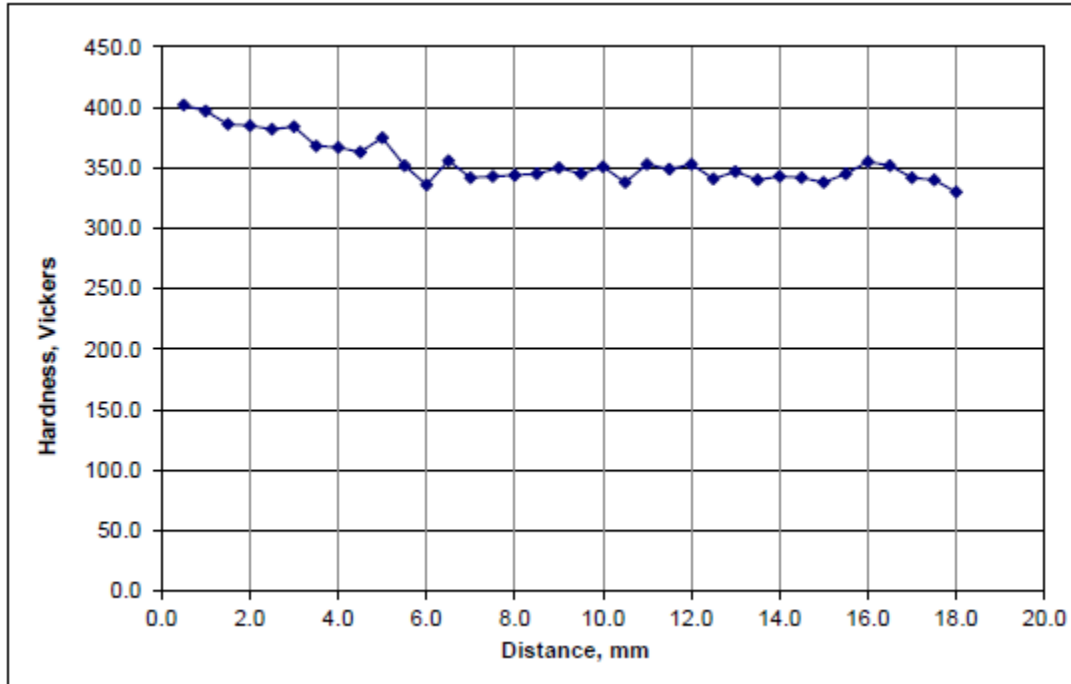


Figure A-51. CSX8 Microhardness in Radial Direction

A.8 Wheel UP9

The wheel was removed due to a VSR fracture which originated from shelling on the tread surface of the wheel. The wheel is shown post-cleaned condition in Figure A-52. Figure A-53 shows a plan view of the VSR.

The tread surface was ultrasonically inspected to determine the extent of delamination, and the extent of the delamination was within the blue parenthesis shown in Figure A-53. No additional delaminated areas were revealed in the failed wheel; no delaminated areas were revealed during inspection of the mate wheel.



Figure A-52. Vertical Split Rim in Wheel UP9

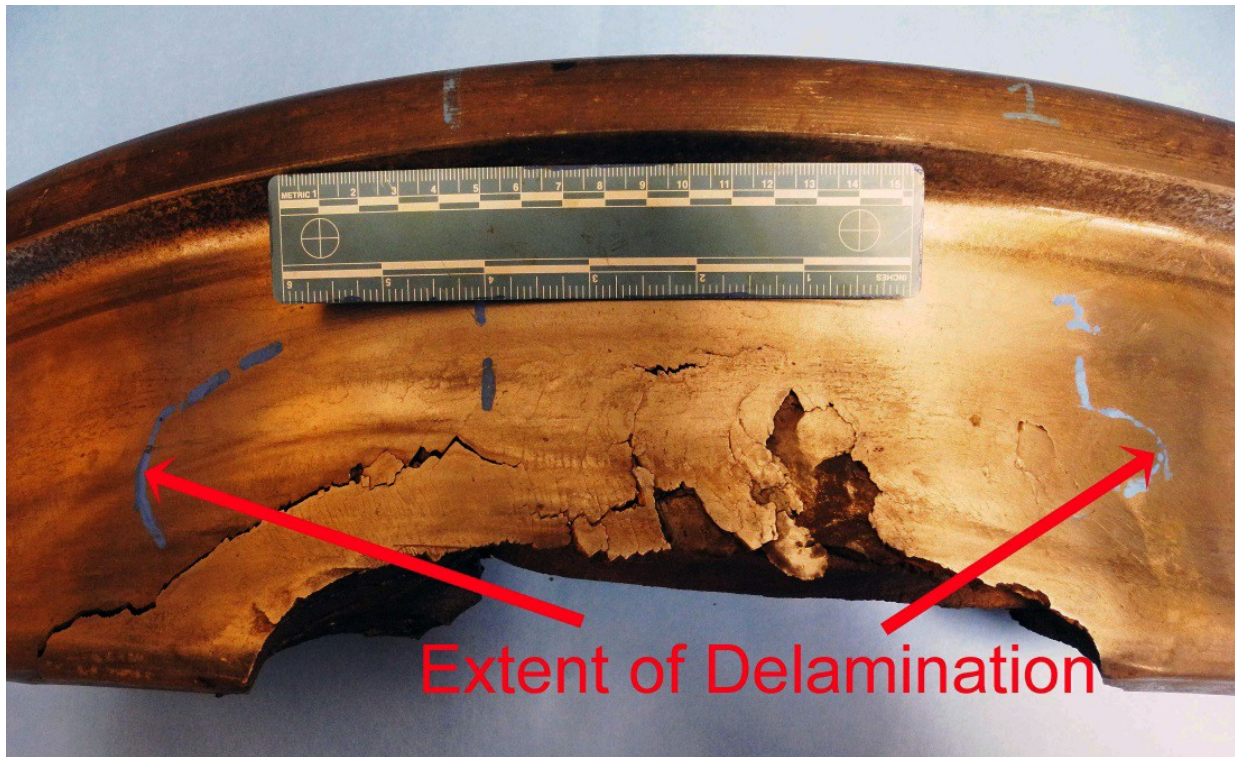


Figure A-53. Extent of Delamination on Failed Wheel UP9, as Revealed by Ultrasonic Inspection

The Brinell hardness of 363 was determined on the front rim face, as required by the AAR M107/M208 specification, and was within the specification requirement of 321 to 363 for Grade C steel. Additionally, the Brinell hardness was measured at 60-degree increments around the failed and mate wheels. The results show that the tread surface had increased in hardness by 25

BHN due to work hardening, except for the location of the VSR, where an increase of 52 Brinell numbers was measured. The corresponding position of the mate did not show an increase in hardness, as seen in Table A-1.

Table A-1. Tread Surface Hardness Around Failed UP9 and Mate Wheel

Distance (in degrees)	Failed Wheel	Mate Wheel
0°	388	388
60°	388	388
120°	388	388
180°	388	388
240°	388	388
360° (VSR)	415	363

The failure occurred in two steps. First, a large layer of separation or delamination, approximately 3/16 of an inch below the tread surface, formed and the initial VSR grew from the tread shell, as shown in Figure A-54. A fatigue crack then initiated and grew until the VSR caused unstable crack growth that separated a portion of the rim, Figure A-55.

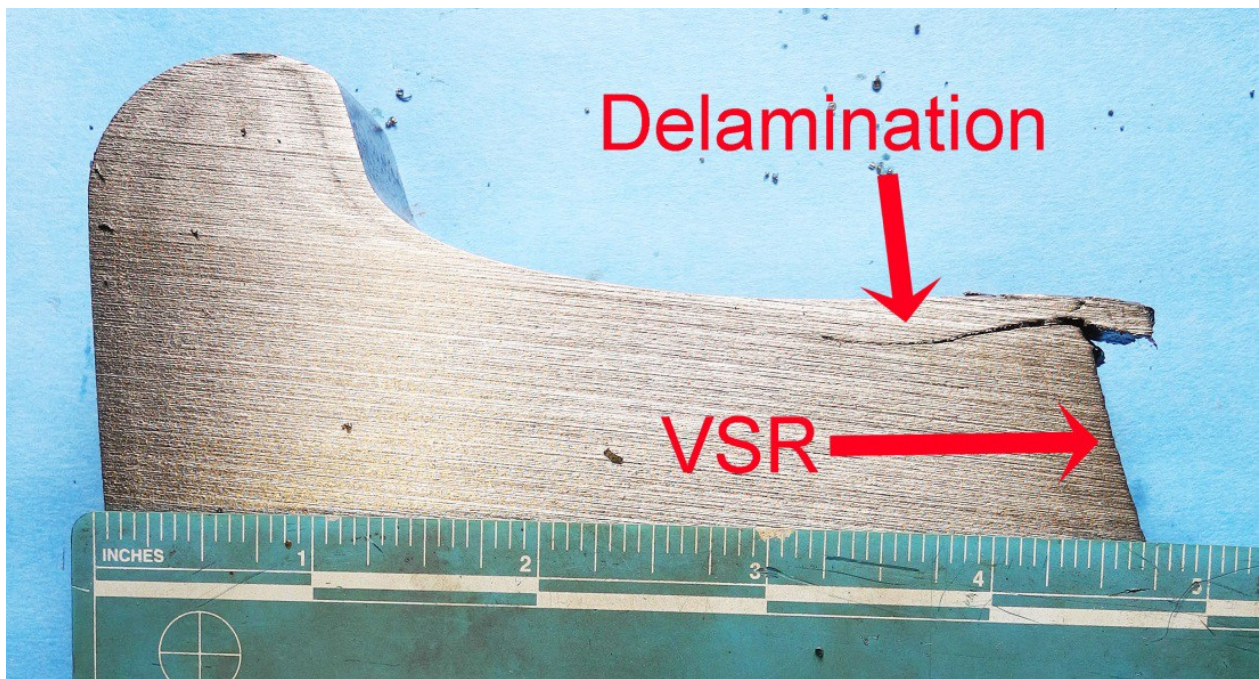


Figure A-54. Cross Section of Wheel UP9 Tread Area

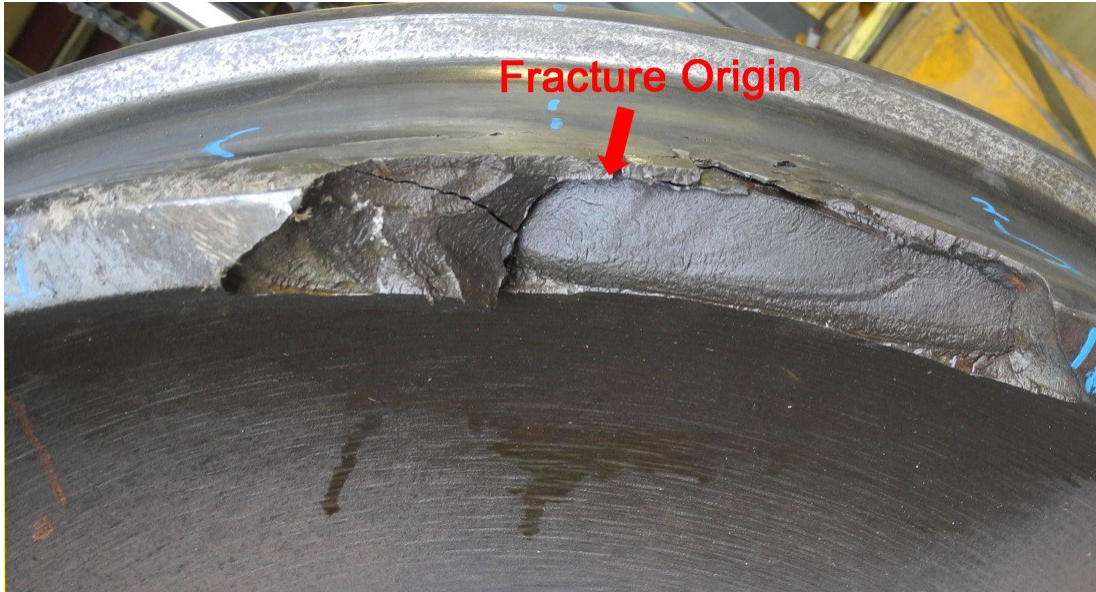


Figure A-55. Fracture Origin of Wheel UP9

The tread surface microstructures of both the failed wheel, Figure A-56, and the mate wheel, Figure A-57, show the expected effects of plastic flow. As is the case with other VSR wheels investigated, oxides that form at high temperature are present with cracks in the vicinity of the VSR formation shown in Figure A-58.

Examination of the fracture surface of the delaminated shelling surface in Figure A-59 shows rolling contact fatigue with the presence of a vertical crack.

The fracture surface of the VSR shown in Figure A-60 is typical of a quasi-cleavage fracture.

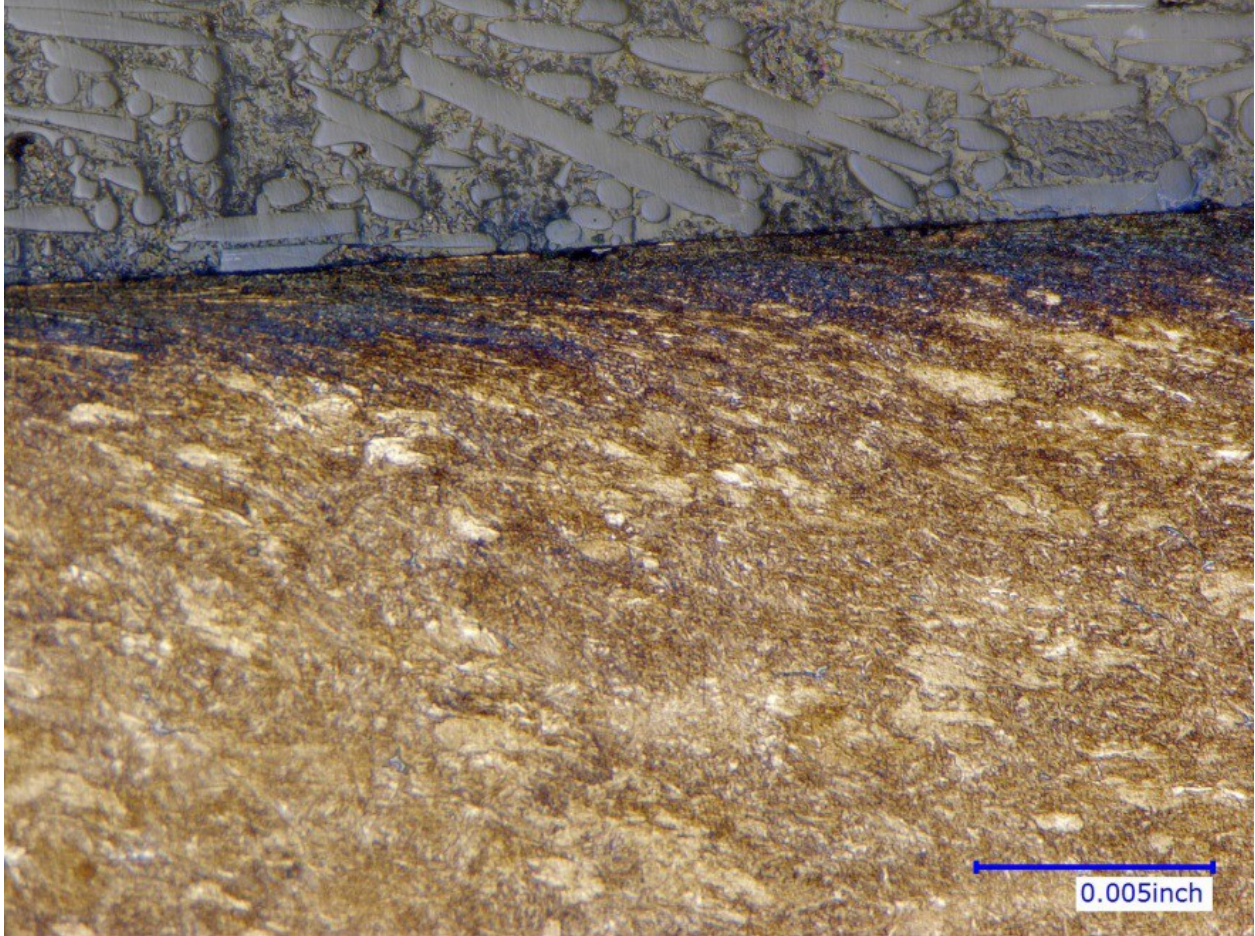


Figure A-56. Microstructure of Failed Wheel UP9 Tread Surface with Plastic Flow to a Depth of Approximately 0.005-Inch, Original Magnification x500, Nital Etch

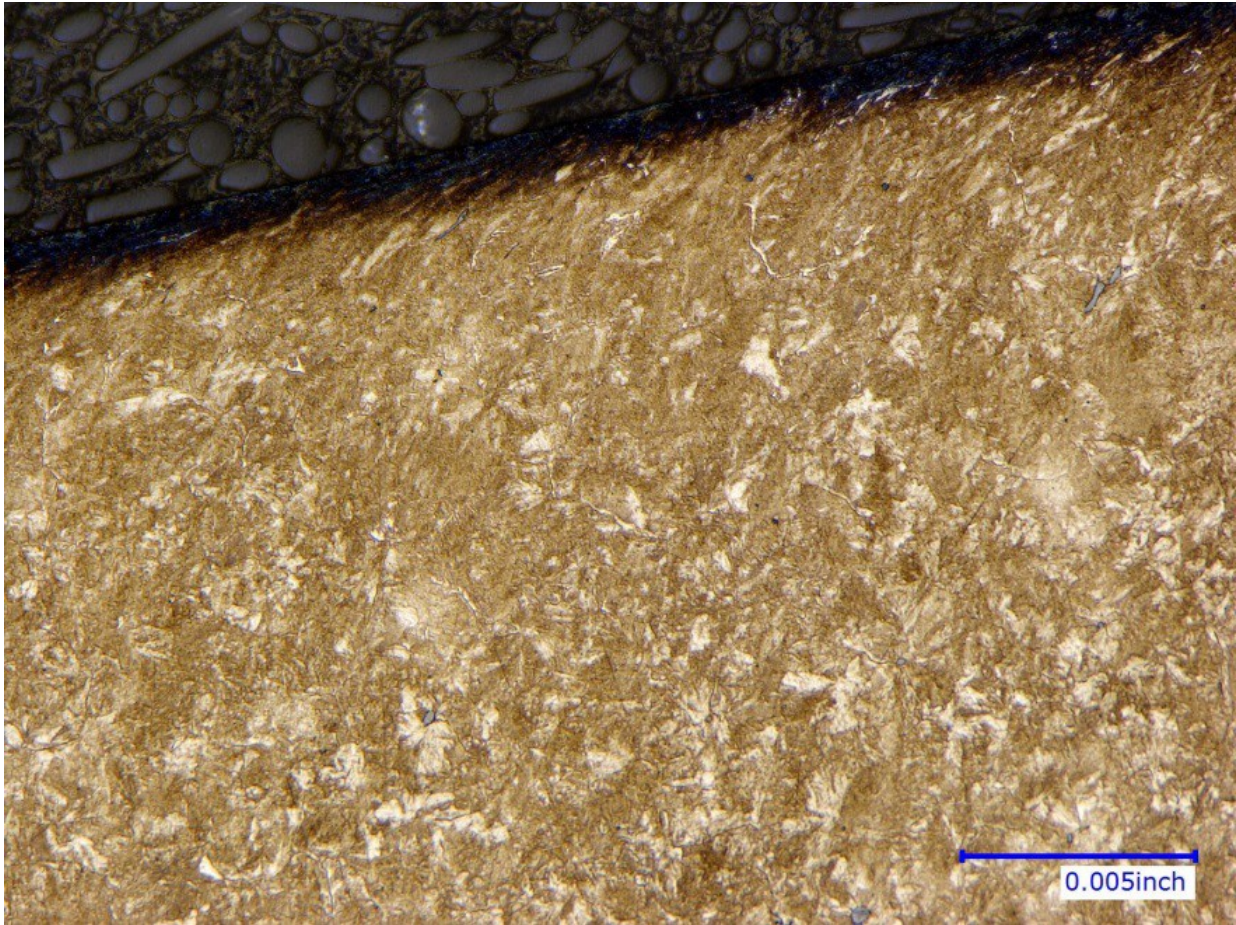


Figure A-57. Microstructure of UP9's Mate Wheel Tread Surface with Plastic Flow to a Depth of Approximately 0.005-Inch, Original Magnification x500, Nital Etch

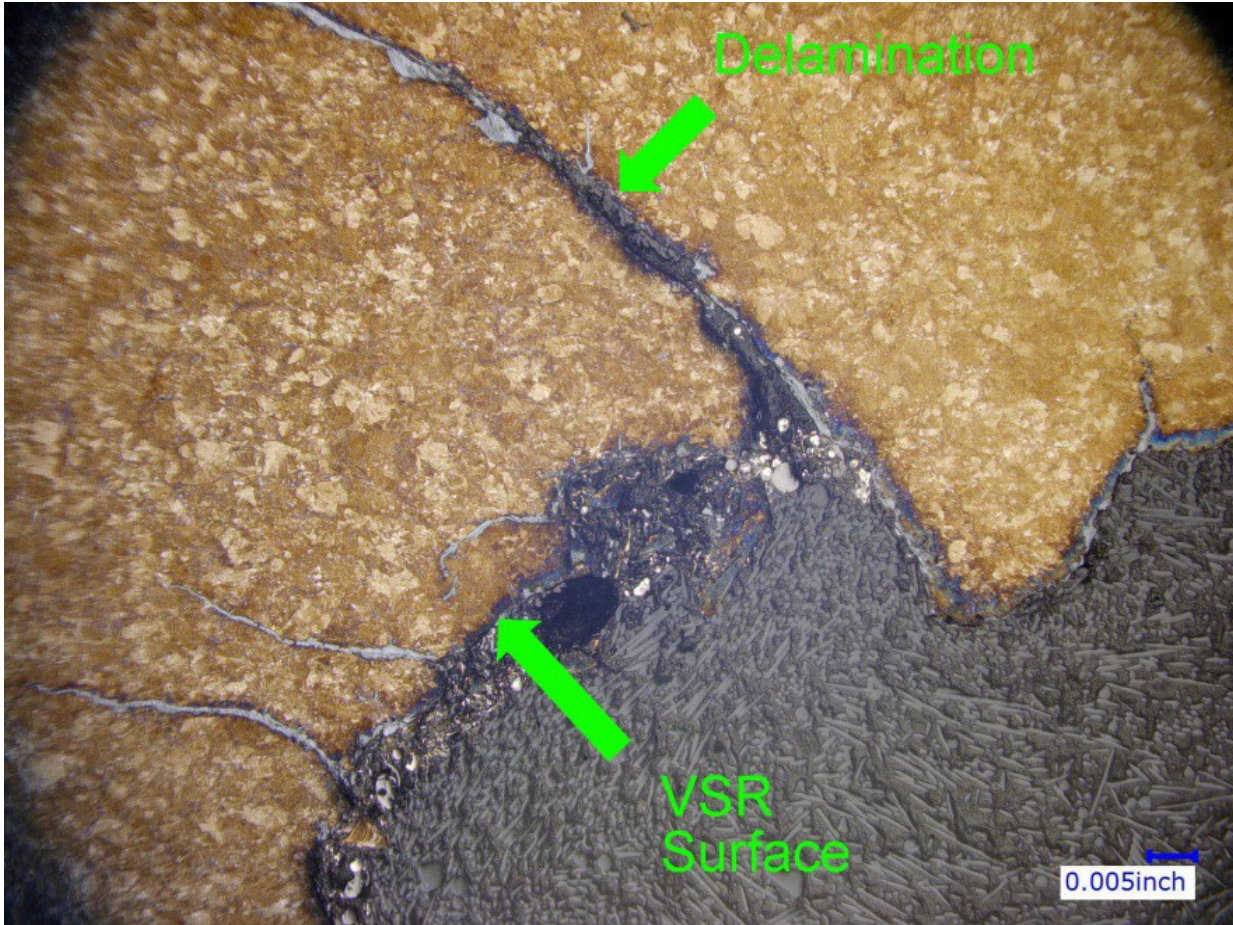
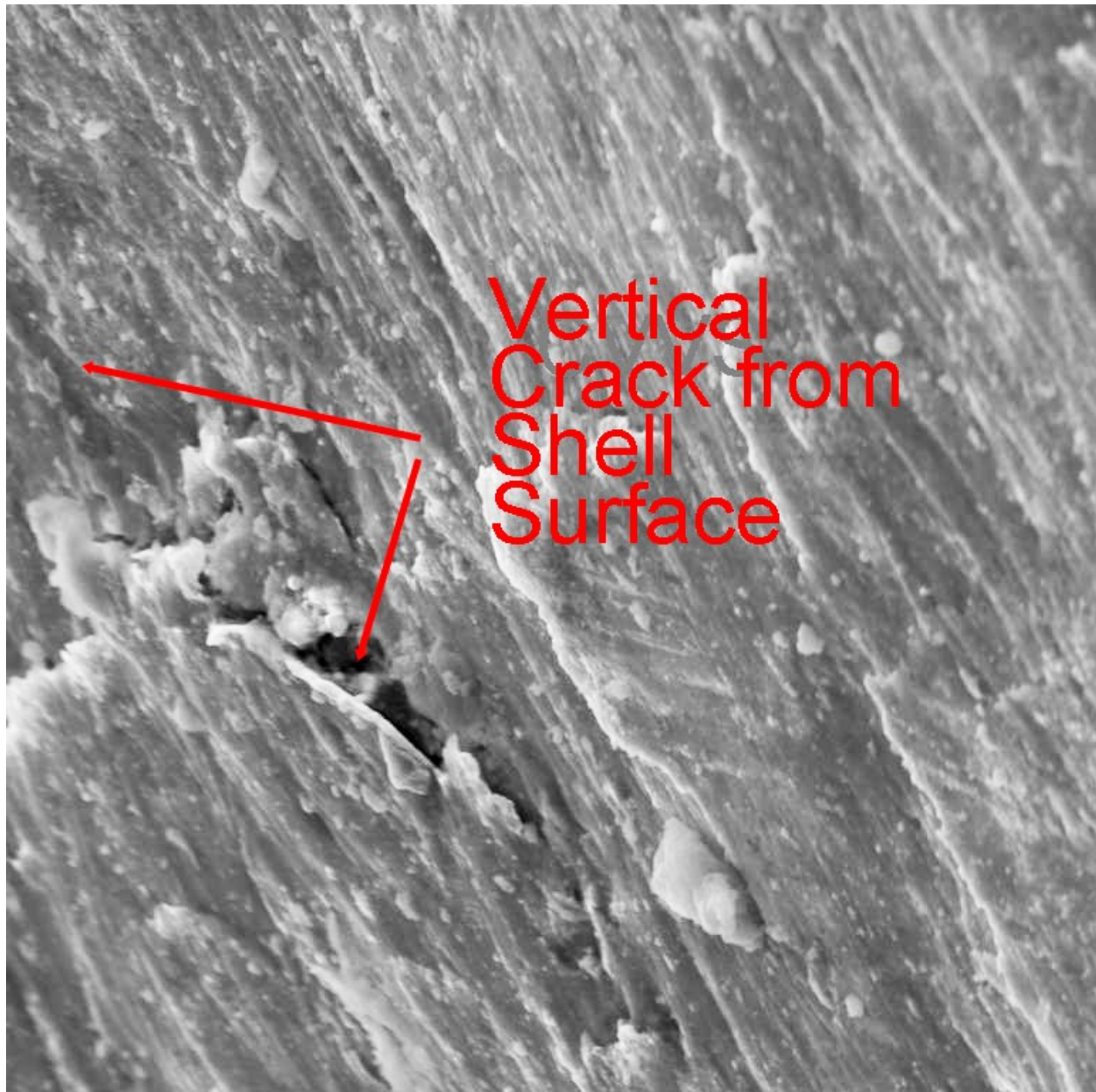


Figure A-58. Transition from Shell to VSR on UP9 with Associated Oxides Within Cracks, Original Magnification x100



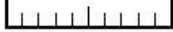

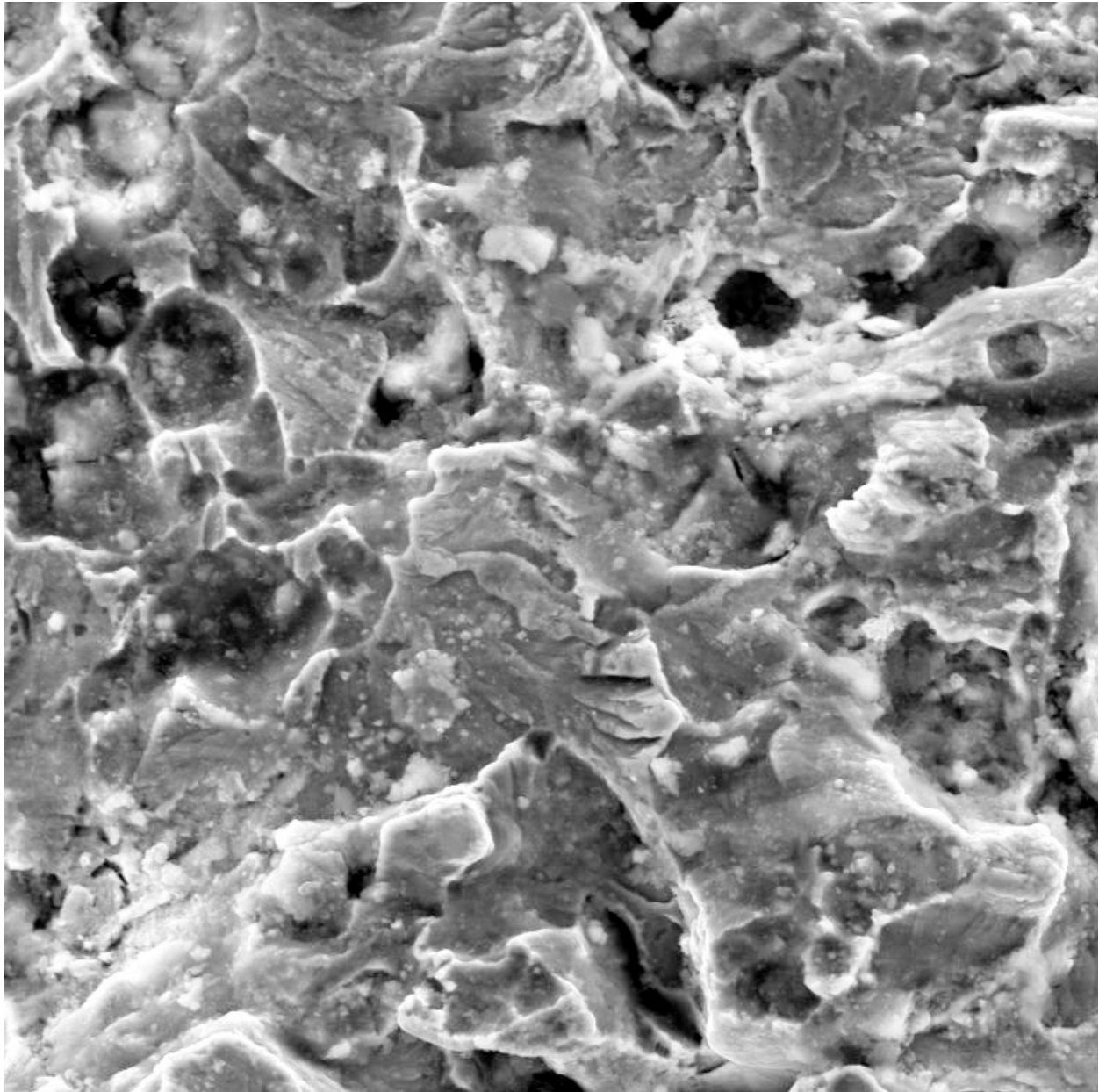
SEM HV: 30.00 kV WD: 25.20 mm  VEGA\\ TESCAN
View field: 150.8 μm Det: SE Detector 20 μm
SEM MAG: 1.00 kx Date(m/d/y): 09/07/18 ESI 

Figure A-59. Scanning Electron Microscope Image of UP9's Delamination Surface, Original Magnification x1,000



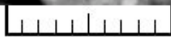

SEM HV: 30.00 kV WD: 15.83 mm  VEGA\\ TESCAN
View field: 150.8 μ m Det: SE Detector 20 μ m
SEM MAG: 1.00 kx Date(m/d/y): 09/07/18 ESI 

Figure A-60. Scanning Electron Microscope Image of Quasi-Cleavage UP9's VSR Fracture Surface. Original Magnification x1,000

A radial microhardness traverse was made from the tread surface to a depth of half of an inch. The results, Figure A-61, show that the surface was work-hardened by approximately 40 Vickers hardness numbers.

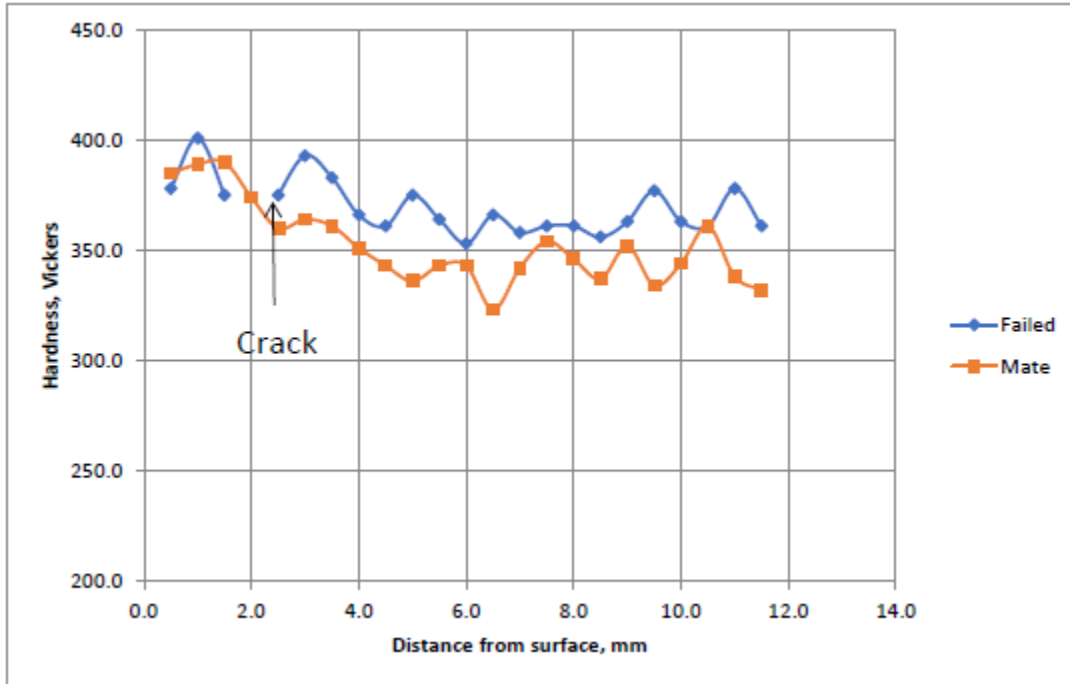


Figure A-61. Radial Microhardness Traverse from UP9 and Mate Tread Surface

The fracture toughness of the failed and mate wheels was determined according to ASTM Standard Method E399. While a valid value of fracture toughness was not determined, K_{q} values were determined. The failed wheel had a K_{q} of 36.6 $\text{ksi}\sqrt{\text{in}}$ while the mate wheel K_{q} was 33.7 $\text{ksi}\sqrt{\text{in}}$. These values are similar to that of 30.8- to 33.8- $\text{ksi}\sqrt{\text{in}}$ reported for a cast wheel in an earlier study of wheel fracture properties [18].

Abbreviations and Acronyms

ACRONYMS	EXPLANATION
ASTM	American Society for Testing and Materials
AWG	Analysis Working Group
AAR	Association of American Railroads
BNSF	Burlington Northern Santa Fe Railway
CN	Canadian National Railway
CP	Canadian Pacific Railway
CSX	CSX Transportation
ESI	Engineering Systems, Inc.
ENSCO	ENSCO, Inc.
FRA	Federal Railroad Administration
FEA	Finite Element Analysis
GATX	GATX Corporation
HA	Head Area
HWD	Hot Wheel Detector
NS	Norfolk Southern Corporation
RRS	Office of Railroad Safety
RD&T	Office Research, Development and Technology
RCF	Rolling Contact Fatigue
SWG	Stakeholder Working Group
TWG	Testing Working Group
TTCI	Transportation Technology Center, Inc.
UP	Union Pacific Railroad
VSF	Vertical Split Flange
VSR	Vertical Split Rims
WILD	Wheel Impact Load Detector